Tito Maldonado

Aspects of climate variability during winter and summer in Central America

UPPSALA
UNIVERSITET

Abstract

Climate variability during winter and summer in Central America is examined. In winter, we focused on the interaction between El Niño Southern Oscillation (ENSO), Pacific Decadal Oscillation (PDO), the Caribbean low-level jet (CLLJ) and precipitation. Using the composite technique it is found that ENSO events are connected to CLLJ anomalies by modulating the sea-level pressure (SLP) near the east coast of the United States and the Aleutian Low. The pattern displayed by the SLP anomalies (SLPa) is also associated with the Pacific/North America pattern (PNA). During warm (cold) ENSO phases, negative (positive) anomalies in the SLP field over the east coast of North America produce cyclonic (anticyclonic) circulations at low levels. However, the ENSO signal in the SLPa and the PNA pattern are modulated by the phases of the PDO. Results indicate that when the ENSO and PDO are in phase (out of phase), the SLPa signal is enhanced (weakened or cancelled), affecting the CLLJ anomalies in both direction and intensity, also changing the spatial distribution of precipitation.

During summer, the midsummer drought (MSD) in Central America is characterised in order to create annual indexes representing the timing of its phases (start, minimum and end), and other features relevant for MSD forecasting such as the intensity and the magnitude. The MSD intensity is defined as the minimum rainfall detected during the MSD, meanwhile the magnitude is the total precipitation divided by the total days between the start and end of the MSD. It is shown that the MSD extends along the Pacific coast, however, a similar MSD structure was detected also in two stations in the Caribbean side of Central America, located in Nicaragua. The MSD intensity and magnitude show a negative relationship with El Niño 3.4 and a positive relationship with the CLLJ index. However for the Caribbean stations the results were not statistically significant, which indicates that other processes might be modulating the precipitation during the MSD over the Caribbean coast. On the other hand, the temporal variables (start, minimum and end) show low and no significant correlations with the same indexes.

The results from canonical correlation analysis (CCA) show good performance to study the MSD intensity and magnitude, however, for the temporal indexes the performance is not satisfactory due to the low skill to predict the MSD phases. Moreover, we find that CCA allows producing forecasts of the MSD intensity and magnitude using sea surface temperatures (SST) with leading times of up to 3 months. Using CCA as diagnostic tool it is found that during June, an SST dipole pattern upon the neighbouring waters to Central America is the main variability mode controlling the inter-annual variability of the MSD features. However, there is also evidence that the regional waters are playing an important role in the annual modulation of the MSD features. The waters in the PDO vicinity might be also controlling the rainfall during the MSD, however, exerting an opposite effect at the north and south regions of Central America.

Sammanfattning

I den här studien har klimatvariationer under vintern och sommaren i Centralamerika undersökts. Betydelsen av El Niño Southern Oscillation (ENSO), Pacific Decadal Oscillation (PDO), Caribbean low-level jet (CLLJ) för nederbördens distribution och magnitude har undersökts. Med hjälp av statistiska metoder visas att ENSO modulerar marktrycket (SLP) nära USA:s östkust och därmed ger avvikelser i CLLJ. Sambandet visar att SLP anomalier (SLPa) också är förknippade med tryckfältet i Stilla Havet/Nordamerika (PNA). Under varma (kalla) ENSO faser producerar negativa (positiva) anomalier i SLP fältet över Nordamerikas ostkust cykloniska (anticykloniska) cirkulationer på låga nivåer. Resultaten visar att när ENSO och PDO är i fas (ur fas), förstärks (försvagas eller avbryts) SLPa-signalen vilket påverkar CLLJ till både riktning och intensitet, så att den geografiska fördelningen av nederbörd förändras.

Under sommaren studerades den s.k. midsommartorkan (MSD) i Centralamerika genom att definiera index som representerar tidpunkten för faserna av MSD (start, minimum och slut), och andra funktioner som är relevanta för MSD prognoser såsom intensitet och omfattning. MSD sträcker sig längs Stillahavskusten, ettMSD-liknande nederbördsmönster uppträder också i data från i två stationer på den karibiska sidan av Centralamerika. MSD-intensitet och magnitud för MSD längs Stilla Havs kusten visar ett negativt samband med El Niño 3.4 och ett positivt samband med CLLJ, för de karibiska stationerna var resultaten inte statistiskt signifikanta, vilket indikerar att andra processer kan modulera nederbörden under MSD längs den karibiska kusten. Däremot visar, visar de temporala variablerna (start, minimum och slut) låg korrelation med samma index.

Canonical correlation analysis (CCA) har använts och visar sig vara är ett bra instrument för att studera MSDs intensitet och omfattning, men för den temporala strukturen är resultaten inte tillfredsställande på grund av att metoden inte kan prediktera MSD faserna. Dessutom kan CCA användas till att producera prognoser för MSD intensitet och omfattning med hjälp av vattenytans temperatur (SST) med upp till 3 månader i förväg. Genom att använda CCA visas att det främst är systematiska SST-mönster (under juni månad) i havsområdens som gränsar till Centralamerika, som styr de årliga variationerna i MSD. Även regionala havsområden spelar en viktig roll i moduleringen av MSD. Havsområden som dominerar PDO- är också väsentliga för nederbörden under MSD.

List of papers

This thesis is based on the following papers, which are referred to in the text by their Roman numerals.

I   Maldonado, T., A. Rutgersson, J. Amador, E. Alfaro, and B. Claremar, 2015: Variability of the Caribbean low-level jet during boreal winter: large-scale forcings. *International Journal of Climatology*. DOI: 10.1002/joc.4472

II   Maldonado, T., A. Rutgersson, E. Alfaro, J. Amador, and B. Claremar, 2015: Interannual variability of the midsummer drought in Central America and the connection with sea surface temperatures. *Submitted*.

Reprints were made with permission from the publishers.

In paper I and II the author had the main responsibility for analysing the data and writing the main text.

Contents

1. Introduction

1.1 About the Centre for Natural Disaster Science

Centre for Natural Disaster Science (CNDS) is a Swedish centre for research on natural disasters. The investigations conducted at CNDS aims to contribute to improving the ability to prevent and deal with risks in society by raising awareness of the dynamics and consequences of natural hazards.

Within the CNDS framework the present thesis examines climate variability aspects and their impact in the precipitation distribution in Central America. The present work also provides tools for both studying and forecasting one of the most interesting climate elements that yearly occurs in the region referred as the mid-summer drought.

1.2 Aims of study

The general objective of this study is to examine the climate variability elements in Central America during both winter and summer affecting the precipitation distribution at monthly scales.

More specific targets are:

- Studying the variability of El Niño and its impact in two relevant climate processes such as the Caribbean low-level jet and precipitation during boreal winter.

- Analysing the inter-annual variability of the mid-summer drought and its relationship with the sea surface temperatures of neighbouring oceans.

Central America and the Caribbean regions are home of about eighty million of people. Formed by countries and islands among the poorest of the Americas and even of the world, many of their inhabitants are living in areas prone to natural disasters. Alfaro et al. (2010) pointed out that most of the natural disaster reports have been related to hydro-meteorological phenomena. Indeed, this region is constantly affected by a wide variety of intense meteorological events, like travelling easterly waves, tropical cyclones, convective systems, cold surges coming from the north hemisphere, the mid-summer drought (in Spanish *canícula or veranillo*), the warm pools, the trades, and an intense low-level jet over the Caribbean Sea. Variations in the intensity of

these elements in combination with social factors (i.e. people living in risky areas), can increase the probability of natural disasters.

The understanding of the annual and seasonal precipitation cycle and its variation through the year, thereby, becomes essential for planning and preparation for the rainy season in the area. The annual rainfall cycle in Central America is known to have two contrasting regimes between the Caribbean and Pacific slopes, due mainly to the interaction of the trades winds with the complex topography in the region While in the Pacific coast a semi annual feature is observed trough the year, with the first rainfall maximum occurring during May-June, and a secondary and more intense peak in August to October, the Caribbean side exhibits wetter and more humid conditions during the winter months, concomitant to a precipitation minimum in the Pacific coast. The reduction in precipitation during July is due to different processes that those at the beginning of the year. Therefore, this relative decrease is a relevant element to explain the annual rainfall cycle. This reduction in rainfall has been called the mid-summer drought (MSD). Furthermore, almost simultaneously with the dry periods and the MSD in the Pacific slope, a strong low-level wind current known as the Caribbean low-level jet (CLLJ) occurs twice per year. Both elements remain as a scientific challenge since little is known about their origins, and interactions with other climate processes in the region.

The precipitation regime in Central America is highly modulated by the interaction of several climate processes that occur every year, that range from local and regional scales such as those mentioned above, to large scales forcing such as El Niño, the Pacific Decadal Oscillation (PDO), and the North Atlantic Oscillation (NAO). El Niño Southern Oscillation (ENSO), however, is the main climate modulator during both winter and summer in the region. ENSO signal, nevertheless, is known to show inherent variability at high and mid latitudes, that in certain cases has been associated to non-linearities, and in other cases to the interaction with the PDO.

At regional scales, previous studies have analysed the influence of the sea surface temperature (SST) anomalies in the precipitation regime in Central America. Enfield and Alfaro (1999) have shown that the magnitude of the precipitation during the rainy season (from May to October) in Central America is highly modulated by the SST anomalies at both oceans, the Pacific and the Atlantic. Alfaro (2007) and Fallas-López and Alfaro (2012b) studied the predictability of the rainfall using canonical correlation analysis (CCA) with SST as predictor. Both studies found that the SST modify the response on precipitation in different ways during each rainfall maximum, the first rainfall peak being modulated mainly by the SST over the tropical Atlantic, and the secondary maximum being controlled by a dipole in the SST anomalies over the neighbour oceans to the Central American coast. Moreover, Fallas-López and Alfaro (2012a) found that the MSD intensity is dependent on several global climate indexes such as the Atlantic Multi-Decadal Oscillation (AMO), Niño 3 (N3), and PDO. Maldonado and Alfaro (2011) and Maldonado et al. (2013)

utilised CCA to explore the distribution of precipitation extreme events during the second precipitation maximum finding that during the second rainfall maximum, the total precipitation and temporal distribution of precipitation events are controlled by a dipole in the SSTs between the Pacific and the Caribbean-North Atlantic waters. Given the above evidence, it would be expected that the SST is involved in the MSD variability at inter-annual scales. In fact, Alfaro (2014) found that warm (cool) conditions of Niño 3.4 tend to be associated to drier (wetter) MSD events in some regions of the North Pacific and Central Valley of Costa Rica.

As mentioned, the general target of this thesis is to examine the climate variability during both dry periods in Central America: winter and summer. Winter is defined as the time spanning from December to February (DJF), while summer is considered from June to August (JJA). Specifically, it is studied what are the main climate variability modes that exert at changes in the temporal and spatial distribution of precipitation during each season at inter-annual scales.

This study contributes to the current knowledge about the weather and climate dynamics in the Central American region. In practical terms, the results of this thesis will contribute to the improvement of the design, planning and implementation of warning and mitigation strategies oriented to the assessment of sever dry conditions, e.g. the droughts reported in the North Pacific region of Costa Rica during July 2014 (Chinchilla-Ramírez, 2014). The results will improve the pool of information currently available to both social and economical sectors, such as emergency offices, water resources, agricultural and hydro-electrical power production parties among others, contributing to better response to an eventual emergency situation linked to winter and summer periods.

2. Background

The geographical location of Central America plays a significant role to describe the climate and the variability of the region. Surrounded by two large water masses, the Eastern Tropical Pacific (ETPac) ocean at the western side (Fiedler and Lavín, 2006), the Caribbean Sea and North Atlantic ocean at the eastern side; along with the Gulf of Mexico, the entire area is known as the Intra-Americas Seas (IAS, Amador 2008) as shown in Fig. 2.1. The IAS is also important for the global climate, because it receives large amounts of radiation coming from the Sun onto the Earth surface, and the regional waters act like an energy reservoir.
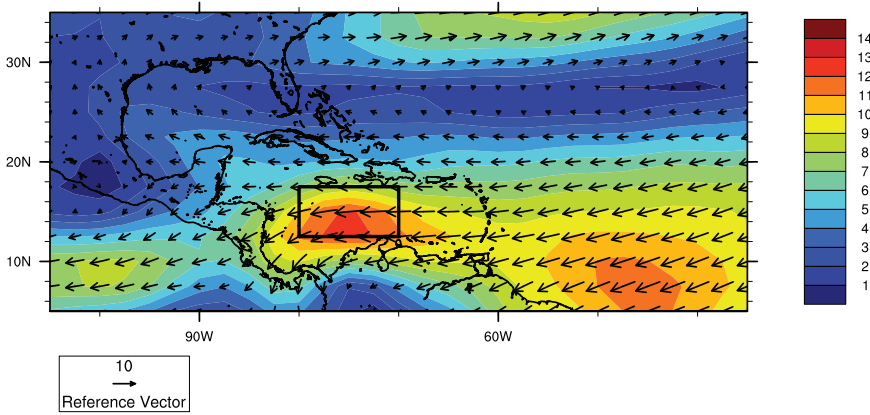

Figure 2.1. The Intra-Americas seas region is the domain bounded by $5°$ S $– 35°$ N, $35° – 105°$ W. The contour colours represent the mean wind speed for February for the period 1950 – 2012. The quivers are the mean wind vectors. Units for both contours and vectors are in ms^{-1}. The square shows the utilised area to define the Caribbean low-level jet index (from Paper I).

The IAS region is sensitive to the effect of both large- and regional-scale dynamical systems acting in its vicinity, such as the North Atlantic Subtropical High (NASH), strong easterly winds, a large latent heat belt, warm sea surface temperature SST and intense precipitation. All of these elements depict the general frame of the regional climate and variability in the region (Wang et al., 2008). Furthermore, the formation of the Western Hemisphere Warm Pool (WHWP, Wang and Enfield 2001, 2003; Wang and Fiedler 2006),

cyclogenesis over the Caribbean Sea (Goldenberg et al., 2001), the influence of the Inter Tropical Convergence Zone (ITCZ) along with the MSD (Magaña et al. 1999; Karnauskas et al. 2013; Herrera et al. 2015, Paper II), and the CLLJ (Amador, 1998, 2008) form part of the vast variety of regional climate components present in this area. Many of the dynamical and physical mechanisms and interactions with the climate of the region are still not fully understood (Amador, 2008).

2.1 The wind field

The trade winds are the low-level tropospheric flow, classically known as part of the equator-ward branch of the Hadley cell transporting a large amount of the moisture, resulting in convergence with uplift and destabilised stratification at the low latitudes. They are responsible of the convective activity and associated precipitation distribution that take places near or within the ITCZ. At local scales, the interaction with the topography helps to explain the temporal and spatial rainfall variability in some areas of Central America (Amador et al., 2003). Two subtropical high-pressure systems located near 30° N, in both the Pacific Ocean (the North Pacific High) and in the North Atlantic Ocean (the Bermuda or Azores High). In average, there is a relative strong meridional pressure gradient between the subtropics and tropics, which accelerates the air masses towards the equator, generating the trade winds.

Monsoonal systems such as the North American Monsoon System (NAMS) and the South American Monsoon System (SAMS) interact in different ways with the trade winds, and are very important mechanisms to explain the precipitation during the warm season in the ETPac. Vera et al. (2006) review both systems with more details. According to Amador et al. (2006), the most relevant for ocean-atmosphere dynamics in the ETPac is the NAMS.

During the northern hemisphere winter, the ITCZ is at its southernmost position (Srinivasan and Smith, 1996), and SSTs over the adjacent areas of the Caribbean and the Pacific are relatively uniform, with values usually below 28 °C (Amador et al., 2003). Trade winds are intensified and a frequent southward displacement of air masses occurs. From December – March cold air masses coming from Canada and the polar regions penetrate deep into the tropics and produce strong wind events associated with intense periods of rainfall (Schultz et al., 1997, 1998). Interaction with topography (i.e. wind is funnelled trough topographical gaps in southern Mexico and Central America), and a strong gradient in the SLP between the basins, a low in the Pacific and a high in the Caribbean, due to the intrusion of the cold fronts (CF), produce strong near-surface wind events that can to extend far in the ETPac. High sea level pressure (SLP) over the southwester Caribbean generates northerly surface winds across the Isthmus of Panama that extend offshore of the Gulf of Panama into the eastern tropical Pacific region (Amador et al., 2006). Dur-

ing this season these intense winds over the Caribbean are associated with the winter branch of the CLLJ (Wang and Lee 2007; Amador 2008, Paper I), and its interaction with mountains forcing rainfall in Central America.

In the boreal summer, more complex circulations than those in winter develop in the IAS region. The NAMS, generated due to the seasonal thermal contrast that occurs in this season over the ETPac, and the North, Central and South America masses (e.g. Higgins et al. 2003). The NAMS has been shown to be associated with the summertime precipitation of the region (Mock, 1996; Higgins et al., 1997). It starts to develop during May – June, and associated with heavy rainfall in late May or early June over southern Mexico, moving north to the south-western United States. The mature phase is reached during July – August and September, and the precipitation regime over North America is related to NAMS (Higgins et al., 1997). Surges of maritime tropical air that move northward and that are associated with rainfall over the Gulf of California and southwester United States (Douglas and Leal, 2003). The decay phase (late September – October) can be characterize as broadly the reverse of the onset phase, though at a slower rate (Higgins et al., 2003).

Other low-level flows occur during the boreal summer, particularly the Gulf of California low-level jet (Douglas, 1995; Douglas et al., 1998), the Chocó low-level jet (Poveda and Mesa, 2000), and the Caribbean low-level jet (Amador, 1998, 2008). The former is parallel to the Gulf axis and has a well defined diurnal and synoptic scale variability. It is located below 2000 m at the northern end of the Gulf of California with wind velocities of $5 - 7 \mathrm{ms}^{-1}$. It is a relevant mechanism for moisture transport into the interior of the continental regions during the monsoon (Douglas and Leal, 2003).

The second mechanism, the Chocó jet (CJ) develops in the western coast of Colombia near $5°$ N. It reaches its maximum by October-November, then decreases its intensity until being almost absent during the period February-March. Low-level warm air and moisture convergence associated with the CJ, low surface pressure and orographic vertical motion on the western Andes, contribute to deep convective activity, which is organized as meso-scale convective complexes.

The third low-level flow, the CLLJ, peaks in both winter and summer (Amador, 1998; Amador et al., 2003; Amador, 2008). The annual mean cycle of the CLLJ index at 925 hPa is shown in Fig. 2.2. During summer, it is barotropically unstable, and has potential interaction with transients, such as easterly waves. From May to July, easterly waves loose energy and momentum strengthening the mean current and causing the low-level jet to peak in July. The CLLJ is an important element to explain the convective activity during July through November, and contributes to understand the climate of the region. In winter, however, its formation is distinct to the summer component (Amador 2008; Wang 2007; Cook and Vizy 2010, Paper I), nevertheless, it is an important mechanism for moisture transport from the Caribbean sea to

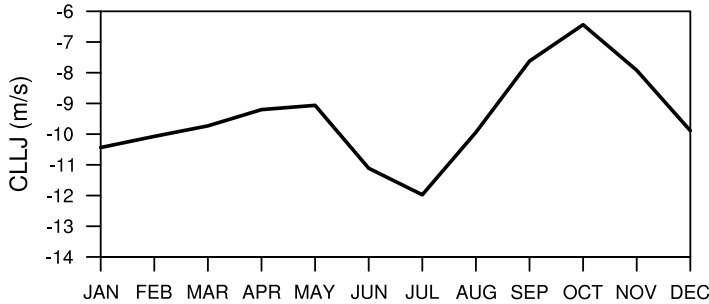Central America and the Gulf of Mexico during both seasons (Durán-Quesada et al., 2010; Gimeno et al., 2012).

Figure 2.2. Mean annual cycle of the Caribbean low-level jet index in ms^{-1}. Note that since the wind is easterly, the negative values mean stronger zonal wind (from Paper I).

According to Amador et al. (2006), the wind stress curl has a strong seasonal cycle with a marked meridional migration of the up-welling (positive curl) and down-welling (negative curl) areas that is mostly associated with the southeast and northeast trade patterns and its north-south migration in the eastern tropical Pacific. The distribution of this variable is almost zonal, and most of the large-scale features are located north of the equator. In general, the fluctuations in the magnitude of the wind stress curl in the tropics are mainly related to seasonal atmospheric circulation and the ITCZ.

2.2 Moisture

Durán-Quesada et al. (2010) identified two main moisture sources for Central America. The first one and the most important is located in the Caribbean. The second appears to exist near the equatorial Pacific region. These results were highlighted also by Gimeno et al. (2012) whose stress that the major amount of humidity in the Continental part of Central America is originated in the nearby oceans. A third source of moisture was found by Durán-Quesada (2012) over Venezuela due to water recycling processes.

The intensity and extent of the moisture sources vary throughout the year. The Caribbean source (CS) does not vary significantly along the year, except a slight displacement towards the Gulf of Mexico during winter. In contrast, the Pacific source (PS) shows significant variation throughout the year, and disappears as a source during winter and spring, mainly due to the influence of the ITCZ (Durán-Quesada et al., 2010). Seasonally, during the boreal summer the humidity transport from the CS is more effective and contributes with the precipitation in Central America, while the moisture that departs from PS is not

15

even able to reach the entire Central America region, contributing only to precipitation in its southernmost portion, specifically at Costa Rica. Through the boreal winter, there is a reduction in the moisture transport. Consistent with the precipitation pattern over this region, exhibiting dry conditions (mainly in the Pacific basin) during this season. Moisture convergence in Central America during winter is clearly less important than during spring (March, April, May) and autumn (September, October, November), when the moisture flux over the continental area of Central America becomes more relevant.

In order to understand the role of the CLLJ for moisture transport, it is worth to say that the CLLJ acts not only as a moisture belt, but also as a humidity collector that is capable of modulating surface evaporation as a result of its moisture content (Wang et al., 2007). Many studies found that the core of CLLJ wind jet is consistent with the maximum nucleus of moisture gain over the Caribbean Sea (Wang, 2007; Wang and Lee, 2007; Wang et al., 2007; Durán-Quesada et al., 2010). The major contribution occurs during boreal summer, and for the case of the CS region this is in good agreement with the maximum observed winds in the core of the CLLJ. However, the second maximum of the CLLJ in boreal winter is not associated with any important transport, mainly due to the incidence of the dry season, which is characterized by less intense jet winds than in summer and a minimal amount of precipitable water.

Durán-Quesada et al. (2010) highlight that the contribution of moisture to Central America that originates in the PS region is partly determined by the presence of the CJ, which in turn allows the development of deep convection in the region. This contribution is more noticeable over northern Colombia when it appears to be combined with the effect of orographic lifting as described by Poveda and Mesa (2000). The importance of the PS region is greatest during those parts of the boreal summer and autumn that coincide with the maximum velocities within the core of the CJ. A significant part of the moisture transported by this jet is unable to reach Central America completely, mainly as a result of the loss of moisture in the ITCZ and the presence of a mountain range in Costa Rica.

2.3 Precipitation

The most relevant synoptic influence present in the Caribbean and Central America area is the NASH. This subtropical high produces strong easterly trades winds towards the equator, being in Central America the dominant wind regime. The interaction between the trades and the topography, plus the location of the isthmus, imprint upon the region particular climate and weather features. This interaction produces two regional climates – Pacific and Caribbean (Taylor and Alfaro, 2005; Amador et al., 2006), nonetheless, the complex orography is capable to produce very local climate and weather

patterns, noted mainly in the high variability observed in precipitation with respect to the altitude (Fernández et al., 1996; Amador et al., 2003).

The Pacific coast presents a bimodal rainfall distribution around the year (Fig. 2.3, upper panel). A first maximum occurs in May-June, due to the migration north of the ITCZ. However, the migration of the ITCZ neither explains the generalized deep convection during the rainy season over the whole region since the ITCZ is not found at latitudes $10° - 12°$ N (Alfaro, 2000), nor explain the beginning and the ending of the rainy spell. Additionally to this migration, the SST of the neighbouring seas have warmed reaching about 29 °C, deep convection activity is developed along with a sub-tropical lower-tropospheric cyclonic circulation anomaly over the subtropics.
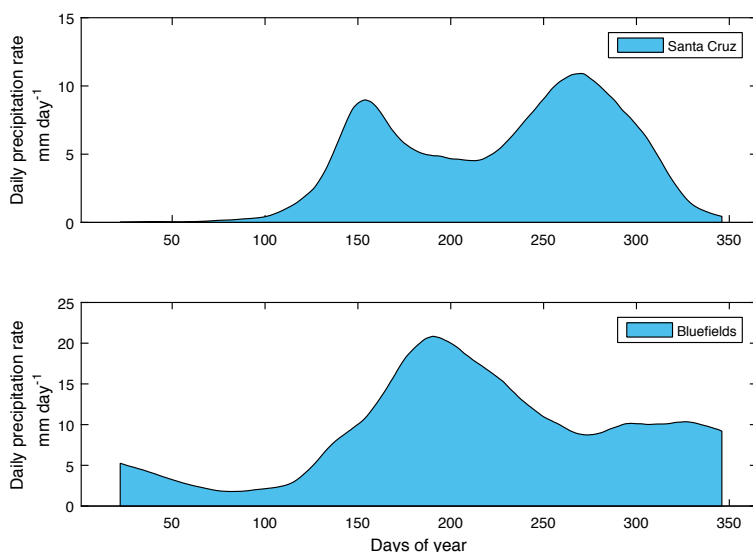

Figure 2.3. Examples of the mean precipitation annual cycle in the Pacific (top) and Caribbean (bottom) coasts.

A relative minimum of precipitation through July-August upon this slope, is due to the MSD (Magaña et al. 1999; Karnauskas et al. 2013; Herrera et al. 2015, Paper II). During the occurrence of the MSD in these months, the convective activity diminishes, due to a decrease of about $1°$ C in the SST over the ETPac, the cyclonic circulation anomaly weakens, corresponding to an anticyclonic acceleration of the low-level flow and, therefore, to an intensification of the trade winds. This leads to a formation of divergence anomalies that inhibit deep convection activity, and the strengthening of the easterlies, forcing upward motion and intense precipitation over the Caribbean side, and subsidence and clear skies upon the Pacific slope (Hidalgo et al., 2015).

The second maximum peaks during August through October due to the presence of fewer deep clouds, which would produce an increment of incom-

ing solar radiation heating the SST above 28° C. Then, this warming in the SST produces an increase of evaporation from the oceans to the atmosphere; in addition, weakened trade winds and a low-level convergence anomaly lead to enhanced deep convection. Normally, this season presents the highest frequency of extreme events over the Pacific slope (Alfaro et al., 2010). While in the Caribbean coast, rainfall decreases during these months, due to a decrease in the strength of the trade winds (Taylor and Alfaro, 2005; Amador et al., 2006). From December to March, the Pacific slope of Central America presents warm and mostly dry conditions. During these moths, the ITCZ is at its southernmost position (Srinivasan and Smith, 1996).

The Caribbean side shows (Fig. 2.3, lower panel) a different rainfall mode, as pointed out by Taylor and Alfaro (2005). Precipitation during the winter months along this coast, is mostly related to humidity convergence, mid-latitude air intrusions (Schultz et al., 1997, 1998), and less frequent low-level cloud systems traveling from the east (Velásquez, 2000).

2.4 Variability elements in the Intra-Americas Seas

2.4.1 Large-scale variability modulators

ENSO is the most influential large scale index on the climate of the IAS (Wang and Fiedler, 2006). Nevertheless, the influence of other variability modes in the Atlantic Ocean such as the AMO, and the NAO have shown to have an important contribution in the variability of the precipitation field of Central America (Enfield and Alfaro 1999; Alfaro 2007; among others). Recently, the influence of the PDO on rainfall over the Central America (Mantua and Hare 2002; Fallas-López and Alfaro 2012b, Paper I), the influence of the Madden-Julian Oscillation (Martin and Schumacher, 2011) on precipitation in the Caribbean islands have also been studied.

El Niño Southern Oscillation
ENSO is a two-component physical mechanism that describes the coupling of SST anomalies in the tropical Pacific Ocean and the fluctuation in tropical SLP gradient in the Western and Eastern Pacific Hemispheres, also known as the Southern Oscillation (SO). El Niño is associated with unusual strong warming events that occur every two to seven years in concert with basin-scale tropical Pacific anomalies (Wang and Fiedler, 2006). ENSO variability in the eastern tropical Pacific is centred along the equator, but is closely related to variability of the tropical WHWP. Authors such as Chen and Taylor (2002) and Bell and Chelliah (2006) suggest that ENSO forces variations in the SST field and vertical wind shear that trigger the inter-annual variability of the hurricane season during ENSO events. Moreover, an increase (decrease) of precipitation has been associated with cold (warm) ENSO phases (Dai and Wigley 2000; Giannini et al. 2000, Paper I).

Variability of the surface winds has been also observed related to ENSO. During summer, the flow over surface has been found to increase during El Niño events while a reduction occurs in the opposite phase. Examples of that, the changes in the CJ (Poveda and Mesa, 2000) and the CLLJ (Wang, 2007; Amador, 2008). The core intensity of the CLLJ varies with ENSO phases in such way that during warm (cold) events the jet core is stronger (weaker) than normal in the boreal summer, surface wind stress and wind stress curl area expected to be stronger (weaker) than normal in the easternmost portion of the eastern tropical Pacific. Contrary to what happens in summers, the jet core is weaker (stronger) than normal during warm (cold) ENSO phases in winter (Amador 2008, Paper I). These variations in the wind field influence the vertical wind shear and cyclone-genetic processes (Amador, 2008; Amador et al., 2010).

It can be followed that ENSO is able to affect precipitation distribution by modulating two different mechanisms: a) evaporation variability linked to SST and surface drag variations and b) transport of moisture due to wind flow modulation.

The Pacific Decadal Oscillation

The PDO is a long-lived El Niño-like pattern of the variability of the Pacific climate (Zhang et al., 1997). Mantua et al. (1997) highlight the PDO as the dominant pattern of Pacific Decadal Variability (PDV). Even when the PDO is referred as an El Niño-like pattern, it differs from ENSO in the time scale of the persistence of events and its fingerprint is more noticeable in the extratropics rather than the tropics (Mantua and Hare, 2002). The pattern of a warm PDO phase is featured by cooler than normal SSTs in the central North Pacific and warmer than normal SSTs along the west coast of the Americas. Symmetry in SST anomalies patterns between northern and southern hemispheres exhibited by the PDO has been noted by Evans et al. (2001). The mechanisms of the PDO are complex and still an open issue, however, some studies suggest the importance of the tropical coupling for the existence of the PDO (Feng et al., 2010). Schneider and Cornuelle (2005), propose the PDO to evolve from a composition between the forcing due to El Niño 3.4 (see Trenberth 1997 or for definition of El Niño regions), and the changes of the Aleutian low (interannual frequencies) and the Kuroshio-Oyashio Extension (decadal time scales). The importance that the PDO may have for global climate is related to a correlation between the PDO index (Mantua et al., 1997) and precipitation anomalies. Warm PDO phases have been found associated with anomalously dry periods in the eastern coasts of Eurasia, Northwest Pacific of USA, Central America and northern South America. While the same phase seems to be related to wetter than normal conditions in the Gulf of Alaska, South-west USA and Mexico, South-east Brazil, South central South America and western Australia. In Paper I is found that during winter the PDO forcing is more appreciable in combination with the El Niño phases. The PDO intensifies El

Niño signal in SLP anomalies, and precipitation if both processes have the same phase. The PDO, however, modulates precipitation mainly over Mexico and southern part of USA.

The North Atlantic Oscillation

Greatbatch (2000) made a detailed revision of the NAO. It is the most important variability mode in the North Atlantic Ocean. One way to define and index for NAO is like the difference between normalized mean winter (December to March) SLP anomalies at Lisbon, Portugal and Stykkisholmur, Iceland (Hurrell, 1996). NAO is an element of the Arctic Oscillation (AO) patterns, then the former is linked with SST anomalies in the East/South-east of Greenland.

NAO has been also associated with the strengthen of the NASH and the North Eastern trade winds, affecting thus the circulation in the IAS. Thereby, the impact of the NAO is associated with the climate features of the IAS, SST in the Tropical North Atlantic, the size of the WHWP and the CLLJ. Seasonal variations of the NAO may be reflected in its influence on the IAS easterly winds and precipitation patterns (Wang, 2007). Malmgren et al. (1998) found that during the boreal summer the NAO index has an inverse relation with the observed precipitation patterns over Puerto Rico.

The Atlantic Multi-Decadal Oscillation

The AMO is a 70 years period mode in SST (Delworth and Mann, 2000; Kerr, 2000). This signal has also been found in different modeling analysis (Delworth et al., 1993; Delworth and Greatbatch, 2000; Latif et al., 2004) and it was detected as the first rotated EOF with a large response in the North Atlantic SST (Mestas-Nuñez and Enfield, 2001). The AMO signal modulates precipitation variations in different regions such as the IAS (Giannini et al., 2000). Wetter (drier) conditions over Central America (north-east Brazil) during JJA (DJF) were found by Zhang and Delworth (2006). AMO has also been determined to be of importance modulating the impact of ENSO on drought. Connection between AMO and other regional features such as the Atlantic Warm Pool (AWP) has been also studied. Wang et al. (2008) show that warm (cool) phases of the AMO are associated with repeated large (small) AWPs, suggesting the relationship between the AMO and Atlantic tropical cyclones. The latter is in agreement with results that indicate the presence of multi-decadal variations in hurricane activity due to the Atlantic SST (Goldenberg et al., 2001). AMO is then of importance related to the low frequency variability of precipitation as it modulates the distribution of moisture and extreme rainfall events (Maldonado et al., 2013).

The Madden-Julian Oscillation

The MJO has been identified as a 40-50 days oscillation in zonal wind anomalies in the tropical Pacific (Madden and Julian, 1994). Zhang (2005) makes a review of the basics of the Madden-Julian Oscillation (MJO). Recent studies

have analyzed both the ocean-MJO relationship (Webber et al., 2010), and the interaction between the MJO and ENSO (Tang and YU, 2008; Moon et al., 2010). Some findings have shown that this oscillation has effects on the tropical troposphere and strong impact on tropical convection. The MJO-related zonal wind anomalies in the ETPac region might be associated with the increase of rainfall in the North America Monsoon region. Also, the amplification of easterly waves as a trigger of gulf surges development that may be related with the variability of the moisture sources that feed the North America Monsoon System (Lorenz and Hartmann, 2006). These authors also suggested that westerly phase of the MJO are associated with the enhancement of favorable conditions for Mesoscale Convective System (MCS) development in the region. Barlow and Salstein (2006) found a positive (negative) phases of the MJO are associated with the increase (decrease) of precipitation in the region. Recently, Martin and Schumacher (2011) showed evidence about a link between the intensity of the CLLJ and the MJO, and it is suggested to lead changes in precipitation. Both of these last studies find some relation between the occurrence of extreme events and the MJO phase.

2.4.2 Regional-scale modulators

Regional circulations systems

Two important regional circulation systems modulate the weather and climate in the region. The first mechanism is the CLLJ over the Caribbean Sea, and the second the Chocó LLJ.

The CLLJ is important for moisture transport in the region, and also to explain the convective activity during the summer months. During the winter, it has a second maximum, nonetheless, it has shown no relation with convection in during this season (Amador et al. 2006; Amador 2008, Paper I). The Chocó LLJ peaks in October-November, and contributes to the moisture transport for the southernmost part of Central America (Durán-Quesada et al., 2010). Furthermore, the Chocó jet is associated with deep convection activity over the western Andes region in Colombia (Poveda and Mesa, 2000).

SST of neighboring oceans

The influence of the SST anomalies in the precipitation variability field has been widely studied (Enfield and Alfaro, 1999; Alfaro, 2000, 2007). The beginning and ending of the rain spells are related to fluctuations in the SST of the Atlantic and Pacific Oceans, and, these anomalies are related to the magnitude of rainfall and frequency of rainy days (Maldonado and Alfaro, 2010, 2011; Maldonado et al., 2013). Amador et al. (2006) pointed out that the seasonal cycle of SST is important in defining key climatological features, especially during summer-autumn, such as the WHWP development (Wang and Enfield, 2001; Wang and Fiedler, 2006), the appearance of MSD (Magaña

et al. 1999; Karnauskas et al. 2013; Herrera et al. 2015, Paper II), and favorable areas for cyclogenesis (Goldenberg et al., 2001). During the northern winter, SST isotherms over the Caribbean and the eastern tropical Pacific are mostly zonally distributed, with values usually below $28 - 29^{\circ}$ C, except in the central eastern tropical Pacific, and to the west of Central America, where there is a maximum of SST all year. A result of this, and a relatively strong vertical trade wind shear, and reduced evaporation, no major convective activity occurs in most of the Pacific coast of Central America during this season. Also, during boreal winter, the ITCZ is at its southernmost position (Srinivasan and Smith, 1996).

During boreal summer, the WHWP dominates the SST distribution over most of the eastern tropical Pacific region (Magaña et al., 1999; Wang and Enfield, 2001, 2003). In the Caribbean warm pool, organized activity is barely observed, due mainly to a strong vertical wind shear and strong subsidence associated with regional scale circulations, such as those associated with the low-level jet described above.

During warm (cold) ENSO phases, the CLLJ shows stronger (weaker) than normal wind speeds (Amador et al., 2003, 2006; Amador, 2008). This fluctuation is reflected in SST anomalies over the Caribbean Sea, north coast of Venezuela; a strong (weak) jet results in negative (positive) SST anomalies over this region due to strong (weak) Ekman transport. In this way, the jet may have a role in coupling SST anomalies in eastern Pacific during El Niño or La Niña events with anomalies over some regions of the Caribbean during summer. Variations in surface variables (precipitation and temperature) in different sectors of Mesoamerica, including its west coast, are the result of a combination of fluctuations in the equatorial tropical Pacific and in the tropical north Atlantic (Amador et al., 2006). Studies such as Alfaro et al. (1998); Alfaro and Cid (1999a,b); Enfield and Alfaro (1999) show that the strongest rainfall signal occurs when tropical north Atlantic and tropical Pacific SST anomalies are in a configuration of meridional dipole (antisymmetric) across the ITCZ, that is, when this anomalies have an opposite sign. The rainy season in south Central America tends to start early and end late in years that begin with warm SST in the tropical North Atlantic. Ending dates are also delayed when the eastern tropical Pacific is cool.

2.4.3 Local-scale modulators

Topography is the main local modulator of the variability in the region. Interaction between the terrain with the induced flow coming from the Pacific ITCZ, due to some prevailing synoptic system, produces a type of disturbance that contributes to precipitation in Central America, which is named the "temporales" (Hanstenrath, 1991; Fernández et al., 1996). These are periods of weak-moderate nearly continuous rain, lasting several days and affecting a

relatively large region. Their definition includes the condition that the wind must be weak; however, Amador et al. (2003) have shown that in some cases winds can be intense and long-lasting.

Fernández et al. (1996) identifies at least four synoptic conditions that can eventually generate conditions for a temporal, such as a deep lower and middle troposphere troughs in the easterlies (hurricanes excluded), intrusions of an upper troposphere troughs in mid-latitude westerlies, outbreaks of cold air from North America, and the direct and indirect effect of hurricanes. Velásquez (2000) also found that westward- traveling, low-level cloud system over the Caribbean reaching the Pacific, which are not necessarily associated with mid-latitude cold air intrusions. The frequency of these events presents a great deal of interannual and intraseasonal variability, and their relationship to ENSO or to other large-scale climatic signal is still unclear (Amador et al., 2006).

The sea-breeze circulations are other relevant regional modulators of the climate, on islands and peninsulas since it favors the development of convective system. Marked by a diurnal cycle due to the thermal contrast between the coastline and the sea, it can be related to a diurnal cycle of precipitation. However, in coastal regions with nearby complex topographical, like Central America, the induced flow can impact the temporal a spatial distribution of the meso-scale features in rainfall. Besides that, there is evidence in regions with similar characteristics to the Central American isthmus (i.e. west coast of Colombia), that the sea breeze can penetrate over near-coastal mountains into a valley until approximately 100 km (Warner et al., 2003). Nevertheless, note that such a feature of the sea breeze circulation has not been reported in Central America yet, but it might be a local modulator on many regions of this area.

3. Data

3.1 Area of study

Two slightly different domains were used for each paper. In Paper I, a domain bounded by 22° S – 63° N and 15° E – 180° W is selected, while, for Paper II the domain was increased to 111° to 15° E, covering basically all the Pacific and Atlantic oceans. Both domains, however, capture the most important global and regional climate variability modes affecting the climate and weather of Central America and the Caribbean, such as El Niño, NAO, AMO, PDO, Pacfic North American (PNA) pattern, WHWP, and TNA.

3.2 Reanalysis data

In Paper I, data from the National Centers for Environmental Prediction-National Center for Atmospheric Research (NCEP-NCAR) reanalysis project (Kalnay et al., 1996) are used because this reanalysis has previously been utilised for climate studies in this region (e.g. Amador 2008; Herrera et al. 2015) and its time series are long enough to capture long-lived events such as the PDO. Thus, in Paper I the period 1950 – 2010 is taken for the SLP and horizontal wind fields.

3.3 Precipitation data

Monthly total precipitation estimates are obtained from the Global Precipitation Climatology Centre (GPCC) (Schneider et al., 2011). The GPCC data are gridded with a 0.5° horizontal resolution. The dataset comprises monitoring products based on quality-controlled gauge station data from 1901 to the present. Nevertheless, in Paper I, the climatology is estimated for the 1950 – 2010 period.

A total of 25 gauge stations with daily observations of precipitation provided by the meteorological services in Central America are used in Paper II. Their location is shown in Fig. 3.1. Note that the majority (23) of the stations are situated along the Pacific coast with only two stations located along the Caribbean coast. The two Caribbean stations possess relevant features to describe the precipitation behaviour in the Caribbean slope, such as their location at the CLLJ exit and their contrasting annual precipitation cycle to that

in the Pacific. Thus, in order to achieve a better representation of the complete region, the Caribbean stations are considered for the analysis. The gaps in the time-series are filled using the methodology described in Alfaro and Soley (2009), which uses autoregressive models of order 1. This method can filter persistent signals comparable to the length of the filter, and the estimated values are consistent with the statistical properties of the time series without external superposition of the data. The precipitation time series length is from 1961 to 2012.
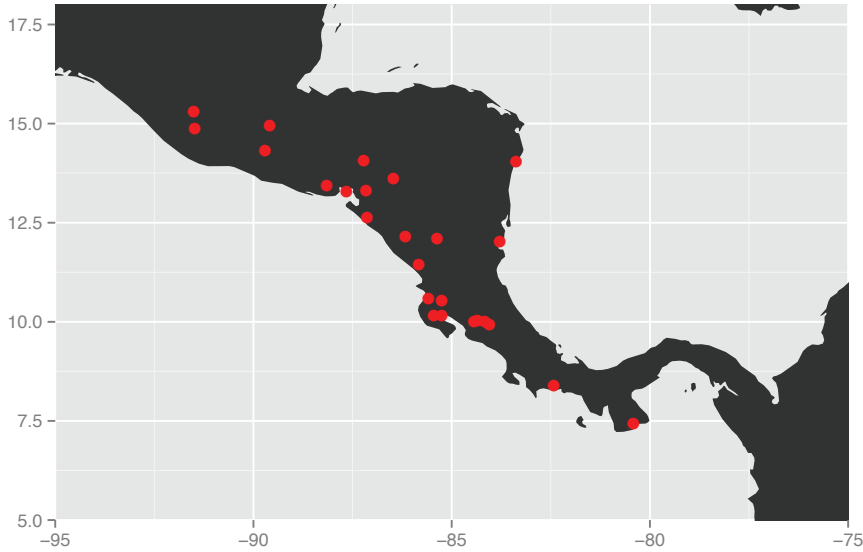
Figure 3.1. Spatial distribution of the gauge stations over Central America. From Paper II.

3.4 Sea surface temperature

The extended reconstructed sea surface temperatures (ERSSTv3b, Xue et al. 2003; Smith et al. 2007) are used in Paper II. The SST anomalies are constructed using a combination of observed data along with models and historical sampling grids. This global database has a horizontal resolution of 2.5 by 2.5 degrees. The domain bounded by -22° to 63° N and 111° to 15° E. Note that this domain is a slight modification of the domain used in Paper I. This change was done in order to have a complete representation of both oceans: the Pacific and Atlantic. The SST anomalies are used as predictors for the canonical correlation analysis method.

3.5 El Niño and PDO indexes

El Niño and PDO indexes are obtained from the National Oceanic and Atmospheric Administration's (NOAA) Earth System Research Laboratory, Physical Sciences Division website[1]. The ENSO episodes were determined using the definition of the Oceanic Niño Index (ONI)[2] from the NOAA's Climate Prediction Centre (CPC). The ONI definition of warm (cold) events consists of a threshold of $\pm 0.5\,^\circ$C for the 3-month running mean of SST anomalies in the Niño 3.4 region, based on centred 30-year base periods updated every 5 years. The MJO index as is defined by the CPC[3].

---

[1]`http://www.esrl.noaa.gov/psd/data/climateindices/list/`
[2]`http://www.cpc.ncep.noaa.gov/products/analysis_monitoring/ensostuff/`
`ensoyears.shtml`
[3]`http://www.cpc.ncep.noaa.gov/products/precip/CWlink/daily_mjo_index/`
`pentad.html`

4. Methods

4.1 Compositing ENSO and PDO

To explore the teleconnections of El Niño, a composite analysis of El Niño and La Niña years is used in Paper I to estimate the monthly mean composite anomalies of SLP, horizontal wind and divergence at 925 hPa and precipitation in February. The composite anomalies were calculated relative to the climatology of neutral years (i.e. neither warm nor cool ENSO events). Table 4.1 shows the ENSO classification of the years using the ONI definition. Note that, according to this definition, the ENSO events from 1950 to 2010 are almost evenly distributed between 18 El Niño and 16 La Niña events.

In Paper I the linear and non-linear effects of the ENSO events were studied by addition and subtraction of the ENSO phases. Assuming that El Niño and La Niña have the opposite signal in the anomalies (linear response) over the same regions, subtracting the anomalies, the signal of ENSO should be amplified in such areas. In regions where the subtraction of the anomalies decreases, this indicates that the ENSO signal in those areas does not have the exact opposite sign during the ENSO phases. With the addition of the anomalies it can identify the regions in which the ENSO signal does not have the opposite signal during each of the ENSO phases, and so a non-linear behaviour.

Similarly, a composite analysis is performed in Paper I to study the influence of the PDO on the perturbation of the wind and precipitation. Table 4.1 also shows the classification of the PDO phases according to CPC. The mean composite anomalies in this case are relative to the 61-year (i.e. 1950 – 2010) climatology for February. Notably, as for the general cases of ENSO, the cases are almost evenly distributed when one considers the combination of ENSO and PDO. This examination of ENSO and PDO events clearly differs from those conducted by, for example, Hoerling et al. (1997); Gershunov and Barnett (1998a); and DeWeaver and Nigam (2002). However, it does capture features that are important relative to the distribution of the ENSO and PDO events, such as the phase shift in La Niña events mentioned by DeWeaver and Nigam (2002). These authors also pointed out that the method used to calculate the composites does not influence the results of estimating the non-linear response of the ENSO events, being more important the distribution of the ENSO events.

Table 4.1. *Classification of ENSO events during February according to ONI. The PDO information is from http://jisao.washintong.edu/pdo (from Paper I).*

	High PDO	Low PDO
El Niño	1983, 1987, 1988, 1992 1995, 1998, 2003, 2010	1953, 1954, 1958, 1959 1964, 1966, 1969, 1973 1977, 1978
La Niña	1985, 1989, 1996, 1999 2000, 2001, 2006, 2008 2009	1950, 1951, 1955, 1956 1974, 1975, 1976
Neutral	1981, 1982, 1984, 1986 1990, 1991, 1993, 1994 1997, 2002, 2004, 2005 2007	1952, 1957, 1960, 1961 1962, 1963, 1965, 1967 1968, 1970, 1972, 1979 1980

4.2 Detection of the MSD

In Paper II the daily precipitation times series were filtered using a running triangular weight average with a window of 31 days, to avoid or minimise interruptions of the MSD due to weakening of the trades and/or approaching of the ITCZ, as suggested by Ramírez (1983) and Alfaro (2014).

An algorithm to systematically identify the features of the MSD was applied to the filtered daily precipitation time series. This algorithm seeks for the timing of each phase of the MSD (start, minimum, and end), besides the intensity and magnitude of the MSD. This approach provides an annual value for each quantity, which were used as indexes to characterise the MSD. The start of the MSD is considered as the moment when the decrease in precipitation initiates, usually after May-Jun. The end of the MSD is when the precipitation stops increasing, normally taking place around September-October. The minimum occurs in between the start and end of the MSD. The MSD intensity is defined as the minimum rainfall detected during the MSD (or the depth of the valley in Fig. 4.1), meanwhile the magnitude is the total precipitation divided by the total number of days between the start and end of the MSD.

The description of the whole MSD detecting process is explained as follows: first, the algorithm scans for the precipitation minimum in the filtered time series within a reasonable range of days for the existence of the MSD, determined by the climatologies of each station, i.e. typically from 1 June to 30 August. If the precipitation minimum falls outside this period, it is not considered a MSD event. Second, the nearest local maxima to the minimum are sought to determine the start and the end of the MSD. The shortest distance allowed between the local mxima and the minimum is 5 days. Consequently, the shortest MSD would have a duration of 10 days. Moreover, the local maxima have the restriction that the difference of precipitation between them and the minimum should be at least 20% per day. It is worth mentioning, that not

all the years present the two local maxima and the minimum. For the scope of Paper II those years missing any of the MSD phases are removed. The causes for those fails in the detection of the MSD phases are several, however, they can be attributed to anomalous years with a extended dry season at the beginning of the year, combined with an earlier and severe MSD, or anomalous drier condition during the secondary precipitation maximum, years with no occurrence MSD at all, and in most cases due to missing data in the observations. Figure 4.1 shows the schematics of this algorithm.
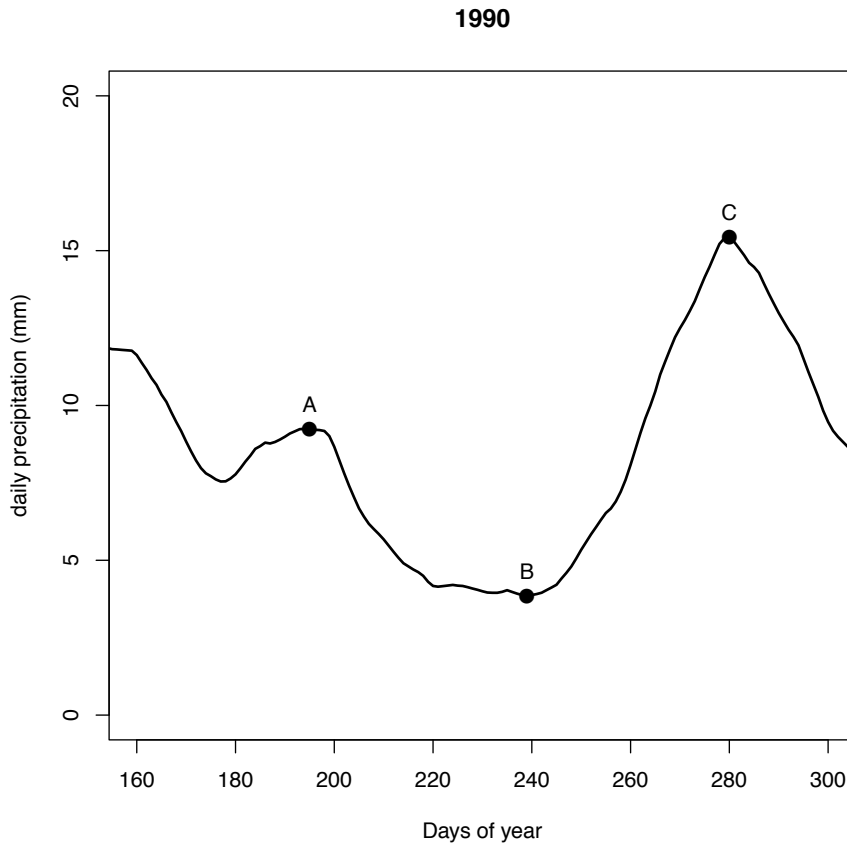
1990

Figure 4.1. Filtered daily time series for the observed precipitation in station La Argentina during 1990. The dots represent the beginning (A), minimum (B) and end (C) of the MSD. In this year the MSD started by day 195 (14 July), reached the minimum at day 239 (27 August) and ended by day 280 (7 Oct). From Paper II.

4.3 Canonical Correlation Analysis

Canonical correlation analysis (CCA, Wilks 2011) is applied to investigate the variability of the MSD. CCA is a statistical technique that searches for pairs of patterns in two multivariate data sets (fields), and constructs sets of transformed data variables by projecting the original data onto those patterns. These new variables maximise the interrelationships between the two fields. The new variables can be used, analogously to the regression coefficient in the multiple regression. The new variables or vector weights are also known as canonical vectors, and their projection with their respective fields as canonical variates. CCA can be useful in different applications, such as: i) to obtain diagnostic aspects of the coupled variability of two fields, in the case when the time series of observations of the two fields are simultaneous, or ii) to perform statistical forecasts, in the case when the time series of observations of one field precede the other (e.g. Alfaro 2007; Maldonado and Alfaro 2011; Fallas-López and Alfaro 2012b; Maldonado et al. 2013).

Therefore in Paper II, CCA is used as a diagnostic tool, however, models for statistical forecasting can be built for future use. Consequently, CCA is employed in order to analyse the relationship between the SSTs monthly anomalies (SSTA, also denoted field X) with each of the indexes (start, minimum, end, intensity and magnitude of MSD) estimated to represent each of the features of the MSD (each index would be the field Y, for the corresponding model), that is, it is sought a statistical relationship between the large and regional scale features of the SSTA and the characteristics of the MSD in each of the stations (local scale).

The above CCA methodology is based on Maldonado et al. (2013) and it is implemented as follows: the fields (SSTA, MSD indexes) are first reduced by means of principal component analysis (PCA) to assure stability in the CCA parameters. A maximum of 17 EOFs and CCA modes in the filtering stage are allowed. This threshold was suggested by Gershunov and Cayan (2003) and Alfaro (2007) to avoid overparameterisation.

The optimal combination of EOFs and CCA modes are calculated by means of the goodness index (R^2, Fig. 5.9) . Notice that any set EOFs will produce unique CCA modes for that especific set, then, once the best combination of EOFs is determined, that set EOF is capturing the maximum variability in each field (X and Y), separately, for each specific CCA model (intensity and magnitude). The maximum possible number of CCA modes, however, is determined first by the minimum number of EOFs between both fields. Then with the goodness index, the maximum number of CCA modes is found for the best fit to avoid any overparameterisation in the model $\hat{Y} = b^T \cdot X$, where the elements of b are the ordinary least-squares regression coefficients computed with CCA, and $\hat{Y}$ is the predicted value of Y.

The R^2 is computed using cross-validation models with 1-month window from 1961-2012 for each station in all the models. This metric also allows

identifying the best month to predict any of the MSD features. It is worth mentioning that at the end the models would not necessarily have 17 EOF and CCA modes. Stations having indexes with more than 30% of missing data (i.e. fails detecting MSD events) are discarded. In total, 21 stations are left for the CCA models. Precipitation data are transformed to a normal distribution using percentiles, to achieve better performance in the EOF. The 21 stations having less than 30% of missing data are filled using the long-term means of each index. Note that filling the data in this step is not the same procedure described previously in Section 3.3.

4.4 Statistical significance

In Paper I, the statistical significance for the composite analysis was tested using bootstrapping estimated in a way similar to that of Gershunov and Barnett (1998a). Using bootstrapping without replacement an artificial time series with normally distributed statistical noise is generated. The anomalies would then be considered significant at the 90% level if the absolute values exceed the 5th or 95th percentiles. A similar relationship between the absolute values of the anomalies was used to estimate the 95% and 99% confidence levels.

5. Results

In the next sections is presented a summary of the results from both paper. In Sections 5.1 and 5.2 describe the interactions between El Niño, PDO, SLP and precipitation found in Paper I, while in Section 5.3 summarises the outcomes from CCA models used in Paper II to study the MSD variability.

5.1 El Niño linearities and non-linearities

The ENSO episode signals in the SLP are shown in Fig. 5.1. During warm episodes (Fig. 5.1(a)), there are significant negative SLPa over the Aleutian Peninsula in Alaska and the east coast of North America (at the 95% and 99% confidence levels, respectively). In contrast, during cold events (Fig. 5.1(b)), almost the opposite pattern is observed, with the SLP being higher than normal in the same regions at the 95% significance level. Hoerling et al. (1997) noted that, during El Niño, the centre of this SLPa pattern extends to the Tropical Northern Hemisphere (TNH) teleconnection, while La Niña extends to the PNA teleconnection pattern. However, La Niña anomalies are shifted south over the Pacific and east over the Atlantic relative to the El Niño signal. Zárate-Hernández (2013) found evidence of a similar configuration of the SLPa associated with the low (high) frequency and penetration of CFs in the Caribbean region.

The linear component of El Niño teleconnections (Fig. 5.1(c)) is dominant over the Aleutian Low and the east coast of the United States. The Gulf of Mexico and the Caribbean region SLPa display linear behaviour, with a higher order of magnitude than the non-linear behaviour for the same reason as explained above. Non-linear anomalies are observed mainly over the Pacific coastal and central United States (Fig. 5.1(d)) and could be associated with the southward shift of the SLPa in the North Pacific during La Niña events. DeWeaver and Nigam (2002) found that the non-linear component of the geopotential field is not negligible over the tropics. Same composites were estimated for a geopotential height of 500 hPa (not shown). Here, El Niño exhibits an asymmetric pattern compared with La Niña pattern. Similar to the low SLPa levels (Fig. 5.1(a)) during El Niño, two significant troughs are located over the Alaskan Peninsula and over the east coast of North America connected by a band of low pressure. A ridge can be observed centred at $60°$ N, $90°$ W. During La Niña over the Alaskan Peninsula and the eastern part of North America, the geopotential height anomalies both have an opposite

sign to El Niño and are relatively lower in intensity. Two ridges separated by a relatively strong trough are centred at 50° N, 120° W. This asymmetry was previously found by DeWeaver and Nigam (2002), who highlighted that the asymmetry observed in these cases could be related to the shift observed in La Niña events in 1976 – 1977, reflecting the inherent variability of ENSO events. The linear component tends to dominate in the mid-latitudes between 30° and 60° N, with relatively important effects in the vicinities of the Caribbean Sea and the Central Pacific. The non-linear component displays more interaction focused in mid-latitudes over the North Pacific to the Alaskan Peninsula, the west coast, and northern North America.

Figure 5.1. February composites of El Niño (a) and La Niña (b) used to estimate the mean SLP anomalies with NCEP-NCAR reanalysis data. The linear component (c) is estimated as the difference between El Niño and La Niña anomalies, whereas the non-linear component (d) is the sum of both. Contour levels are spaced 2 hPa apart. Shaded regions are significant anomalies with confidence levels of 90 – 95% (horizontal lines), 95 – 99% (vertical lines), and >99% (slant lines). From Paper I.

Composites of the horizontal wind anomalies at 925 hPa during warm and cold episodes (Fig. 5.2(a) and (b)) confirm previous results reported by Amador et al. (2003) and Amador (2008). Warm (cold) episodes during boreal winter and lower (higher) than normal SLPa over the east coast of the United States and over the Alaskan Peninsula (described above) are associated with cyclonic (anti-cyclonic) circulation at low levels, resulting in westerly (easterly) wind anomalies and weakening (enhancing) the intensity of the CLLJ. However, the anomalies over the Gulf of Mexico and the Caribbean Sea are mainly dominated by the linear (Fig. 5.2(c)) rather than the non-linear component (Fig. 5.2(d)). This indicates that, at low atmospheric levels, El Niño signal behaves linearly over this region, as do the jet anomalies during ENSO phases.

Precipitation composites exhibit a dominant contrasting pattern during El Niño and La Niña events. Drier conditions are found from the Yucatan Penin-
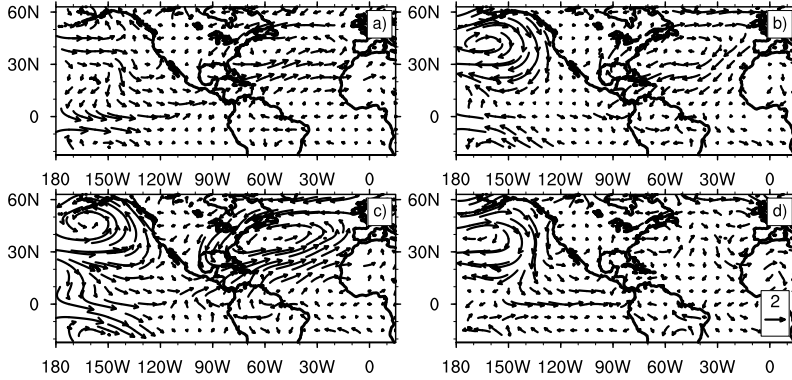
Figure 5.2. February horizontal wind anomalies at 925 hPa for (a) El Niño, (b) La Niña, (c) El Niño - La Niña (linear anomalies), and (d) El Niño + La Niña (non-linear anomalies). The reference vector is in ms^{-1} (Paper I).

sula to northern South America during warm events, while Mexico and Cuba experience wetter conditions (Fig. 5.3(a)). During cold episodes, the inverse pattern of rainfall anomalies is observed, with essentially the same spatial distribution (Fig. 5.3(b)) as during warm events, except for Yucatan Peninsula, Guatemala, Honduras, and El Salvador, where precipitation anomalies are mostly negative in both phases. Durán-Quesada (2012) pointed out that these contrasting precipitation patterns arise due to the relationship between the CLLJ and the ENSO phases. During warm (cold) events, the CLLJ is weakened (enhanced), the moisture transport efficiency is weakened (enhanced), and less (more) humidity is transported to Central America. Non-linear anomalies are observed in the rainfall having the same order of magnitude as does the linear counterpart (Fig. 5.3(d)), however, with no statistical significance. These non-linear anomalies in the rainfall result in wetter conditions over Costa Rica and the west coast of southern Mexico, and drier conditions over the rest of Central America and Mexico. The cause of the non-linear rainfall anomalies is difficult to determine; however, from these results, it cannot be related to the non-linear signal in the horizontal wind over the Caribbean Sea or in the pressure pattern over the Atlantic, as the non-linear signal in those fields is very low relative to the linear counterpart.

Comparing the mean precipitation anomalies with the divergence composites (Fig. 5.4), convergence (divergence) is observed over regions with drier (wetter) conditions during El Niño or La Niña (Fig. 5.4(a) and (b)). The linear component of the divergence dominates over continental Central America (Fig. 5.4(c)). The non-linear component (Fig. 5.4(d)) makes a significant contribution over southern Central America, even though the other fields analysed previously indicated that the non-linear component can be ignored in the tropics. However, the non-linearity of precipitation cannot be linked only to
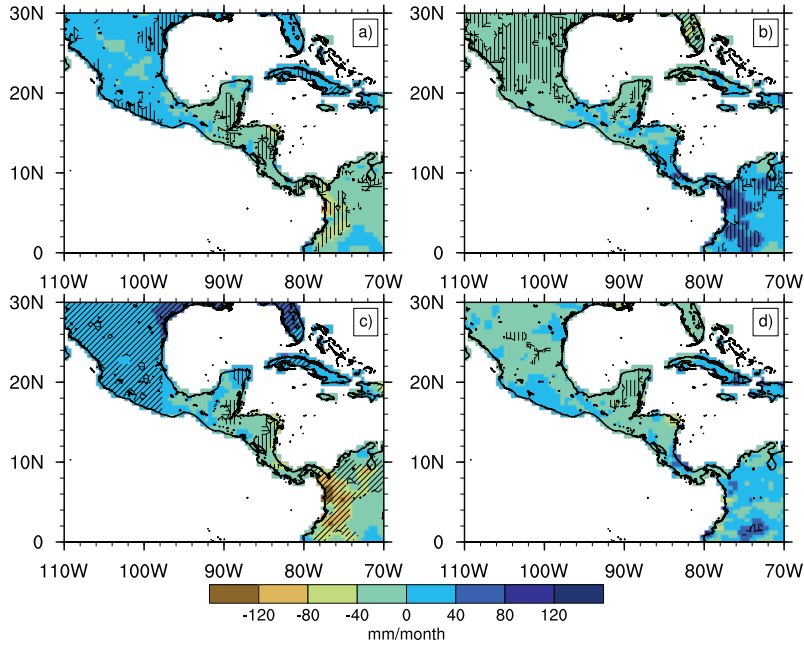
Figure 5.3. February anomalies of total monthly precipitation in millimetres (mm) for (a) El Niño, (b) La Niña, (c) El Niño – La Niña (linear anomalies), and (d) El Niño + La Niña (non-linear anomalies). Shaded regions are significant anomalies with confidence levels of 90 – 95% (horizontal lines), 95 – 99% (vertical lines), and >99% (slant lines). From Paper I.

the divergence. Other regional elements could control the precipitation distribution, such as the interaction of the mean wind with topography or other geographical elements present in the region. DeWeaver and Nigam (2002) pointed out that PDO might be responsible for some observed variability in ENSO events, and in some cases such variability has been taken erroneously as the non-linearity of El Niño episodes.

5.2 Influence of the PDO

Since the PDO is a long-lived phenomenon lasting approximately 30 – 40 years, a 30-year running average (not shown) was applied to the PDO index. This procedure reveals a negative PDO phase dominating from 1950 to 1981 and a positive PDO phase from 1981 to 2010. Table 4.1 lists the classification of El Niño and PDO phases. The anomalies are estimated relative to the climatology of the 61-year period from 1950 to 2010.

Figure 5.5(a) shows the SLPa for the El Niño and positive PDO (PDO+) sub-composite. Note the similarity between the spatial distribution of the
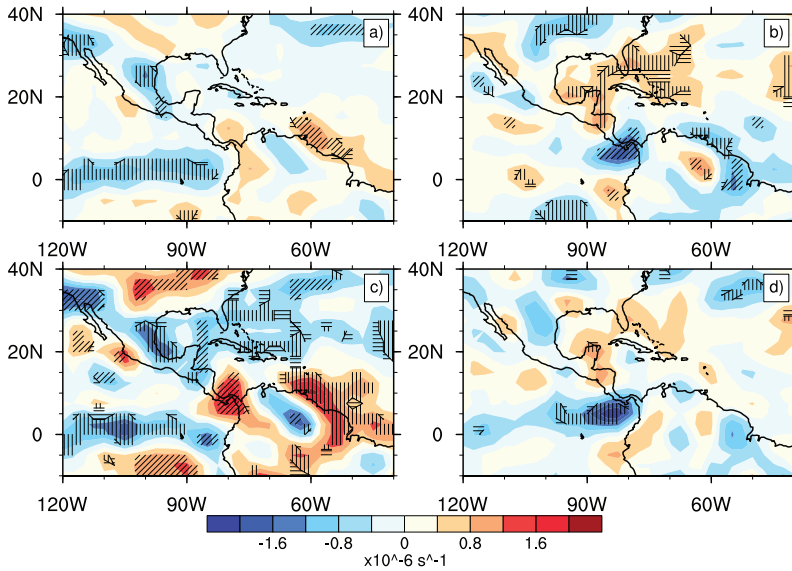
Figure 5.4. As in Fig. 5.2 but showing the wind divergence at 925 hPa. Contour levels are spaced every 0.4×10^{-6} s $^{-1}$ (from Paper I).

SLPa and the SLPa pattern found for the El Niño composites (Fig. 5.1(a)). Nevertheless, the SLPa are intensified and shifted south relative to the El Niño case shown in Fig. 5.1(a), while a lower-than-normal pressure band is located over Central North America, conditions that enhance the Northern Hemisphere storms that reach low latitudes (Gershunov and Barnett, 1998b). This configuration of the SLPa spatial distribution is called a constructive pattern. In addition, significant negative SLPa (at 95 – 99% confidence levels) are located near each coast of North America, along with cyclonic circulation that weakens the trades and the jet over the Caribbean Sea (Fig. 5.6(a)). Rainfall anomalies indicate drier-than-normal conditions over Central America and the Yucatan Peninsula and wetter-than-normal conditions in southern Mexico (Fig. 5.7(a)). Significant anomalies in rainfall are found in south-western Mexico (positive), Nicaragua, and Panama (negative).

The other constructive case is that of La Niña and negative PDO (PDO-) Fig. 5.5(d)). In this case, the spatial distribution of SLPa is similar to the SLPa pattern found in La Niña composites (Fig. 5.1(b)). La Niña signal in the SLPa is modulated by the PDO-, producing more intense and extended SLPa. This condition can also block storms from the north, preventing them from reaching southern latitudes (Gershunov and Barnett, 1998b). Significant SLPa over the eastern North America are accompanied by anticyclonic circulation,
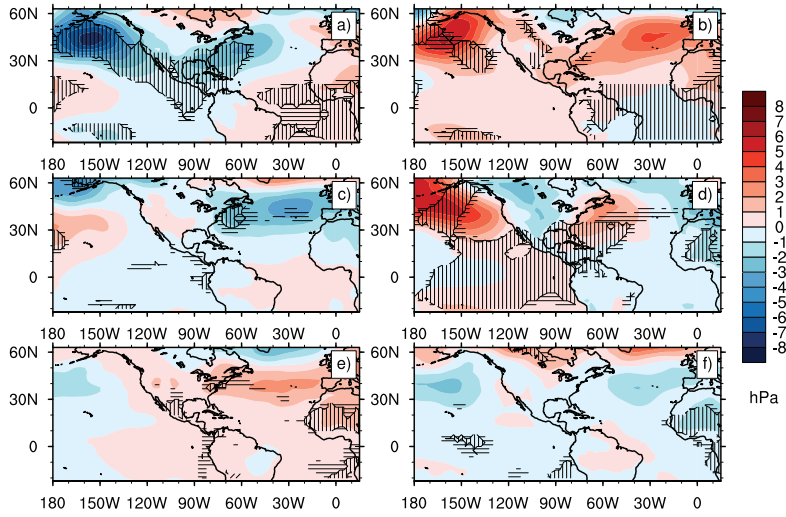
Figure 5.5. February mean SLP anomalies for the El Niño and PDO phase sub-composites: (a) El Niño and PDO+, (b) La Niña and PDO+, (c) El Niño and PDO-, (d) La Niña and PDO-, (e) neutral and PDO+, and (f) neutral and PDO-. Contours are spaced every 1 hPa. Shaded regions are significant anomalies with confidence levels of 90 – 95% (horizontal lines), 95 – 99% (vertical lines), and >99% (slant lines). From Paper I.

enhancing the trades and the CLLJ (Fig. 5.6(d)). Rainfall anomalies present conditions that are drier than normal over Mexico and wetter than normal over Central America and the Yucatan Peninsula (Fig. 5.7(d)).

In the combination of El Niño with PDO-, or of La Niña with PDO+, the ENSO signal is modulated differently in comparison with the constructive cases mentioned above. Therefore, the condition in which ENSO and PDO are out of phase is regarded as a destructive pattern. Note that in Fig. 5.5(b) the spatial distribution of the SLPa is different from that of the constructive case (Fig. 5.5(d)), the high pressure anomaly centres being shifted to $160°$ W (over the north Pacific) and $30°$ W (north Atlantic). In the Atlantic, the trades are enhanced and, in addition, the wind over the Caribbean changes in direction (becoming south-easterly, Fig. 5.6(b)) compared with the constructive case. Precipitation anomalies display similar distributions but with wetter conditions in Central America (Fig. 5.7(b)).

In the El Niño and PDO- case (Fig. 5.5(c)), the SLPa pattern is also distorted. In the Pacific, the SLPa are located farther north and their extent and intensity are decreased. In the Atlantic, the SLPa are located farther east and their intensity is also reduced. The circulation linked to the SLPa in the Atlantic does not greatly modify the trades over the Caribbean (Fig. 5.6(c)).
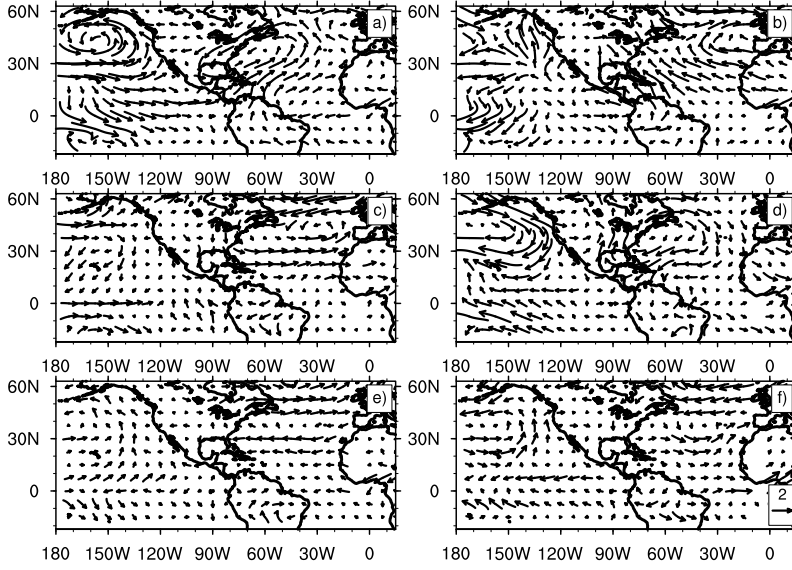
Figure 5.6. February horizontal wind anomalies at 925 hPa for (a) El Niño and PDO+, (b) La Niña and PDO+, (c) El Niño and PDO-, (d) La Niña and PDO-, (e) neutral and PDO+, and (f) neutral and PDO-. The reference vector is in ms $^{-1}$ (from Paper I).

Rainfall anomalies (Fig. 5.7(c)) display a distribution similar to that of their constructive counterparts, though south-western Mexico is drier than normal. Note that the rainfall anomalies are not statistically significant in Mexico or Central America.

The influence of the PDO on the perturbations of the Central American climate is measured during neutral ENSO conditions (Fig. 5.5(e) and (f)). The SLPa spatial distribution in the Atlantic is similar during each phase, but with opposite sign. Consequently, the magnitude of the SLPa is less than when combined with ENSO events. On the other hand, negative SLPa are found over the Pacific during each PDO phase, though negative SLPa are intensified during PDO-. Moreover, in each PDO phase, the observed SLPa do not produce marked changes in the horizontal wind at 925 hPa over the Caribbean (Fig. 5.6), so the association between the PDO and the perturbation in the CLLJ's intensity and direction is negligible or non-existent. Although the rainfall anomalies (Fig. 5.7(e) and (f)) tend to be positive during PDO+ (PDO-) phases in most of the study domain, these results are not statistically significant.

The divergence field is shown in Fig. 5.8. In the constructive cases (Fig. 5.8(a) and (d)), the divergence anomaly pattern represents an intensification of the pattern found during both the El Niño and La Niña phases, besides having the opposite sign in each case. During El Niño (La Niña) positive (negative) anomalies are observed mainly over Costa Rica and Panama, and
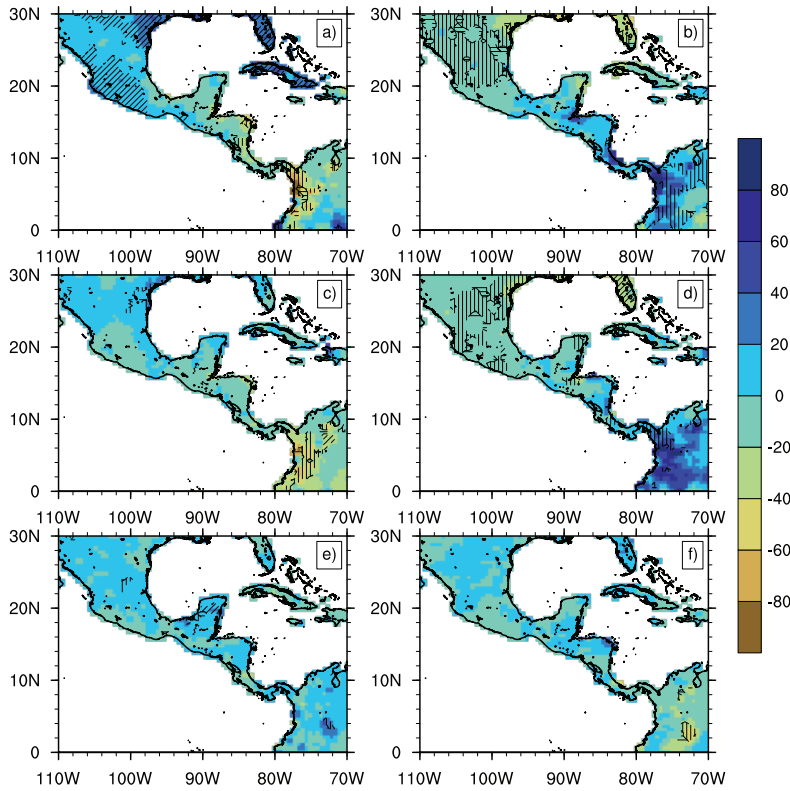
Figure 5.7. February anomalies of total monthly precipitation in millimetres (mm) for (a) El Niño and PDO+, (b) La Niña and PDO-, (c) El Niño and PDO-, (d) La Niña and PDO-, (e) neutral and PDO+, and (f) neutral and PDO-. Shaded regions are significant anomalies with confidence levels of 90 – 95% (horizontal lines), 95 – 99% (vertical lines), and >99% (slant lines). From Paper I.

over the north-eastern coast of South America, separated by negative (positive) anomalies over Colombia and Venezuela. In the destructive cases, however, each combination behaves differently. During the El Niño and PDO- case (Fig. 5.8(c)), larger changes are observed from $15°$ N towards the North Pole, over continental North America, and in the equatorial eastern Pacific. Note that the same region displays similar behaviour in the changes in distribution of the precipitation anomalies (Fig. 5.7(a) and (c)). The other destructive case, i.e. La Niña and PDO+ (Figure 5.8(b)), occurs in a different manner: negative anomalies are intensified over Costa Rica, Panama, and South America, but significant positive anomalies are centred on $40°$ N and $90°$ W where reduced precipitation is observed. In the neutral cases, nevertheless, relevant changes happen only near the equator over continental South America. Regarding the influence of the PDO on rainfall, it is worth mentioning that the modulated
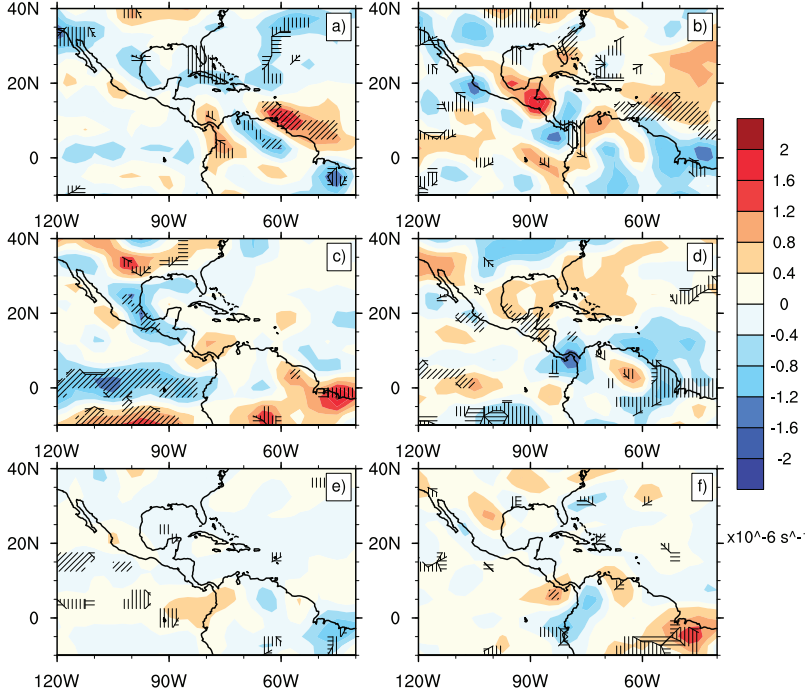
Figure 5.8. February divergence anomalies at 925 hPa for (a) El Niño and PDO+, (b) La Niña and PDO+, (c) El Niño and PDO-, (d) La Niña and PDO-, (e) neutral and PDO+, and (f) neutral and PDO-. Contours levels are spaced every 0.4×10^{-6} s^{-1} (from Paper I).

divergence helps to explain some observed changes in the spatial distribution of precipitation, though there are other mechanisms related to combinations of the PDO with PNA and/or El Niño. These mechanisms are associated with changes in the distribution of the latent and sensible heat flux anomalies, modulating mainly the SST anomalies in the Gulf of Mexico (Muñoz et al., 2010) that could also be associated with changed precipitation distribution in the mid latitudes or with the changed storm tracks observed in the Northern Hemisphere by Gershunov and Barnett (1998a) and Zárate-Hernández (2013).

5.3 Influence of the SST during summer

Correlations of the MSD features with El Niño 3.4 and the CLLJ indexes (Paper II) show that the MSD intensity and magnitude have a negative relationship

with El Niño 3.4 and a positive relationship with the Caribbean low-level jet (CLLJ) index, however, for the Caribbean stations the results were not statistically significant, which is indicating that other processes might be modulating the precipitation during the MSD over the Caribbean coast. On the other hand, the temporal variables (start, minimum and end) show low and no significant correlations with the same indexes.

Such results are also observed in models based on CCA. Using the SST anomalies as predictor (X field), CCA identifies SST patterns that are related to the perturbations of the MSD features (Y field, predictant). The goodness index (R^2) is shown in Fig. 5.9. The intensity and magnitude show the best skill score compared to the other indexes. These results show that the models to study the timing of the MSD phases have a poor performance using the CCA technique. Consequently, those models are not considered in the further analysis. Both CCA models for MSD intensity and magnitude show one of the highest values of R^2 in April, which means in operational terms, information concerning the MSD intensity and magnitude can be retrieve up to 3 months in advance of an event. This would be valuable for preparation and planning of the societal, economical and agricultural activities during the MSD period. Notice that both models also shown the highest results in July, concurrently with the existence of the MSD, and the CLLJ.
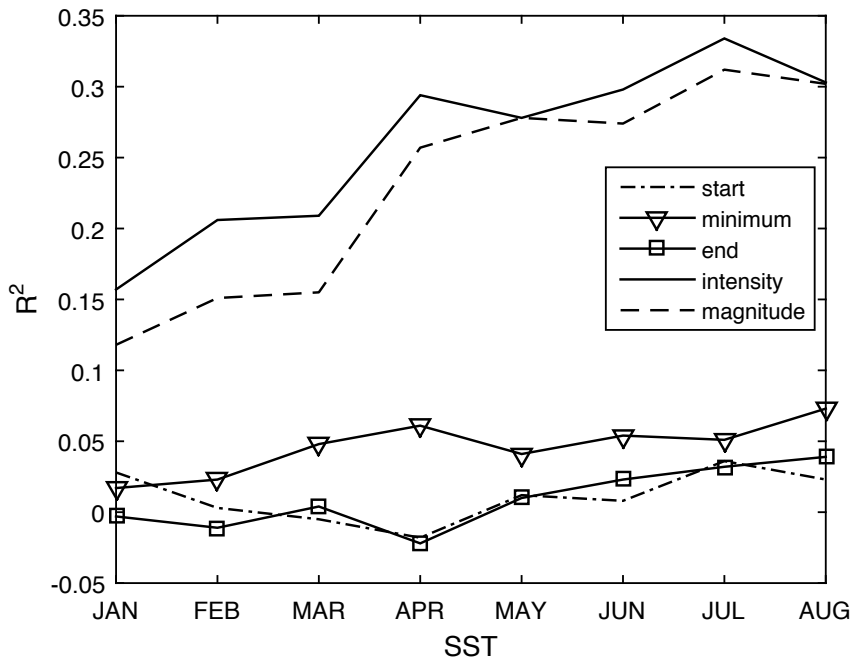

Figure 5.9. Goodness index (R^2) estimated as the average of the Pearson correlation between synthetic time series generated by cross-validation models and the observed MSD features per station (Paper II).

In Paper II, however, the SSTA patterns identified by the model in June is analysed, since for that month, CCA models show a relative high R^2, and there is also 1-month leading time for forecasting the MSD. Besides, the SST does not change significantly from June to July, when the CCA models have the best performance, thus, the SST in July is expected to be close to the SST in June. The best combination of EOF and CCA modes for the MSD intensity are $X = 14$, $Y = 4$ EOFs and 2 CCA modes, and for the MSD magnitude $X = 11$, $Y = 6$ EOFs and 3 CCA modes, meaning that for each model (for intensity and magnitude respectively) the best fit is achieved when using 2 and 3 modes (canonical variates) respectively, capturing the maximum influence of the SST on the precipitation field, and specifically in the modulation of the MSD. Figure 5.10 shows the Pearson correlation between the predicted time series generated using cross-validation models and the observations of both intensity and magnitude in each station. In each case, the station exhibits relatively high significant correlation, about 0.35 in average.

The X loadings (correlation between the canonical vectors of the SST and the SSTA) of the first mode controlling the MSD intensity shows a dipolar pattern in the correlation with the SSTAs surrounding Central America (Fig. 5.11a,b). The highest positive correlations are found over the Pacific in the El Niño region, whereas the highest negative correlation are found over the Tropical North Atlantic and near to the Brasil coast. The influence of this variability mode on the precipitation in Central America has been previously studied by Enfield and Alfaro (1999); Maldonado and Alfaro (2011) and Maldonado et al. (2013), but for the secondary peak of precipitation during August-October (ASO), thus, this results shows that the rainfall during the MSD is governed by the same variability mode present during the highest precipitation season in Central America. On the other hand, for the MSD magnitude, the first mode exerts more influence of the SSTA over the El Niño region, and the regional waters close the west Mexican coast. Notice that in both cases also high positive correlations are found near the western coast of Mexico revealing that both models are affected by the influence of regional waters, varying with the same phase that the superficial temperatures in the El Niño region. The Y loadings in both models are negatively correlated with most of the stations (Fig. 5.11c,d). That means for a state in which the water over the Pacific is warmer (colder) than normal, plus the SST over the Atlantic colder (warmer) than normal, the intensity and magnitude of the MSD drier (wetter). This results also connects the MSD period with the second rainfall peak, that is, SSTs conditions for drier MSDs, would persist leading to less rainfall during the second peak, following the results in Maldonado et al. (2013). The temporal scores (canonical variates) of this mode in both models show that this mode has mainly inter-annual variations (Fig. 5.11e,f).

The X loadings of the second mode are shown in Fig. 5.12a,b. The MSD intensity is dominated by negative correlations with SST anomalies in the Tropical North Atlantic, the Caribbean and Gulf of Mexico and the eastern Pacific,
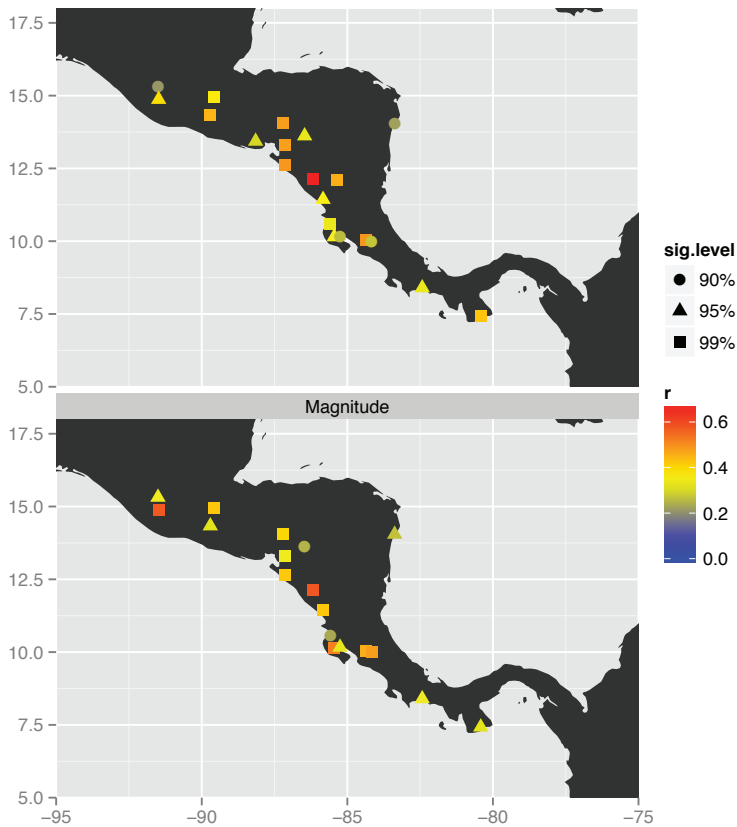
Figure 5.10. Pearson correlation of the CCA models with the time series of intensity (top) and magnitude (bottom) of MSD. Only significant correlations are plotted (Paper II).

being more important than the first region. The *X* loadings for the MSD magnitude on the other hand, reveal a tripolar configuration in the North Pacific. This tripolar setting is located in the region where the PDO develops. The PDO has shown more influence in the southern USA and northern Mexico than in Central America (Muñoz et al. 2010, Paper I), and that could be the reason that its influence is observed in the second mode. The *Y* loadings in both cases (Fig. 5.12c,d) show a non-uniform distribution of the correlation. For the MSD intensity (Fig. 5.12c), the stations are positively correlated with this mode, meanwhile, the MSD magnitude (Fig. 5.12d) shows a clear division between northern and southern Central America, being the former region (Guatemala, El Salvador, Honduras and west Nicaragua) negatively correlated and the latter region (Costa Rica, Panama and east Nicaragua) positively correlated. The temporal scores for the intensity model exhibit mainly inter-annual variability with a negative trend after 1990 (Fig. 5.12e), while the temporal
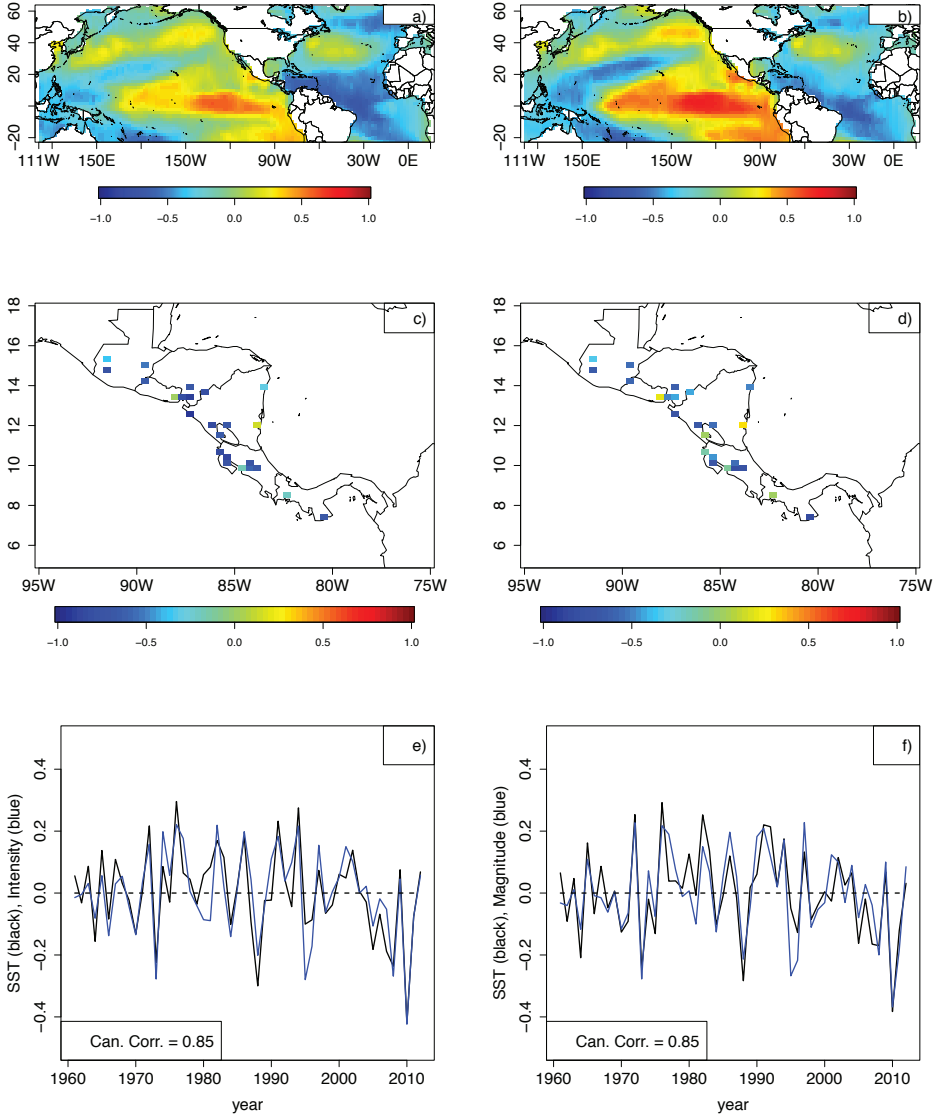
Figure 5.11. CCA mode 1 for both MSD intensity and magnitude. In the left column are the X (upper) and Y(middle) loadings, and the time scores (bottom) for the intensity. In the right column the same but for the magnitude (Paper II).

scores of the magnitude (Fig. 5.12f) present a decadal variation, that again possibly relates to the influence of the PDO.
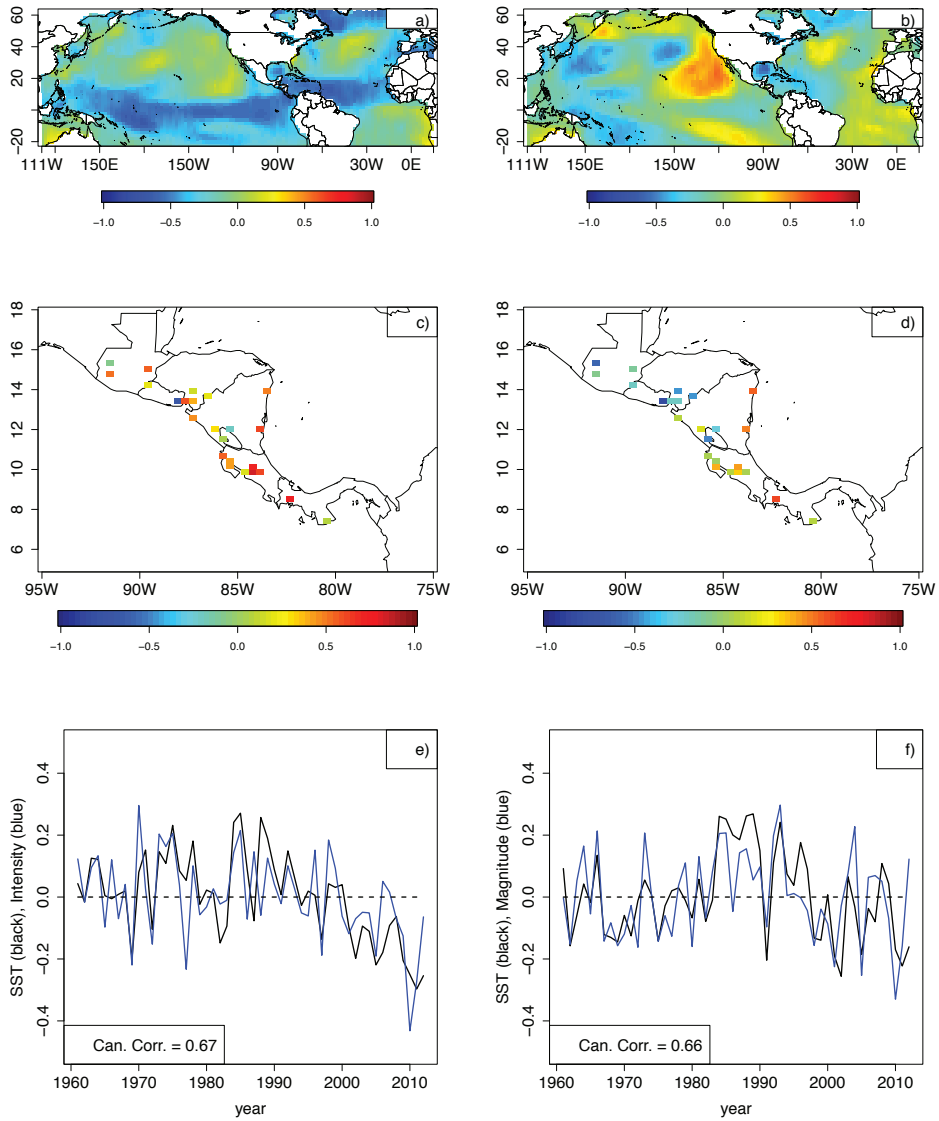
Figure 5.12. Same as Fig. 5.11 but for Mode 2 (Paper II).

The MSD magnitude is the only feature with a third mode, the *X* loadings (Fig. 5.13a) reveal that this mode is dominated by regional SSTs in the Pacific and Tropical North Atlantic. The north and south Pacific show a dipole being positive and negative correlations respectively. The *Y* loadings (Fig. 5.13b)

show a north/south division being positively correlated to the north and nega-
tively to the south, while the temporal scores (Fig. 5.13c) reveal an interannual
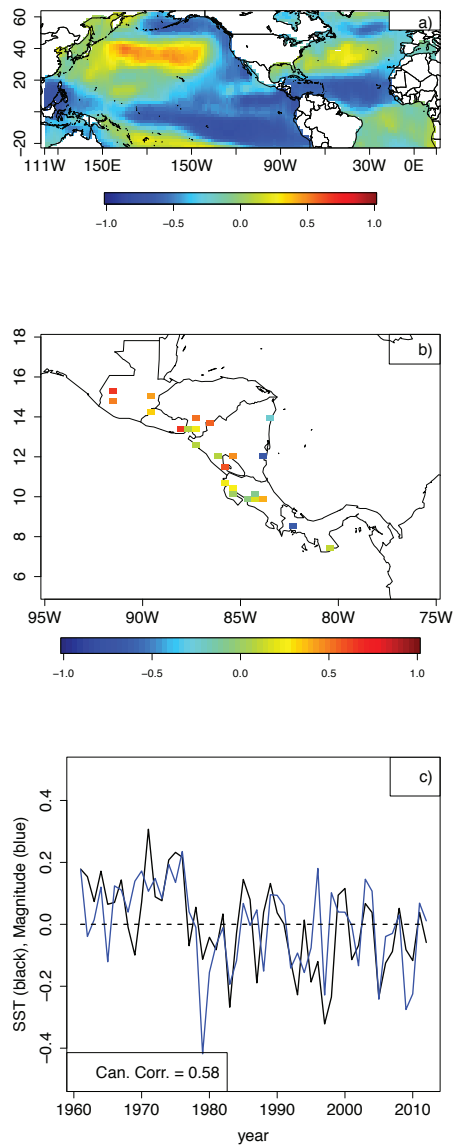variation of this mode.

Figure 5.13. CCA mode 3 for MSD magnitude. *X* (a) and *Y* (b) loadings, and (c) the
time scores (Paper II).

6. Concluding remarks

The interaction between El Niño and the PDO was studied in Paper I using composite analysis. The interaction between these two variability modes during boreal winter is summed up as follows:

- During warm (cold) events, the SLPa align with the PNA teleconnection pattern, and cyclonic (anticyclonic) circulation is observed, resulting in westerly (easterly) wind anomalies over the Caribbean Sea, weakening (enhancing) the jet intensity. The PDO enhances or attenuates the ENSO signal in the SLPa (i.e. during El Niño events concomitant with a positive PDO, the PNA teleconnection pattern is enhanced), whereas during El Niño in combination with negative PDO, the PNA pattern is not observed, resulting in no significant modification of the circulation over the Caribbean Sea.

- Changes in the circulation due to the PDO phases during La Niña episodes are observed in the direction change of the meridional wind anomalies in the Caribbean Basin. Cold events plus positive (negative) PDO result in an anomalous northward (southward) wind component. Due to the Rossby problem adjustment, the relationship between the SLPa and the CLLJ anomalies needs further study.

- Despite large changes in the circulation pattern found due to the influence of the PDO, changes in the monthly cumulative precipitation anomaly were minimal over the Central American Isthmus. The small perturbations in rainfall were related to small fluctuations in the divergence in the tropical regions of the American continent.

The outputs of CCA models tailored in Paper II show:

- that the MSD intensity is mainly modulated by a dipolar configuration in the SST anomalies formed between the Pacific and the Tropical North Atlantic and Caribbean sea, meanwhile, the first mode controlling the MSD magnitude shows more influence from El Niño and the regional waters close to the western coast of Mexico and Central America. This variability mode in both models has an inter-annual scale, with negative effects in precipitation, i.e. when this mode is positive for both intensity and magnitude, a reduction in rainfall is observed in almost all the stations. Similar SST dipole has been reported to influence the anomalies

in rainfall during the months of the highest precipitation events (August-November), and it has been associated with intensification/reduction of the trades, leading to a decrease/increase of precipitation in Central America during the second rainfall period, however, these results show this mode is present prior to the quarter ASO and is also modulating the precipitation during boreal summer.

- The second mode in both models presents more complex structures, and it is difficult to distinguish a general pattern affecting the intensity as well as magnitude of the MSD. For the intensity model, the SST shows a negative correlation pattern over the equatorial Pacific and North Atlantic waters, nevertheless, the latter region dominates; the time series for this mode show a negative trend after 1990. Meanwhile, for the magnitude, a tripolar configuration over the vicinity of the PDO development region is found. Also negative correlations are found over the Gulf of Mexico. The influence of the PDO should be taken with caution and needs more analysis since the PDO has shown more influence in the southern USA and northern Mexico than in Central America. The time series exhibited inter-decadal variability. As previously mentioned, the correlations between both variables (intensity and magnitude) and this mode, however, do not depict a clear pattern in the stations; for the MSD intensity the correlations reveal a positive association with the SSTA, meanwhile, for the MSD magnitude shows a division between the north and south Central America, being the north (Guatemala, Honduras, El Salvador and west Nicaragua) affected negatively and the south and Caribbean (Costa Rica, Panama and east Nicaragua) positively. It is clear that the second mode is not controlling the precipitation in both models in the same way . The North Atlantic waters become more important for the MSD intensity, hence, could be associated with the same controlling mechanism present during the first precipitation maximum (Alfaro, 2007; Fallas-López and Alfaro, 2012b). While for the MSD magnitude the tripolar configuration might suggest the influence of the PDO, also noted in the contrasting effects of this mode between north and south Central America.

- The MSD magnitude is the only variable with higher CCA modes. The third mode reveals the influence of regional waters close to the Central America Pacific and a dipole formed between the north (positive) and south (negative) Pacific, affecting with opposite sign the eastern (negative) and western (positive) part of Central America. This mode presents an inter-annual variability scale.

- The CCA allows identifying patterns of the SST affecting variables describing the MSD such as the intensity and magnitude, however, it shows

a poor performance related to the temporal variables. Another benefit achieved using CCA was the identification of particular months suitable for prediction of the intensity and magnitude of the MSD, being capable of forecasting up to 3 months in advance, which is a reasonable time in terms of practical matters related to prevention and planing for the season. Finally, it is worth pointing out that this analysis also provides a systematic method to study the MSD features, that can be used for statistical forecasts of such a phenomenon.

7. Future work

The project contemplates the elaboration of at least two papers more. The objectives of those studies are summarised next.

- A further study of MSD extreme events using CCA analysis. This technique has shown good performance to capture the main variability processes affecting the precipitation distribution mainly during the second half of the year. Moreover, improving the understanding about the MSD extreme events contributes to the scientific knowledge about the climate in the region, also provides a systematic method to analyse and predict the rainfall during the boreal summer. Besides, it is planed to match the reports from affected sectors such as agricultural, and hydro-electrical power production with the MSD forecast produced using CCA to evaluate the information obtained with this approach in terms of natural disasters.

- It is planed to study the CLLJ momentum sources through an integrated model such as an Earth System Model, allowing to integrate all the climate elements at global and regional scales, since the interaction of the CLLJ is known to encompass all these scales. Understanding the mechanisms involved in the formation, maintenance and dissipation of the CLLJ will also provide better knowledge of its interactions with other meteorological processes such as the MSD or the hurricanes occurring frequently during the second half of the year.

8. Acknowledgements

I would like to thank my supervisor team Anna Rutgersson, Bjön Claremar, Eric Alfaro and Jorge Amador for their full support. Without their guidance, collaboration and effort this licentiate would never happen. Big thanks to all PhD students in the meteorology group, present and former for sharing laughs and burdens.

References

Alfaro, E., 2000: Eventos cálidos y fríos en el Atlántico tropical norte. *Atmosfera*, **13 (2)**, 109–119.

Alfaro, E., 2007: Uso del análisis de correlación canónica para la predicción de la precipitación pluvial en Centroamérica. *Ingeniería y Competitividad*, **9 (2)**, 33–48, URL `http: //bibliotecadigital.univalle.edu.co/xmlui/handle/10893/1622`.

Alfaro, E., 2014: Caracterización del "veranillo" en dos cuencas de la vertiente del Pacífico de Costa Rica, América Central (Characterization of the Mid Summer Drought in two Pacific slope river basins of Costa Rica, Central America). Spanish. *International Journal of Tropical Biology*, **62 (4)**, 1–15, URL `https://www.academia.edu/9493294/Caracterizaci%C3%B3n_del_ veranillo_en_dos_cuencas_de_la_vertiente_del_Pac%C3%ADfico_de_ Costa_Rica_Am%C3%A9rica_Central_Characterization_of_the_Mid_ Summer_Drought_in_two_Pacific_slope_river_basins_of_Costa_Rica_ Central_America_._Spanish`.

Alfaro, E. ., L. Cid, and D. Enfield, 1998: Relaciones entre la precipitación en Centroamérica y los Océanos Pacífico y Atlántico Tropical. *Investigaciones Marinas*, **26**, 59–69.

Alfaro, E. and L. Cid, 1999a: Ajuste de un modelo VARMA para los campos de anomalías de precipitación en Centroamérica y los índices de los océanos Pacífico y Atlántico Tropical. *Atmosfera*, **12**, 205–222.

Alfaro, E. and L. Cid, 1999b: Análisis de las anomalías en el inicio y el término de la estación lluviosa en Centroamérica y su relación con los océanos Pacífico y Atlántico Tropical. *Tópicos Meteorológicos Oceanográficos*, **6**, 1–13.

Alfaro, E. and J. Soley, 2009: Descripción de dos métodos de rellenado de datos ausentes en series de tiempo meteorológicas. *Revista de Matemáticas: Teoría y Aplicaciones.*, **16 (1)**, 59–74, URL `http: //revistas.ucr.ac.cr/index.php/matematica/article/view/1419`.

Alfaro, E. J., A. Quesada, and F. Solano, 2010: Análisis del impacto en Costa Rica de los ciclones tropicales ocurridos en el mar Caribe desde 1968 al 2007. *Diálogos Revista Electrónica de Historia*, **11 (2)**, 22–38, URL `http://www.scielo.sa.cr/scielo.php?script=sci_abstract&pid= S1409-469X2010000200002&lng=en&nrm=iso&tlng=pt`.

Amador, J. A., 1998: A Climatic Feature of the Tropical Americas: The Trade Wind Easterly Jet. *Top. Meteor. Oceanogr.*, **5 (2)**, 91–102, URL `http://imn.ac.cr/publicaciones/revista/1998/diciembre/ 1-Amador,Jorge-dic98.pdf.pdf`.

Amador, J. A., 2008: The Intra-Americas Sea Low-level Jet Overview and Future Research. *Annals of the New York Academy of Sciences*, **1146 (1)**, 153–188, doi:10.1196/annals.1446.012, URL `http: //onlinelibrary.wiley.com/doi/10.1196/annals.1446.012/abstract`.

Amador, J. A., E. J. Alfaro, O. G. Lizano, and V. O. Magaña, 2006: Atmospheric forcing of the eastern tropical Pacific: A review. *Progress In Oceanography*, **69 (2–4)**, 101–142, doi:10.1016/j.pocean.2006.03.007, URL `http://www.sciencedirect.com/science/article/pii/S0079661106000292`.

Amador, J. A., E. J. Alfaro, E. R. Rivera, and B. Calderón, 2010: Climatic Features and Their Relationship with Tropical Cyclones Over the Intra-Americas Seas. *Hurricanes and Climate Change*, Springer Netherlands, Netherlands, Vol. 2, 149–173.

Amador, J. A., J. R. Chacón, and S. Laporte, 2003: Climate and climate variability in the Arenal Basin of Costa Rica. *Climate, Water and Trans-boundary Challenges in the Americas*, H. Díaz and B. Morehouse, Eds., Academic Publishers, Kluwer, 317–349.

Barlow, M. and D. Salstein, 2006: Summertime influence of the Madden-Julian Oscillation on daily rainfall over Mexico and Central America. *Geophysical Research Letters*, **33 (21)**, n/a–n/a, doi:10.1029/2006GL027738, URL `http://onlinelibrary.wiley.com/doi/10.1029/2006GL027738/abstract`.

Bell, G. D. and M. Chelliah, 2006: Leading Tropical Modes Associated with Interannual and Multidecadal Fluctuations in North Atlantic Hurricane Activity. *Journal of Climate*, **19 (4)**, 590–612, doi:10.1175/JCLI3659.1, URL `http://journals.ametsoc.org/doi/abs/10.1175/JCLI3659.1`.

Chen, A. A. and M. A. Taylor, 2002: Investigating the link between early season Caribbean rainfall and the El Niño+ 1 year. *Int. J. Climatol.*, **22 (1)**, 87–106, doi:10.1002/joc.711.

Chinchilla-Ramírez, G., 2014: Resumen Meteorológico Julio 2014. Boletín Meteorológico Mensual. Instituto Meteorológico Nacional, San José, Costa Rica, URL `http://www.imn.ac.cr/boletin_meteo/historial/2014/BMET072014.pdf`, 1–42 pp.

Cook, K. H. and E. K. Vizy, 2010: Hydrodynamics of the Caribbean Low-Level Jet and Its Relationship to Precipitation. *Journal of Climate*, **23 (6)**, 1477–1494, doi:10.1175/2009JCLI3210.1, URL `http://journals.ametsoc.org/doi/abs/10.1175/2009JCLI3210.1`.

Dai, A. and T. M. L. Wigley, 2000: Global patterns of ENSO-induced precipitation. *Geophysical Research Letters*, **27 (9)**, 1283–1286, doi:10.1029/1999GL011140, URL `http://onlinelibrary.wiley.com/doi/10.1029/1999GL011140/abstract`.

Delworth, T., S. Manabe, and R. J. Stouffer, 1993: Interdecadal Variations of the Thermohaline Circulation in a Coupled Ocean-Atmosphere Model. *Journal of Climate*, **6 (11)**, 1993–2011, doi:10.1175/1520-0442(1993)006<1993:IVOTTC>2.0.CO;2, URL `http://journals.ametsoc.org/doi/abs/10.1175/1520-0442(1993)006%3C1993%3AIVOTTC%3E2.0.CO%3B2`.

Delworth, T. L. and R. J. Greatbatch, 2000: Multidecadal Thermohaline Circulation Variability Driven by Atmospheric Surface Flux Forcing. *Journal of Climate*, **13 (9)**, 1481–1495, doi:10.1175/1520-0442(2000)013<1481:MTCVDB>2.0.CO;2, URL `http://journals.ametsoc.org/doi/abs/10.1175/1520-0442(2000)013%`

3C1481%3AMTCVDB%3E2.0.CO%3B2.

Delworth, T. L. and M. E. Mann, 2000: Observed and simulated multidecadal variability in the Northern Hemisphere. *Climate Dynamics*, **16 (9)**, 661–676, doi:10.1007/s003820000075, URL `http://link.springer.com/article/10.1007/s003820000075`.

DeWeaver, E. and S. Nigam, 2002: Linearity in ENSO's Atmospheric Response. *J. Climate*, **15**, 2446 – 2461.

Douglas, M. W., 1995: The Summertime Low-Level Jet over the Gulf of California. *Monthly Weather Review*, **123 (8)**, 2334–2347, doi:10.1175/1520-0493(1995)123<2334:TSLLJO>2.0.CO;2, URL `http://journals.ametsoc.org/doi/abs/10.1175/1520-0493(1995)123%3C2334%3ATSLLJO%3E2.0.CO%3B2`.

Douglas, M. W. and J. C. Leal, 2003: Summertime Surges over the Gulf of California: Aspects of Their Climatology, Mean Structure, and Evolution from Radiosonde, NCEP Reanalysis, and Rainfall Data. *Weather and Forecasting*, **18 (1)**, 55–74, doi:10.1175/1520-0434(2003)018<0055:SSOTGO>2.0.CO;2, URL `http://journals.ametsoc.org/doi/abs/10.1175/1520-0434(2003)018%3C0055:SSOTGO%3E2.0.CO%3B2`.

Douglas, M. W., A. Valdez-Manzanilla, and R. Garcia Cueto, 1998: Diurnal Variation and Horizontal Extent of the Low-Level Jet over the Northern Gulf of California. *Monthly Weather Review*, **126 (7)**, 2017–2025, doi:10.1175/1520-0493(1998)126<2017:DVAHEO>2.0.CO;2, URL `http://journals.ametsoc.org/doi/abs/10.1175/1520-0493(1998)126%3C2017%3ADVAHEO%3E2.0.CO%3B2`.

Durán-Quesada, A. M., 2012: Sources of moisture for Central America and transport based on a Lagrangian approach: variability, contributions to precipitation and transport mechanisms. Ph.D. thesis, Universidade de Vigo.

Durán-Quesada, A. M., L. Gimeno, J. A. Amador, and R. Nieto, 2010: Moisture sources for Central America: Identification of moisture sources using a Lagrangian analysis technique. *Journal of Geophysical Research: Atmospheres*, **115 (D5)**, n/a–n/a, doi:10.1029/2009JD012455, URL `http://onlinelibrary.wiley.com/doi/10.1029/2009JD012455/abstract`.

Enfield, D. B. and E. J. Alfaro, 1999: The Dependence of Caribbean Rainfall on the Interaction of the Tropical Atlantic and Pacific Oceans. *Journal of Climate*, **12 (7)**, 2093–2103, doi:10.1175/1520-0442(1999)012<2093:TDOCRO>2.0.CO;2, URL `http://journals.ametsoc.org/doi/abs/10.1175/1520-0442(1999)012%3C2093%3ATDOCRO%3E2.0.CO%3B2`.

Evans, M. N., M. A. Cane, D. P. Schrag, A. Kaplan, B. K. Linsley, R. Villalba, and G. M. Wellington, 2001: Support for tropically-driven Pacific decadal variability based on paleoproxy evidence. *Geophys. Res. Lett*, **28 (19)**, 3689–3692, URL `http://ic.ltrr.arizona.edu/pp/pdv.pdf`.

Fallas-López, B. and E. J. Alfaro, 2012a: Uso de herramientas estadísticas para la predicción estacional del campo de precipitación en América Central como apoyo a los Foros Climáticos Regionales. 1: Análisis de tablas de contingencia. *Revista de Climatología, 2012, 12: 61-79*, URL `http://webs.ono.com/reclim7/reclim12e.pdf`.

Fallas-López, B. and E. J. Alfaro, 2012b: Uso de herramientas estadísticas para la predicción estacional del campo de precipitación en América Central como apoyo a los Foros Climáticos Regionales. 2: Análisis de Correlación Canónica. *Revista de Climatología*, **12**, URL `http://webs.ono.com/reclim8/reclim12g.pdf`.

Feng, L., D. Wu, X. Lin, and X. Meng, 2010: The effect of regional ocean-atmosphere coupling on the long-term variability in the Pacific Ocean. *Advances in Atmospheric Sciences*, **27 (2)**, 393–402, doi:10.1007/s00376-009-8195-3, URL `http://www.springerlink.com/index/10.1007/s00376-009-8195-3`.

Fernández, W., R. Chacón, and Melgarejo, 1996: On the rainfall distribution with altitude over Costa Rica. *Revista Geofísica*, **44**, 57–72.

Fiedler, P. C. and M. F. Lavín, 2006: Introduction: A review of eastern tropical Pacific oceanography. *Progress in Oceanography*, **69 (2-4)**, 94–100, doi:10.1016/j.pocean.2006.03.006, URL `http://linkinghub.elsevier.com/retrieve/pii/S0079661106000280`.

Gershunov, A. and T. Barnett, 1998a: ENSO influence on intraseasonal extreme rainfall and temperature frequencies in the contiguous United States: Observations and model results. *J. Climate*, **11 (7)**, 1575–1586, doi:10.1175/1520-0442(1998)011<1575:EIOIER>2.0.CO;2.

Gershunov, A. and T. Barnett, 1998b: Interdecadal modulation of ENSO teleconnections. *Bull. Am. Meteor. Soc.*, **79 (12)**, 2715–2725, doi:10.1175/1520-0477(1998)079<2715:IMOET>2.0.CO;2.

Gershunov, A. and D. R. Cayan, 2003: Heavy Daily Precipitation Frequency over the Contiguous United States: Sources of Climatic Variability and Seasonal Predictability. *Journal of Climate*, **16 (16)**, 2752–2765, doi:10.1175/1520-0442(2003)016<2752:HDPFOT>2.0.CO;2, URL `http://journals.ametsoc.org/doi/abs/10.1175/1520-0442%282003%29016%3C2752%3AHDPFOT%3E2.0.CO%3B2`.

Giannini, A., Y. Kushnir, and M. A. Cane, 2000: Interannual Variability of Caribbean Rainfall, ENSO, and the Atlantic Ocean*. *Journal of Climate*, **13 (2)**, 297–311, doi:10.1175/1520-0442(2000)013<0297:IVOCRE>2.0.CO;2, URL `http://journals.ametsoc.org/doi/abs/10.1175/1520-0442(2000)013%3C0297%3AIVOCRE%3E2.0.CO%3B2`.

Gimeno, L., et al., 2012: Oceanic and terrestrial sources of continental precipitation. *Reviews of Geophysics*, **50 (4)**, n/a–n/a, doi:10.1029/2012RG000389, URL `http://onlinelibrary.wiley.com/doi/10.1029/2012RG000389/abstract`.

Goldenberg, S. B., C. W. Landsea, A. M. Mestas-Nuñez, and W. M. Gray, 2001: The Recent Increase in Atlantic Hurricane Activity: Causes and Implications. *Science*, **293 (5529)**, 474–479, doi:10.1126/science.1060040, URL `http://www.sciencemag.org/content/293/5529/474`.

Greatbatch, R. J., 2000: The North Atlantic Oscillation. *Stochastic Environmental Research and Risk Assessment*, **14 (4-5)**, 213–242, doi:10.1007/s004770000047, URL `http://link.springer.com/article/10.1007/s004770000047`.

Hanstenrath, S., 1991: *Climate Dynamics of the Tropics*. Kluwer Academic Publishers.

Herrera, E., V. Magaña, and E. Caetano, 2015: Air–sea interactions and dynamical processes associated with the midsummer drought. *Int. J. Climatol.*, **35**,

1569–1578, doi:10.1002/joc.4077, URL
`http://onlinelibrary.wiley.com/doi/10.1002/joc.4077/abstract`.

Hidalgo, H. G., A. M. Durán-Quesada, J. A. Amador, and E. J. Alfaro, 2015: The Caribbean Low-Level Jet, the Inter-Tropical Convergence Zone and Precipitation Patterns in the Intra-Americas Sea: A Proposed Dynamical Mechanism. *Geografiska Annaler: Series A, Physical Geography*, **97 (1)**, 41–59, doi:10.1111/geoa.12085, URL
`http://onlinelibrary.wiley.com/doi/10.1111/geoa.12085/abstract`.

Higgins, R. W., Y. Yao, and X. L. Wang, 1997: Influence of the North American Monsoon System on the U.S. Summer Precipitation Regime. *Journal of Climate*, **10 (10)**, 2600–2622,
doi:10.1175/1520-0442(1997)010<2600:IOTNAM>2.0.CO;2, URL
`http://journals.ametsoc.org/doi/abs/10.1175/1520-0442(1997)010%`
`3C2600%3AIOTNAM%3E2.0.CO%3B2`.

Higgins, R. W., et al., 2003: Progress in Pan American CLIVAR Research: The North American Monsoon System. *Atmósfera*, **16 (1)**, URL
`http://revistas.unam.mx/index.php/atm/article/view/8504`.

Hoerling, M., A. Kumar, and M. Zhong, 1997: El Niño, La Niña, and the nonlinearity of their teleconnections. *J. Climate*, **10 (8)**, 1769–1786,
doi:10.1175/1520-0442(1997)010<1769:ENOLNA>2.0.CO;2.

Hurrell, J. W., 1996: Influence of variations in extratropical wintertime teleconnections on northern hemisphere temperature. *Geophys. Res. Lett.*, **23 (6)**, 665–668, doi:10.1029/96GL00459, URL
`http://onlinelibrary.wiley.com/doi/10.1029/96GL00459/abstract`.

Kalnay, E., et al., 1996: The NCEP/NCAR 40-Year Reanalysis Project. *Bull. Amer. Meteor. Soc.*, **77 (3)**, 437–471,
doi:10.1175/1520-0477(1996)077<0437:TNYRP>2.0.CO;2, URL `http:`
`//dx.doi.org/10.1175/1520-0477(1996)077<0437:TNYRP>2.0.CO;2`.

Karnauskas, K. B., R. Seager, A. Giannini, and A. J. Busalacchi, 2013: A simple mechanism for the climatological midsummer drought along the Pacific coast of Central America. *Atmósfera*, **26 (2)**, 261–281,
doi:10.1016/S0187-6236(13)71075-0, URL `http:`
`//www.sciencedirect.com/science/article/pii/S0187623613710750`.

Kerr, R. A., 2000: A North Atlantic Climate Pacemaker for the Centuries. *Science*, **288 (5473)**, 1984–1985, doi:DOI:10.1126/science.288.5473.1984.

Latif, M., et al., 2004: Reconstructing, Monitoring, and Predicting Multidecadal-Scale Changes in the North Atlantic Thermohaline Circulation with Sea Surface Temperature. *Journal of Climate*, **17 (7)**, 1605–1614,
doi:10.1175/1520-0442(2004)017<1605:RMAPMC>2.0.CO;2, URL
`http://journals.ametsoc.org/doi/abs/10.1175/1520-0442(2004)017%`
`3C1605%3ARMAPMC%3E2.0.CO%3B2`.

Lorenz, D. J. and D. L. Hartmann, 2006: The Effect of the MJO on the North American Monsoon*. *Journal of Climate*, **19 (3)**, 333–343,
doi:10.1175/JCLI3684.1, URL
`http://journals.ametsoc.org/doi/abs/10.1175/JCLI3684.1`.

Madden, R. A. and P. R. Julian, 1994: Observations of the 40–50-Day Tropical Oscillation—A Review. *Mon. Wea. Rev.*, **122 (5)**, 814–837,

doi:10.1175/1520-0493(1994)122<0814:OOTDTO>2.0.CO;2, URL
`http://journals.ametsoc.org/doi/abs/10.1175/1520-0493(1994)122%`
`3C0814:OOTDTO%3E2.0.CO;2.`

Magaña, V., J. A. Amador, and S. Medina, 1999: The Midsummer Drought over
Mexico and Central America. *Journal of Climate*, **12 (6)**, 1577–1588,
doi:10.1175/1520-0442(1999)012<1577:TMDOMA>2.0.CO;2, URL
`http://journals.ametsoc.org/doi/abs/10.1175/1520-0442%281999%`
`29012%3C1577%3ATMDOMA%3E2.0.CO%3B2.`

Maldonado, T. and E. Alfaro, 2010: Comparación de las salidas del modelo MM5v3
con datos observados en la Isla del Coco, Costa Rica. *Tecnología en Marcha*,
23 (4), 3–28.

Maldonado, T. and E. Alfaro, 2011: Predicción estacional para ASO de eventos
extremos y días con precipitación sobre las vertientes Pacífico y Caribe de
América Central, utilizando análisis de correlación canónica. *InterSedes*, **12 (24)**,
78–108, URL `http://www.intersedes.ucr.ac.cr/ojs/index.php/`
`intersedes/article/view/301.`

Maldonado, T., E. Alfaro, B. Fallas-López, and L. Alvarado, 2013: Seasonal
prediction of extreme precipitation events and frequency of rainy days over Costa
Rica, Central America, using Canonical Correlation Analysis. *Adv. Geosci.*, **33**,
41–52, doi:10.5194/adgeo-33-41-2013, URL
`http://www.adv-geosci.net/33/41/2013/.`

Malmgren, B. A., A. Winter, and D. Chen, 1998: El Niño–Southern Oscillation and
North Atlantic Oscillation Control of Climate in Puerto Rico. *Journal of Climate*,
11 (10), 2713–2717,
doi:10.1175/1520-0442(1998)011<2713:ENOSOA>2.0.CO;2, URL
`http://journals.ametsoc.org/doi/abs/10.1175/1520-0442(1998)011%`
`3C2713%3AENOSOA%3E2.0.CO%3B2.`

Mantua, N. J. and S. R. Hare, 2002: The Pacific Decadal Oscillation. *Journal of
Oceanography*, **58 (1)**, 35–44, doi:10.1023/A:1015820616384, URL
`http://link.springer.com/article/10.1023/A%3A1015820616384.`

Mantua, N. J., S. R. Hare, Y. Zhang, J. M. Wallace, and R. C. Francis, 1997: A
Pacific Interdecadal Climate Oscillation with Impacts on Salmon Production. *Bull.
Amer. Meteor. Soc.*, **78 (6)**, 1069–1079,
doi:10.1175/1520-0477(1997)078<1069:APICOW>2.0.CO;2, URL
`http://journals.ametsoc.org/doi/abs/10.1175/1520-0477(1997)078%`
`3C1069:APICOW%3E2.0.CO;2.`

Martin, E. R. and C. Schumacher, 2011: Modulation of Caribbean Precipitation by
the Madden–Julian Oscillation. *Journal of Climate*, **24 (3)**, 813–824,
doi:10.1175/2010JCLI3773.1, URL
`http://journals.ametsoc.org/doi/abs/10.1175/2010JCLI3773.1.`

Mestas-Nuñez, A. M. and D. B. Enfield, 2001: Eastern equatorial Pacific SST
variability: ENSO and non-ENSO components and their climatic associations.
Journal of Climate, **14 (3)**, 391–402, URL
`http://journals.ametsoc.org/doi/pdf/10.1175/1520-0442(2001)014%`
`3C0391%3AEEPSVE%3E2.0.CO%3B2.`

Mock, C. J., 1996: Climatic controls and spatial variations of precipitation in the
western United States. *Journal of climate*, **9 (5)**, 1111–1125, URL

http://cat.inist.fr/?aModele=afficheN&cpsidt=3095716.

Moon, J.-Y., B. Wang, and K.-J. Ha, 2010: ENSO regulation of MJO teleconnection. *Climate Dynamics*, **37 (5-6)**, 1133–1149, doi:10.1007/s00382-010-0902-3, URL http://www.springerlink.com/index/10.1007/s00382-010-0902-3.

Muñoz, E., C. Wang, and D. Enfield, 2010: The Intra-Americas Sea springtime surface temperature anomaly dipole as fingerprint of remote influence. *J. Climate*, **23**, 43–56, doi:http://dx.doi.org/10.1175/2009JCLI3006.1.

Poveda, G. and O. J. Mesa, 2000: On the existence of Lloró (the rainiest locality on earth): Enhanced ocean-land-atmosphere interaction by a low-level jet. *Geophysical Research Letters*, **27 (11)**, 1675–1678, doi:10.1029/1999GL006091.

Ramírez, P., 1983: Estudio Meteorológico de los Veranillos en Costa Rica. Nota de investigación. 5, Instituto Meteorológico Nacional, Ministerio de Agricultura y Ganadería., San José, Costa Rica.

Schneider, N. and B. D. Cornuelle, 2005: The Forcing of the Pacific Decadal Oscillation*. *Journal of Climate*, **18 (21)**, 4355–4373, doi:10.1175/JCLI3527.1, URL http://journals.ametsoc.org/doi/abs/10.1175/JCLI3527.1.

Schultz, D. M., W. E. Bracken, and L. F. Bosart, 1998: Planetary- and Synoptic-Scale Signatures Associated with Central American Cold Surges. *Monthly Weather Review*, **126 (1)**, 5–27, doi:10.1175/1520-0493(1998)126<0005:PASSSA>2.0.CO;2, URL http://journals.ametsoc.org/doi/abs/10.1175/1520-0493(1998)126%3C0005:PASSSA%3E2.0.CO%3B2.

Schultz, D. M., W. E. Bracken, L. F. Bosart, G. J. Hakim, M. A. Bedrick, M. J. Dickinson, and K. R. Tyle, 1997: The 1993 Superstorm Cold Surge: Frontal Structure, Gap Flow, and Tropical Impact. *Mon. Wea. Rev.*, **125 (1)**, 5–39, doi:10.1175/1520-0493(1997)125<0005:TSCSFS>2.0.CO;2, URL http://dx.doi.org/10.1175/1520-0493(1997)125<0005:TSCSFS>2.0.CO;2.

Smith, T., R. Reynolds, T. C. Peterson, and J. Lawrimore, 2007: Improvements to NOAA's Historical Merged Land–Ocean Surface Temperature Analysis (1880–2006). *J. Climate*, **21**, 2283 – 2296.

Srinivasan, J. and G. L. Smith, 1996: Meridional Migration of Tropical Convergence Zones. *Journal of Applied Meteorology*, **35 (8)**, 1189–1202, doi:10.1175/1520-0450(1996)035<1189:MMOTCZ>2.0.CO;2, URL http://journals.ametsoc.org/doi/abs/10.1175/1520-0450(1996)035%3C1189:MMOTCZ%3E2.0.CO%3B2.

Tang, Y. and B. YU, 2008: An Analysis of Nonlinear Relationship between the MJO and ENSO. *Journal of the Meteorological Society of Japan. Ser. II*, **86 (6)**, 867–881, URL http://japanlinkcenter.org/JST.JSTAGE/jmsj/86.867?from=Google.

Taylor, M. A. and E. J. Alfaro, 2005: Climate of Central America and the Caribbean. *Encyclopedia of World Climatology*, J. E. Oliver, Ed., Springer, Netherlands, 183–186.

Trenberth, K. E., 1997: The Definition of El Niño. *Bulletin of the American Meteorological Society*, **78 (12)**, 2771–2777, doi:10.1175/1520-0477(1997)078<2771:TDOENO>2.0.CO;2, URL http://journals.ametsoc.org/doi/abs/10.1175/1520-0477(1997)078%3C2771%3ATDOENO%3E2.0.CO%3B2.

Velásquez, R., 2000: Mecanismos físicos de variabilidad climática y eventos extremos en Venezuela. Lic. thesis, Departamento de Física Atmosférica, Oceánica y Planetaria, Escuela de Física, Universidad de Costa Rica.

Vera, C., et al., 2006: Toward a unified view of the American monsoon systems. *Journal of Climate*, **19 (20)**, 4977–5000, URL `http://journals.ametsoc.org/doi/pdf/10.1175/JCLI3896.1`.

Wang, C., 2007: Variability of the Caribbean Low-Level Jet and its relations to climate. *Clim Dyn*, **29 (4)**, 411–422, doi:10.1007/s00382-007-0243-z, URL `http://link.springer.com/article/10.1007/s00382-007-0243-z`.

Wang, C. and D. B. Enfield, 2001: The Tropical Western Hemisphere Warm Pool. *Geophysical Research Letters*, **28 (8)**, 1635–1638, doi:10.1029/2000GL011763, URL `http://onlinelibrary.wiley.com/doi/10.1029/2000GL011763/abstract`.

Wang, C. and D. B. Enfield, 2003: A Further Study of the Tropical Western Hemisphere Warm Pool. *J. Climate*, **16 (10)**, 1476–1493, doi:10.1175/1520-0442(2003)016<1476:AFSOTT>2.0.CO;2, URL `http://journals.ametsoc.org/doi/abs/10.1175/1520-0442%282003%29016%3C1476%3AAFSOTT%3E2.0.CO%3B2`.

Wang, C. and P. C. Fiedler, 2006: ENSO variability and the eastern tropical Pacific: A review. *Prog. Oceanogr.*, **69 (2–4)**, 239–266, doi:10.1016/j.pocean.2006.03.004, URL `http://www.sciencedirect.com/science/article/pii/S0079661106000334`.

Wang, C. and S.-k. Lee, 2007: Atlantic warm pool, Caribbean low-level jet, and their potential impact on Atlantic hurricanes. *Geophysical Research Letters*, **34 (2)**, 1–5, doi:10.1029/2006GL028579, URL `http://onlinelibrary.wiley.com/doi/10.1029/2006GL028579/abstract`.

Wang, C., S.-k. Lee, and D. B. Enfield, 2007: Impact of the Atlantic Warm Pool on the Summer Climate of the Western Hemisphere. *Journal of Climate*, **20 (20)**, 5021–5040, doi:10.1175/JCLI4304.1, URL `http://journals.ametsoc.org/doi/abs/10.1175/JCLI4304.1`.

Wang, C., S.-K. Lee, and D. B. Enfield, 2008: Climate Response to Anomalously Large and Small Atlantic Warm Pools during the Summer. *Journal of Climate*, **21 (11)**, 2437–2450, doi:10.1175/2007JCLI2029.1, URL `http://journals.ametsoc.org/doi/abs/10.1175/2007JCLI2029.1`.

Warner, T. T., B. E. Mapes, and M. Xu, 2003: Diurnal Patterns of Rainfall in Northwestern South America. Part II: Model Simulations. *Monthly Weather Review*, **131 (5)**, 813–829, doi:10.1175/1520-0493(2003)131<0813:DPORIN>2.0.CO;2, URL `http://journals.ametsoc.org/doi/abs/10.1175/1520-0493%282003%29131%3C0813%3ADPORIN%3E2.0.CO%3B2`.

Webber, B. G. M., A. J. Matthews, and K. J. Heywood, 2010: A dynamical ocean feedback mechanism for the Madden–Julian Oscillation. *Quarterly Journal of the Royal Meteorological Society*, **136 (648)**, 740–754, doi:10.1002/qj.604, URL `http://onlinelibrary.wiley.com/doi/10.1002/qj.604/abstract`.

Wilks, D. S., 2011: *Statistical Methods in the Atmospheric Sciences, Volume 100, Third Edition*. 3d ed., Academic Press, Amsterdam ; Boston.

Xue, Y., T. Smith, and R. Reynolds, 2003: Interdecadal changes of 30-yr SST normals during 1871-2000. *JOURNAL OF CLIMATE*, **16 (10)**, 1601–1612, doi:10.1175/1520-0442-16.10.1601.

Zárate-Hernández, E., 2013: Climatología de masas invernales de aire frío que alcanzan Centroamérica y el Caribe y su relación con algunos índices árticos. *Top. Meteor. Oceanogr.*, **12 (1)**, 35 – 55.

Zhang, C., 2005: Madden-Julian Oscillation. *Reviews of Geophysics*, **43 (2)**, n/a–n/a, doi:10.1029/2004RG000158, URL `http://onlinelibrary.wiley.com/doi/10.1029/2004RG000158/abstract`.

Zhang, R. and T. L. Delworth, 2006: Impact of Atlantic multidecadal oscillations on India/Sahel rainfall and Atlantic hurricanes. *Geophysical Research Letters*, **33 (17)**, n/a–n/a, doi:10.1029/2006GL026267, URL `http://onlinelibrary.wiley.com/doi/10.1029/2006GL026267/abstract`.

Zhang, Y., J. M. Wallace, and D. S. Battisti, 1997: ENSO-like interdecadal variability: 1900-93. *Journal of Climate*, **10 (5)**, 1004–1020, URL `http://journals.ametsoc.org/doi/abs/10.1175/1520-0442(1997)010%3C1004%3AELIV%3E2.0.CO%3B2`.

Paper I

RMetS

Royal Meteorological Society

Variability of the Caribbean low-level jet during boreal winter: large-scale forcings

Tito Maldonado,* Anna Rutgersson,[†] Jorge Amador,[‡] Eric Alfaro[§] and Björn Claremar[†]

Department of Earth Sciences, Uppsala University, Sweden

ABSTRACT: An index capturing the anomalies of the zonal wind at 925 hPa from 1950 to 2010 was defined to explore the relationship between the fluctuations of the Caribbean low-level jet (CLLJ) and the main climate variability modes affecting the Intra-Americas Sea Region. El Niño Southern Oscillation (ENSO) events, here defined using the Niño 3.4 index, are found to be the most important variability modes for the jet anomalies, in agreement with previous studies. However, the Pacific Decadal Oscillation (PDO) and the Pacific/North American (PNA) teleconnection pattern also show significant correlations with the CLLJ anomaly index during February. The North Atlantic Oscillation (NAO) and the Arctic Oscillation (AO) reveal a possible interaction with the jet anomalies that could be connected with the cold fronts and cold air surges arriving to the Caribbean basin from the Northern Hemisphere during winter. A composite technique is used to explain the correlations with the Pacific indexes. We found that ENSO events are connected to CLLJ anomalies by modulating the sea-level pressure (SLP) near the east coast of the United States and the Aleutian Low. The pattern displayed by the SLP anomalies (SLPa) is also associated with the PNA. During warm (cold) ENSO phases, negative (positive) anomalies in the SLP field over the east coast of North America produce cyclonic (anticyclonic) circulations at low levels. However, the ENSO signal in the SLPa and the PNA pattern are modulated by the phases of the PDO. Results indicate that when the ENSO and PDO are in phase (out of phase), the SLPa signal is enhanced (weakened or cancelled), affecting the CLLJ anomalies in both direction and intensity, also changing the spatial distribution of precipitation.

KEY WORDS   El Niño Southern Oscillation; Pacific Decadal Oscillation; Caribbean low-level jet; climate variability; ENSO non-linearities

Received 25 March 2015; Revised 29 June 2015; Accepted 15 July 2015

1. Introduction

The Central American climate is known to be controlled by the trade winds (trades), the dominant wind regime year-round (e.g. Alfaro, 2002; Taylor and Alfaro, 2005; Amador *et al.*, 2006). The trades are generated by the North Atlantic subtropical high (NASH) and by the pressure gradient between the NASH and the low-pressure belt formed over the intertropical convergence zone (ITCZ). The interaction of the trades with the complex topography of Central America leads to a marked contrast in annual precipitation distribution between the Pacific and Caribbean coasts of Central America. On the Pacific coast, precipitation displays a bimodal annual cycle, peaking in May–June and August–October, the second precipitation maximum being more intense than the first. A relative reduction of rainfall for several weeks in July and August is known as the mid-summer drought (MSD; Magaña *et al.*, 1999; Herrera *et al.*, 2015). On the western Caribbean (Greater Antilles), annual rainfall also exhibits a bimodal structure (Martin and Schumacher, 2011b), with an initial maximum in May, a minimum in approximately July–August, and a second maximum in September–October (Jury *et al.*, 2007, Gamble *et al.*, 2008). The minimum that separates the two rainfall peaks has also been termed the MSD based on its similarity to the rainfall minimum that occurs on the Pacific coast of Central America (Magaña *et al.*, 1999).

In the Caribbean Sea, a strong low-level wind flow is present year-round. This wind current displays a bimodal annual cycle that peaks in February (winter) and July (summer) at approximately 925 hPa (Amador, 1998, 2008; Amador *et al.*, 2010). This strong wind current is usually called the Intra-Americas Sea low-level jet (IALLJ; Amador, 2008) or, for concision, the Caribbean low-level jet (CLLJ). The CLLJ occurrence coincides with reduced precipitation on the Pacific coast and relatively increased rainfall on the Caribbean coast of Central America. In winter, the CLLJ transports moisture from the Caribbean

* Correspondence to: T. Maldonado, Department of Earth Sciences, Uppsala University, Villav. 16, 752 36 Uppsala, Sweden; Centre for Geophysical Research, University of Costa Rica, San Pedro de Montes de Oca, 11501-2060 San Jose, Costa Rica. E-mail: tito.maldonado@geo.uu.se

[†]Present address: Department of Earth Sciences, Uppsala University, Villav. 16, 752 36 Uppsala, Sweden.
[‡]Present address: Centre for Geophysical Research and School of Physics, University of Costa Rica, San Pedro de Montes de Oca, 11501-2060 San Jose, Costa Rica.
[§]Present address: Centre for Geophysical Research, Centre for Research in Marine Sciences and Limnology and School of Physics, University of Costa Rica, San Pedro de Montes de Oca, 11501-2060 San Jose, Costa Rica.

Sea to the eastern Central American continent and, due to ascending motion at the jet exit, precipitation occurs over relatively flat areas of Costa Rica and Nicaragua (Amador, 2008). Cold fronts (CFs) arriving from the Northern Hemisphere and terrain concavity are also elements producing precipitation during the winter months on the Caribbean coast (Amador *et al.*, 2006; Zárate-Hernández, 2013). On the other hand, in summer, the CLLJ plays a significant role in Central American convective activity. The CLLJ is the main element generating the MSD in July and August (Herrera *et al.*, 2015). The CLLJ also modulates the vertical wind shear in the Caribbean Sea, one of the mechanisms controlling the formation of tropical cyclones in the region (Amador, 2008; Amador *et al.*, 2010).

Previous studies (e.g. Amador, 2008; Amador *et al.*, 2010) have noted that these two peaks in the CLLJ wind speed might differ in origin, with distinct dynamic and physical mechanisms in each season. Many studies (e.g. Wang, 2007; Wang and Lee, 2007; Muñoz *et al.*, 2008; Cook and Vizy, 2010) have attributed the origin of the CLLJ to geostrophic balance produced by the meridional pressure gradient (due to the NASH) in the neighbourhood of the jet. This reasoning, however, could be debatable because of the mass field adjustment (or Rossby adjustment) problem (Gill, 1982; Holton, 2004). Herrera *et al.* (2015) point out that the length scale of the CLLJ (∼1500 km) suggests that geostrophic equilibrium is achieved through the adjustment of the mass field to the wind; in other words, the meridional pressure gradient in this region adapts to the circulation, and not the reverse as most studies suggest. Ranjha *et al.* (2013), nevertheless, found that the CLLJ did not follow their classification of coastal low-level jets, thus, the sources of CLLJ momentum in winter and summer remain unknown, and exploration of them is beyond the scope of this paper.

Amador (2008) has identified El Niño Southern Oscillation (ENSO) events as the main climate variability mode responsible for the inter-annual variability of the jet in each season. It should be mentioned that when the impact of ENSO phases on the climate over Central America is analysed, it is usually assumed that the signals of both episodes (i.e. El Niño and La Niña) have opposite effects, that is, their teleconnections have the same spatial distribution but with the inverse sign of the atmospheric field anomalies. Hoerling *et al.* (1997) analysed the effects of the linear and non-linear teleconnections of El Niño in North America during boreal winter. Their findings indicated that precipitation in the tropics displays non-linear behaviour, evidenced by the shift in the maximum anomalies of tropical rainfall. They also found a large non-linear component in the surface climate anomalies in North America, consistent with a phase shift in teleconnections. Later, DeWeaver and Nigam (2002) found that ENSO sea surface temperatures (SSTs) directly affect the large-scale atmospheric circulation through their impact on diabatic heating and subsequent upper-level divergence over the equatorial Pacific. In previous studies (e.g. Wang, 2007; Amador, 2008), CLLJ anomalies have been assumed to behave linearly in response to El Niño events, as has the

impact of wind fluctuation on precipitation distribution; nonetheless, non-linearity might appear because of the inherent non-linearity of ENSO events.

The variability of the CLLJ during each season is reportedly associated with different forcings, the fluctuations of the jet during winter being related to large-scale features such as SST anomalies over the Niño 3.4 region (−5° to 5°N, 120° to 170°W), whereas the CLLJ perturbations in summer are associated with regional-scale forcings such as the difference in the SSTs of the tropical North Atlantic (TNA) and El Niño regions (Amador *et al.*, 2010). Jury and Malmgren (2012) found evidence that the variability of the CLLJ is associated with SLP anomalies over the Amazons and the Atlantic ITCZ, rather than the North Atlantic anticyclone. Recently, Hidalgo *et al.* (2015) presented evidence that the CLLJ during summer is modulated by a pattern of divergence between lower and higher levels of the troposphere over the Intra-Americas Sea region.

Besides the CLLJ variability associated with ENSO events, other climate variability modes have been associated with the CLLJ anomalies in winter. Wang (2007) mentioned that the North Atlantic Oscillation (NAO) might modulate the jet anomalies through controlling the pressure difference between the NASH and the Icelandic Low, although he presented no supporting evidence. Moreover, Muñoz and Enfield (2011) found that the NAO is not correlated with the jet's anomalies during spring, although the NAO decays during that season. In addition, Muñoz and Enfield (2011) documented the influence of other important climate variability indexes, such as the Pacific Decadal Oscillation (PDO) and Pacific/North American Pattern (PNA), related to the wind fluctuations in spring over the Caribbean Sea and to the jet region. Gershunov and Barnett (1998b) explored the influence of the PDO in modulating El Niño signal during winter in North America. Their findings indicate that the PDO intensifies (or weakens) El Niño signal in the sea-level pressure (SLP) field. Durán-Quesada (2012) pointed out that the CLLJ variability in winter associated with large-scale indexes, such as the ENSO, PDO, NAO, and Madden–Julian Oscillation (MJO), could alter the moisture transport from the Caribbean to Central America. Under certain circumstances, this transport could provoke intensified dry conditions leading to severe drought events. Notably, although most of these studies describe the association between climate variability indexes and CLLJ anomalies, the connection between CLLJ fluctuations and climate variability modes is still an open scientific question. CFs or cold surges from the Northern Hemisphere (Amador *et al.*, 2006, Zárate-Hernández, 2013) are additional sources of variability in winter; however, their interaction with the CLLJ has not previously been explored.

This study examines the CLLJ variability in February (winter) to identify and establish a relationship between the CLLJ fluctuations in this season and the main climate variability modes affecting the Intra-Americas Sea. Section 2 describes the data, while the analytical methodology and techniques are described in Section 3.

Results are presented in Section 4 and the summary and conclusions in Section 5.

2. Data

To study the influence of the large- and regional-scale modulators of the CLLJ, we selected the domain bounded by 22°S–63°N and 15°E–180°W. This domain captures the most important global and regional climate variability modes affecting the climate and weather of Central America and the Caribbean, such as El Niño as well as the NAO, Atlantic Multidecadal Oscillation (AMO), PDO, PNA, Western Hemisphere Warm Pool (WHWP), and TNA.

2.1. Reanalysis data

In this study, data from the National Centers for Environmental Prediction-National Center for Atmospheric Research (NCEP-NCAR) reanalysis project (Kalnay *et al.*, 1996) are used because this reanalysis has been extensively utilised for climate studies in this region (e.g. Amador, 2008; Herrera *et al.*, 2015) and its time series are long enough to capture long-lived events such as the PDO.

The NCEP-NCAR reanalysis has previously displayed deficiencies in its representation of precipitation in the tropics, mainly at regional scales, although the large-scale and inter-annual variability features are rendered in good agreement with observations (Janowiak *et al.*, 1998). On the other hand, Janowiak *et al.* (1998) also pointed out that reanalysis fields such as wind, geopotential height, and temperature contained proper estimates of the observed values. Herrera *et al.* (2015) mentioned that this reanalysis can capture important features of the climate in Central America, such as the MSD. Therefore, the NCEP-NCAR reanalysis is good enough for exploring the large-scale and inter-annual variability of the CLLJ for two reasons: (1) it is similar to other reanalyses, such as ERA-Interim (Dee *et al.*, 2011), in capturing the variability in dynamic fields (e.g. horizontal wind, geopotential height, and SLP) and (2) its time coverage exceeds 60 years, which is sufficient for studying long-lived phenomena such as the PDO. Consequently, the horizontal wind at 925 hPa and SLP data are taken from this reanalysis database. The monthly means for the 1950–2010 period were used to estimate the monthly climatology of both fields for February, to enable examination of the mean atmospheric conditions when the CLLJ peaks.

2.2. Precipitation data

Monthly total precipitation estimates are obtained from the Global Precipitation Climatology Centre (GPCC) (Schneider *et al.*, 2011). The GPCC data are gridded with a 0.5° horizontal resolution. The dataset comprises monitoring products based on quality-controlled gauge station data from 1901 to the present. Nevertheless, in this study, the climatology is estimated for the 1950–2010 period.

2.3. Global and regional climate variability indexes

Global climate variability indexes such as the Caribbean index (CAR), PNA, NAO, TNA, PDO, Arctic Oscillation (AO), WHWP, and AMO, were obtained from the National Oceanic and Atmospheric Administration's (NOAA's) Earth System Research Laboratory, Physical Sciences Division website (http://www.esrl.noaa.gov/psd/data/climateindices/list/, last viewed 23 February 2015). The ENSO episodes were determined using the definition of the Oceanic Niño Index (ONI: http://www.cpc.ncep.noaa.gov/products/analysis_monitoring/ensostuff/ensoyears.shtml, last viewed 23 February 2015) from the NOAA's Climate Prediction Centre (CPC). The ONI definition of warm (cold) events consists of a threshold of ±0.5 °C for the 3-month running mean of SST anomalies in the Niño 3.4 region, based on centred 30-year base periods updated every 5 years. The MJO index as is defined by the CPC (http://www.cpc.ncep.noaa.gov/products/precip/CWlink/daily_mjo_index/pentad.html, last viewed 23 February 2015). In this study the MJO index 7 (40°W) is used as presented by Durán-Quesada (2012). We define an index to represent the number of CFs arriving in the Caribbean Sea and northern South America, based in Zárate-Hernández (2013), who numbered the CFs reaching this region. The count is divided into monthly scores from November to February covering the period 1978–2012. Hence, the February score for 1979–2010 is selected for the CFs index.

3. Methods

3.1. CLLJ anomaly index

As the aim of this paper is to study the variability of the maximum wind speed in winter, the February monthly means were chosen. The maximum wind speed in January or February has been reported as statistically not different (Wang, 2007), while using the monthly means the results do not show a significant difference with the seasonal means (not shown). The CLLJ anomaly (CLLJa) index was defined as the areal average of zonal wind anomalies in the region bounded by 12.5°–17.5°N and 70°–80°W at 925 hPa (square in Figure 1(a)), in order to describe the monthly fluctuations of zonal wind velocity in February, relative to the climatology over the 61 years from 1950 to 2010. Using this definition of the CLLJ index allows us to have a good and simple representation of the mean features of the jet core, whereas it can be applied to measure other features of the wind such as the wind shear in the jet area as is described below. Thus, having a positive (negative) anomaly means a weaker (stronger) CLLJ. The annual climatology of monthly means for the index is shown in Figure 1(b). To explore the variability of the vertical structure of the jet, another index is defined as the difference between the monthly anomalies of the U-component at 925 and 1000 hPa in February. Amador (2008) described the main features of the jet in each season. The jet is weaker in winter than in summer (Figure 1(b)). The jet's vertical structure also differs between winter and summer, being less strong but more confined to 925 hPa in February. In addition, in February, the CLLJ has a single well-defined
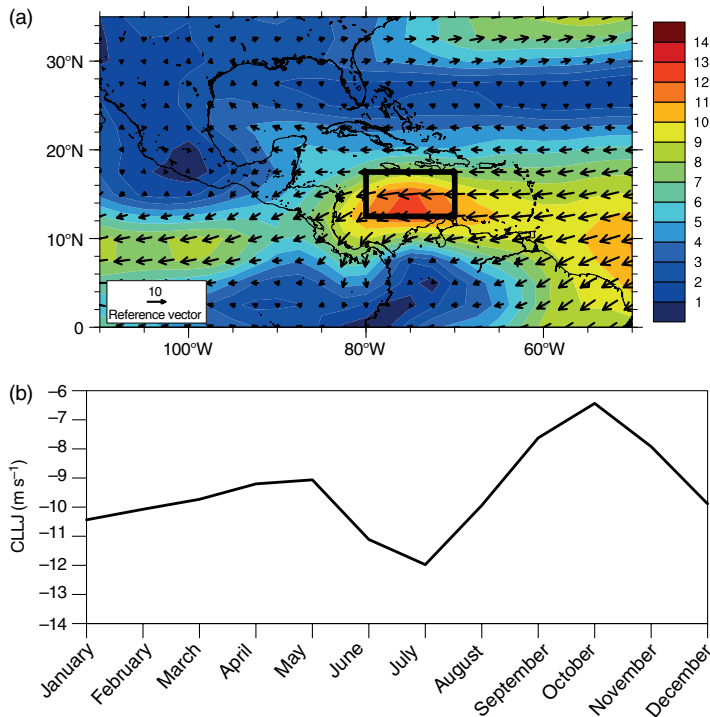
Figure 1. (a) February mean horizontal wind at 925 hPa for the 1950–2010 period using the NCEP-NCAR reanalysis. Contour lines are spaced 1 m s^{-1} apart and represent the wind magnitude. Arrows show the mean wind direction and magnitude. The CLLJ index is defined as the February monthly anomalies of the zonal wind in the area enclosed by the black square. Latitude and longitude coordinates are in degrees. (b) Annual cycle of the CLLJ monthly means index.

southward branch, whereas in July, it presents two ramifications, one extending towards Central America and the other extending to the Gulf of Mexico. This branching of the CLLJ suggests a connection between the jet and the Americas Monsoon System (AMS), as the jet is the main moisture transport from the Caribbean Sea to the AMS. Figure 2 shows the time series of the CLLJa index. It is to be noted from this figure that the variability of the wind speed, ranges from approximately −3 to 3 m s^{-1}. This time series also indicates that some observed anomalies in the CLLJ can be related to ENSO episodes.

3.2. Compositing ENSO and PDO

The winter variability of the CLLJa is found to be mainly associated with El Niño events (Figure 2 and Table 1), in agreement with previous studies (e.g. Amador, 2008). To explore how the teleconnections of El Niño influence the CLLJ anomalies, a composite analysis of El Niño and La Niña years is used to estimate the monthly mean composite anomalies of SLP, horizontal wind and divergence at 925 hPa and precipitation in February. The composite anomalies were calculated relative to the climatology of neutral years (i.e. neither warm nor cool ENSO events). Table 2 shows the ENSO classification of the years using

the ONI definition. Note that, according to this definition, the ENSO events from 1950 to 2010 are almost evenly distributed between 18 El Niño and 16 La Niña events.

The linear and non-linear effects of the ENSO events were studied by addition and subtraction of the ENSO phases. Assuming that El Niño and La Niña have the opposite signal in the anomalies (linear response) over the same regions, subtracting the anomalies, the signal of ENSO should be amplified in such areas. In regions where the subtraction of the anomalies decreases, this indicates that the ENSO signal in those areas does not have the exact opposite sign during the ENSO phases. With the addition of the anomalies we can identify the regions in which the ENSO signal does not have the opposite signal during each of the ENSO phases, and so a non-linear behaviour.

Similarly, a composite analysis is performed to study the influence of the PDO on the perturbation of the wind and precipitation. Table 2 also shows the classification of the PDO phases according to CPC. The mean composite anomalies in this case are relative to the 61-year (i.e. 1950–2010) climatology for February. Notably, as for the general cases of ENSO, the cases are almost evenly distributed when one considers the combination of ENSO and PDO. This examination of ENSO and PDO events
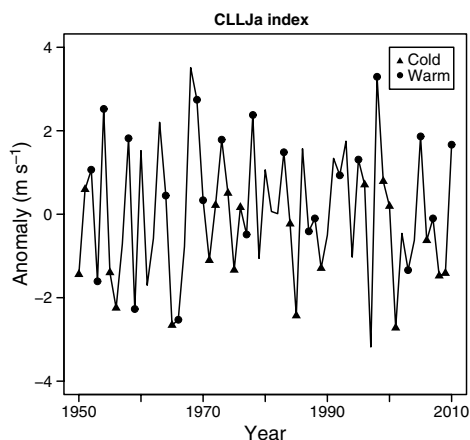
Figure 2. CLLJa index defined as the areal average of the anomalies for February 1950–2010, in the region bounded by 12.5°–17.5°N and 70°–80°W. The x-axis shows the temporal coordinates and the y-axis the anomalies of the CLLJ in m s^{-1}. The warm (cold) ENSO episodes are represented by dots (triangles).

Table 1. February Pearson correlation coefficients (r) between the CLLJa index and global and regional climate modulators. Significance levels are 90% (italic), 95% (bold), and 99% (bold italic).

Index	r
Niño 3.4	***0.36***
PDO	*0.22*
PNA	**0.35**
NAO	*−0.21*
AMO	−0.18
CAR	0.13
TNA	0.22
WHWP	**0.31**
MJO	***−0.40***
CS (CF)	***0.44***
AO	**−0.31**

clearly differs from those conducted by, for example, Hoerling *et al.* (1997), Gershunov and Barnett (1998a), and DeWeaver and Nigam (2002). However, it does capture features that are important relative to the distribution of the ENSO and PDO events, such as the phase shift in La Niña events mentioned by DeWeaver and Nigam (2002). These authors also pointed out that the method used to calculate the composites does not influence the results of estimating the non-linear response of the ENSO events, being more important the distribution of the ENSO events.

Statistical significance was estimated in a way similar to that of Gershunov and Barnett (1998a), using bootstrapping without replacement. In this approach, an artificial time series with normally distributed statistical noise is generated. The anomalies would then be considered significant at the 90% level if the absolute values exceed the 5th or 95th percentiles. A similar relationship between the

absolute values of the anomalies was used to estimate the 95% and 99% confidence levels.

4. Results

Figure 2 shows the time series of the CLLJ anomaly index. It is to be noted from this figure that there is a relationship between the jet fluctuations and ENSO episodes, i.e. during warm (cold) events, the jet is weakened (enhanced) due to an increase in westerly (easterly) wind anomalies over the jet core region. This association between ENSO episodes and CLLJ perturbations was previously reported by, for example, Amador *et al.* (2003), Wang (2007), and Amador (2008). However, not all CLLJ anomalies can be explained by ENSO events, as shown in Figure 2. This reveals an inherent ENSO variability due to either non-linearities or the presence of additional external forcings that affect the CLLJa.

The Pearson correlation of the CLLJ index with the global and regional indexes was estimated in order to determine and study what variability modes (besides ENSO) are important in explaining the CLLJ variability. The same was done with the vertical structure index. In addition, to explore the lead time between the time series, and so to determine which indexes are suitable for seasonal forecasting of the wind over the Caribbean Sea, correlations considering up to 5 months in advance, from September to January were calculated, and with the simultaneous correlation in February (perfect prognosis) to study the relationship with the anomalies of the CLLJ. The results for both the intensity and vertical structure indexes are shown in Tables 3 and 4.

Tables 3 and 4 present similar results. The Niño 3.4 SST and the WHWP anomalies have the highest correlation values, peaking in December. This result suggests that, by knowing the state of the SST in the Niño 3.4 region by December or January, one could forecast the expected intensity and vertical structure of the jet in February. Other variability modes, such as PDO, PNA, NAO and AO, display relatively high correlations in winter months, specifically in February, concurrent with the jet maximum, making them suitable for diagnostic studies. The simultaneous correlations of the CLLJ anomaly index and the majority of the climate modulators considered in this study reinforce the use of the February monthly means for the composite analysis.

Gershunov and Barnett (1998b) have documented that the influence of the PDO in the ENSO signal intensifies (reduces) the response to ENSO in winter, if both modes are in phase (out of phase). Moreover, the PNA teleconnection pattern is known to reach its mature phase in winter and is highly correlated with ENSO events. The relationship between the ENSO, PDO, and PNA is explored in the next section using composites.

Wang (2007) has suggested that the NAO might be associated with the fluctuations and formation of the CLLJ, because the NAO is the main mechanism associated with the pressure difference between the Icelandic Low and

Table 2. ENSO events in February classified according to ONI. The PDO information is from http://jisao.washington.edu/pdo (last viewed 23 February 2015).

	High PDO	Low PDO
El Niño	1983, 1987, 1988, 1992, 1995, 1998, 2003, 2010	1953, 1954, 1958, 1959, 1964, 1966, 1969, 1973, 1977, 1978
La Niña	1985, 1989, 1996, 1999, 2000, 2001, 2006, 2008, 2009	1950, 1951, 1955, 1956, 1974, 1975, 1976
Neutral	1981, 1982, 1984, 1986, 1990, 1991, 1993, 1994, 1997, 2002, 2004, 2005, 2007	1952, 1957, 1960, 1961, 1962, 1963, 1965, 1967, 1968, 1970, 1972, 1979, 1980

Table 3. Pearson correlation between the CLLJ anomalies index and the most important global and regional climate modulators for the Caribbean Basin. Significance levels are 90% (italic), 95% (bold), and 99% (bold italic).

	Niño 3.4	PDO	PNA	NAO	AMO	CAR	WHWP	TNA	AO
September	*0.33*	0.20	0.11	0.02	−0.20	0.07	0.17	0.01	0.06
October	**0.36**	0.18	0.12	0.00	−0.20	0.07	*0.24*	0.13	−0.07
November	**0.39**	0.07	0.12	0.09	−0.18	0.16	**0.26**	0.10	0.10
December	***0.41***	−0.08	0.12	−0.02	−0.18	0.16	***0.33***	0.09	0.21
January	**0.39**	*−0.01*	−0.05	0.15	−0.18	0.19	***0.31***	*0.08*	0.02
February	**0.36**	*0.22*	**0.35**	*−0.21*	−0.18	0.13	***0.31***	0.22	**−0.31**

the NASH. Table 1 presents estimated Pearson correlation coefficients. The NAO and the AO show simultaneous significant negative correlation with the jet anomalies; however, this result is expected since the close relationship of these two indexes (Ambaum *et al.*, 2001). A scatter plot of these modes and the CLLJ index is shown in Figure 3 in order to help with the interpretation of their correlations. The high dispersion of the dots reflects the relatively low correlations of the ENSO, PDO, PNA, NAO, and AO with the CLLJ index in February.

Regional climate indexes such as the CAR exhibit low and no significant correlation with the CLLJa, while the TNA indexes exhibit a significant positive correlation only in February. On the other hand, the WHWP SSTs show significant positive correlation with the wind fluctuation during the months considered, which reveals the importance of the regional waters in the interaction with the wind; however, this interaction is not completely clear and needs further analysis (Hidalgo *et al.*, 2015). It should be noted that the WHWP is also strongly modulated by the influence of the ENSO SSTs (Wang and Enfield, 2003; Wang and Fiedler, 2006) and by the phases of the PNA and PDO (Muñoz *et al.*, 2010).

The interaction of the MJO and CLLJ with the precipitation over the Caribbean has already been studied by Martin and Schumacher (2011a). They found that precipitation anomalies are above (below) average in phases 1 and 2 (5 and 6), and that the wind decreases (increases) in the region of the low-level jet. In contrast, we found that the MJO index 7 is significantly negatively correlated with the CLLJa, meaning that a positive MJO phase 7 in February would result in increased wind intensity and decreased precipitation if the mechanisms Martin and Schumacher (2011a) examined are valid for the MJO phase 7 in winter. Note, however, that how this interaction affects the temporal and spatial distribution of precipitation over Central America remains an open question that is not addressed here due to the low temporal resolution of the data series used. Adequately resolving MJO would require weekly or daily data.

The frequency and variability of CFs and cold surges arriving in the Gulf of Mexico, Central America, and the Caribbean region have been studied by Zárate-Hernández (2013). He found that CF frequency and penetration into northern South America are modulated by temperatures in the Arctic Belt between 70° and 90°N and by the AO phases. Using the results of Zárate-Hernández (2013), a CF index is defined to account for the number of CFs arriving in the Caribbean region in February from 1979 to 2010. The correlation between the CLLJa and the CFs is significant and positive, meaning that if the number of CFs increases, the jet intensity decreases. This finding agrees with the fact that when a CF arrives in the Caribbean region, low SLPa weakens the trades, increasing the westerly anomalies and thus reducing the jet intensity. This correlation is also corroborated by the AO, which exhibits a significant negative correlation. According to Zárate-Hernández (2013), the number of CFs increases if the AO is in its negative phase. The latter shows a possible connection of NAO, AO, and CF with the CLLJ anomalies that needs further study.

4.1. El Niño composites

The ENSO episode signals in the SLP are shown in Figure 4. SLPa as shown in Figure 4(a) and (b) is in agreement with previous results, such as those of Hoerling *et al.* (1997) and Gershunov and Barnett (1998b). During warm episodes (Figure 4(a)), there are significant negative SLPa over the Aleutian Peninsula in Alaska and the east coast of North America (at the 95% and 99% confidence levels, respectively). In contrast, during cold events (Figure 4(b)), almost the opposite pattern is observed, with the SLP being

Table 4. Pearson correlation between the vertical structure anomalies index and the most important global and regional climate modulators for the Caribbean Basin. Significance levels are 90% (italic), 95% (bold), and 99% (bold italic).

	Niño 3.4	PDO	PNA	NAO	AMO	CAR	WHWP	TNA	AO
September	*0.41*	**0.27**	0.11	0.03	−0.04	0.12	*0.23*	0.01	0.07
October	*0.45*	*0.22*	0.12	−0.02	−0.04	0.10	**0.28**	0.15	−0.10
November	*0.48*	0.11	0.12	0.11	−0.02	0.19	**0.29**	0.10	0.05
December	*0.50*	−0.01	0.13	0.01	−0.01	0.22	*0.46*	0.09	0.20
January	*0.50*	0.07	0.02	0.17	−0.01	*0.25*	*0.46*	0.09	0.00
February	*0.49*	*0.31*	*0.38*	*−0.24*	−0.01	0.18	*0.48*	**0.27**	*−0.34*
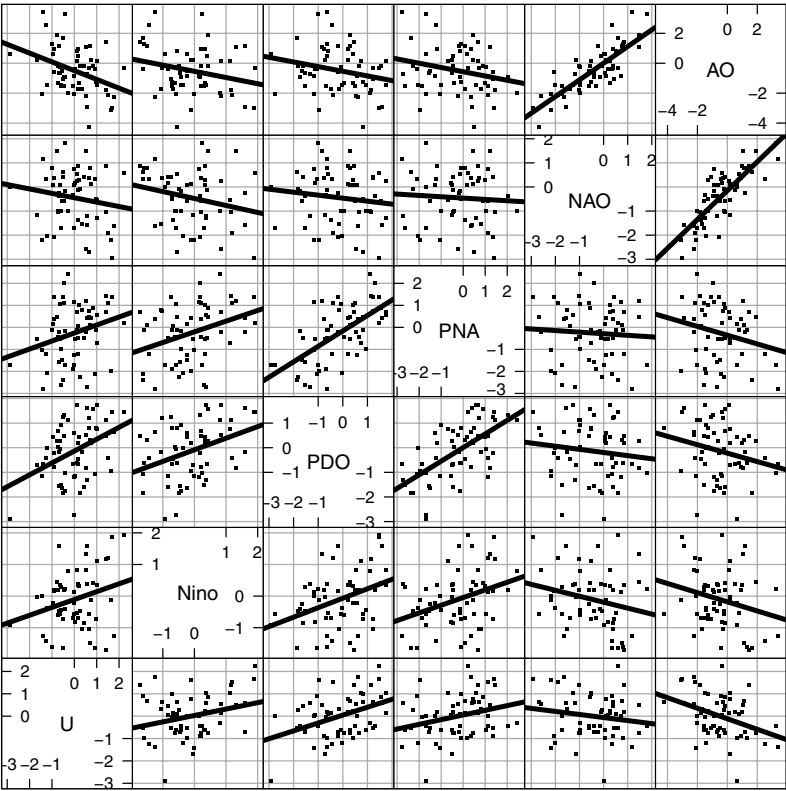
Figure 3. Scatter plot matrix showing the relationship of the CLLJ anomalies with Niño 3.4, PDO, PNA, NAO, and AO. This matrix also shows the association among each of these indexes.

higher than normal in the same regions at the 95% significance level. Hoerling *et al.* (1997) noted that, during El Niño, the centre of this SLPa pattern extends to the Tropical Northern Hemisphere (TNH) teleconnection, while La Niña extends to the PNA teleconnection pattern. However the La Niña anomalies are shifted south over the Pacific and east over the Atlantic relative to the El Niño signal. Zárate-Hernández (2013) found evidence of a similar configuration of the SLPa associated with the low (high) frequency and penetration of CFs in the Caribbean region.

The linear component of El Niño teleconnections (Figure 4(c)) is dominant over the Aleutian Low and the

east coast of the United States. The Gulf of Mexico and the Caribbean region SLPa display linear behaviour, with a higher order of magnitude than the non-linear behaviour for the same reason as explained above. Non-linear anomalies are observed mainly over the Pacific coastal and central United States (Figure 4(d)) and could be associated with the southward shift of the SLPa in the North Pacific during La Niña events. DeWeaver and Nigam (2002) found that the non-linear component of the geopotential field is not negligible over the tropics. Same composites were estimated for a geopotential height of 500 hPa (not shown). Here, El Niño exhibits an asymmetric
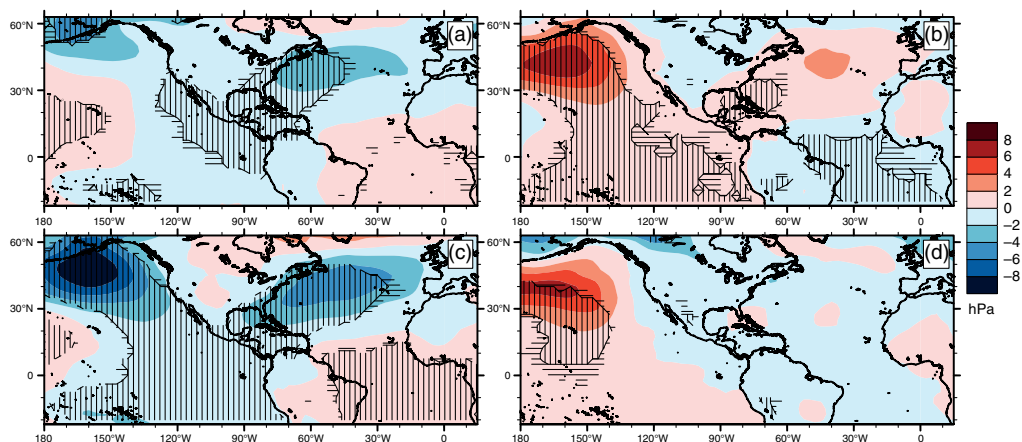
Figure 4. February composites of El Niño (a) and La Niña (b) used to estimate the mean SLP anomalies with NCEP-NCAR reanalysis data. The linear component (c) is estimated as the difference between El Niño and La Niña anomalies, whereas the non-linear component (d) is the sum of both. Contour levels are spaced 2 hPa apart. Shaded regions are significant anomalies with confidence levels of 90–95% (horizontal lines), 95–99% (vertical lines), and >99% (slant lines).
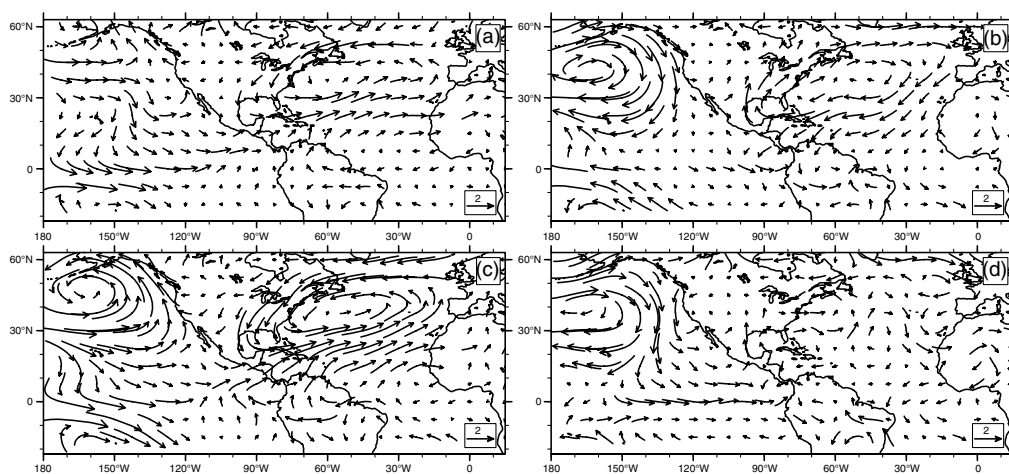

Figure 5. February horizontal wind anomalies at 925 hPa for (a) El Niño, (b) La Niña, (c) El Niño – La Niña (linear anomalies), and (d) El Niño + La Niña (non-linear anomalies). The reference vector is in m s^{-1}.

pattern compared with La Niña pattern. Similar to the low SLPa levels (Figure 4(a)) during El Niño, two significant troughs are located over the Alaskan Peninsula and over the east coast of North America connected by a band of low pressure. A ridge can be observed centred at 60°N, 90°W. During La Niña over the Alaskan Peninsula and the eastern part of North America, the geopotential height anomalies both have an opposite sign to El Niño and are relatively lower in intensity. Two ridges separated by a relatively strong trough are centred at 50°N, 120°W. This asymmetry was previously found by DeWeaver and Nigam (2002), who highlighted that the asymmetry observed in these cases could be related to the shift

observed in La Niña events in 1976–1977, reflecting the inherent variability of ENSO events. The linear component tends to dominate in the mid-latitudes between 30° and 60°N, with relatively important effects in the vicinities of the Caribbean Sea and the Central Pacific. The non-linear component displays more interaction focused in mid-latitudes over the North Pacific to the Alaskan Peninsula, the west coast, and northern North America.

Composites of the horizontal wind anomalies at 925 hPa during warm and cold episodes (Figure 5(a) and (b)) confirm previous results reported by Amador *et al.* (2003) and Amador (2008). Warm (cold) episodes during boreal winter and lower (higher) than normal SLPa over the east
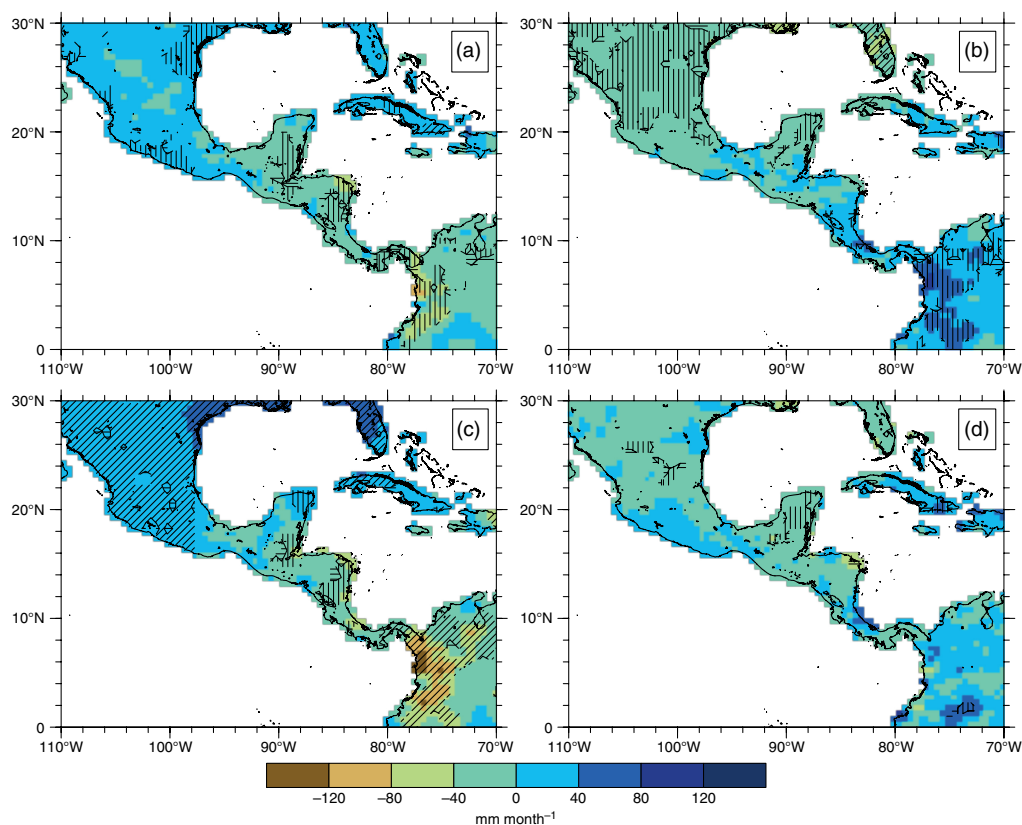
Figure 6. February anomalies of cumulative monthly precipitation in millimetres (mm) for (a) El Niño, (b) La Niña, (c) El Niño – La Niña (linear anomalies), and (d) El Niño + La Niña (non-linear anomalies). Shaded regions are significant anomalies with confidence levels of 90–95% (horizontal lines), 95–99% (vertical lines), and >99% (slant lines).

coast of the United States and over the Alaskan Penin-sula (described above) are associated with cyclonic (anti-cyclonic) circulation at low levels, resulting in westerly (easterly) wind anomalies and weakening (enhancing) the intensity of the CLLJ. However the anomalies over the Gulf of Mexico and the Caribbean Sea are mainly dom-inated by the linear (Figure 5(c)) rather than the non-linear component (Figure 5(d)). This indicates that, at low atmo-spheric levels, El Niño signal behaves linearly over this region, as do the jet anomalies during ENSO phases.

The implication of these results for the precipita-tion distribution in Central America is as follows. Precipitation composites exhibit a dominant contrast-ing pattern during El Niño and La Niña events. Drier conditions are found from the Yucatan Peninsula to north-ern South America during warm events, while Mexico and Cuba experience wetter conditions (Figure 6(a)). During cold episodes, the inverse pattern of rainfall anomalies is observed, with essentially the same spa-tial distribution (Figure 6(b)) as during warm events, except for Yucatan Peninsula, Guatemala, Honduras, and

El Salvador, where precipitation anomalies are mostly negative in both phases. Durán-Quesada (2012) pointed out that these contrasting precipitation patterns arise due to the relationship between the CLLJ and the ENSO phases. During warm (cold) events, the CLLJ is weakened (enhanced), the moisture transport efficiency is weakened (enhanced), and less (more) humidity is transported to Central America. Non-linear anomalies are observed in the rainfall having the same order of magnitude as does the linear counterpart (Figure 6(d)), however, with no statistical significance. These non-linear anomalies in the rainfall result in wetter conditions over Costa Rica and the west coast of southern Mexico, and drier conditions over the rest of Central America and Mexico. The cause of the non-linear rainfall anomalies is difficult to determine; however, from these results, it cannot be related to the non-linear signal in the horizontal wind over the Caribbean Sea or in the pressure pattern over the Atlantic, as the non-linear signal in those fields is very low relative to the linear counterpart. Nevertheless, comparing the mean precipitation anomalies with the divergence composites
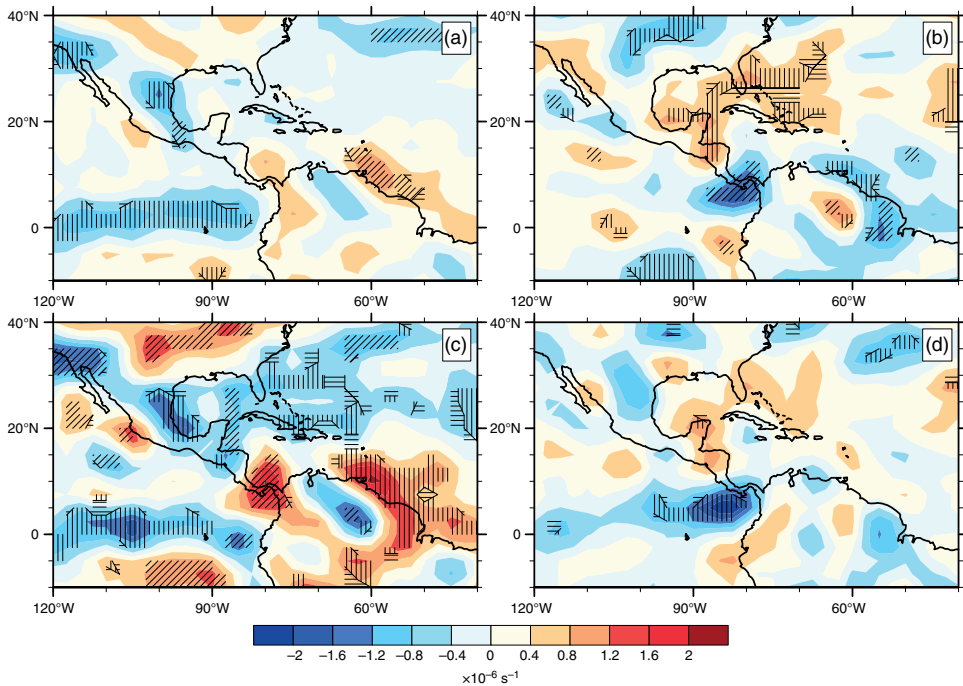
Figure 7. As in Figure 5 but showing the divergence at 925 hPa. Contour levels are spaced every $0.4 \times 10^{-6}\,\mathrm{s}^{-1}$.

(Figure 7), convergence (divergence) is observed over regions with drier (wetter) conditions during El Niño or La Niña (Figure 7(a) and (b)). The linear component of the divergence dominates over continental Central America (Figure 7(c)). The non-linear component (Figure 7(d)) makes a significant contribution over southern Central America, even though the other fields analysed previously indicated that the non-linear component can be ignored in the tropics. However, the non-linearity of precipitation cannot be linked only to the divergence. Other regional elements could control the precipitation distribution, such as the interaction of the mean wind with topography or other geographical elements present in the region. DeWeaver and Nigam (2002) pointed out that PDO might be responsible for some observed variability in ENSO events, and in some cases such variability has been taken erroneously as the non-linearity of El Niño episodes. In the following section, we explore the influence of the PDO on the ENSO teleconnection in Central America.

4.2. Influence of the PDO

In the previous subsection, the ENSO signal in the anomalies of fields such as SLP, horizontal wind at 925 hPa, and precipitation in February were examined using a composite analysis of ENSO events. Here, the effects of the PDO are examined by constructing sub-composites of ENSO events and PDO phases. The objective is to determine the effects of changes in the ENSO signal on SLP, horizontal wind at 925 hPa, and precipitation due to the influence of the PDO in February. Because the PDO is a long-lived phenomenon lasting approximately 30–40 years, a 30-year running average (not shown) was applied to the PDO index described in Section 2. This procedure reveals a negative PDO phase dominating from 1950 to 1981 and a positive PDO phase from 1981 to 2010. Table 2 lists the classification of El Niño and PDO phases. The anomalies are estimated relative to the climatology of the 61-year period from 1950 to 2010.

Figure 8(a) shows the SLPa for the El Niño and positive PDO (PDO+) sub-composite. Note the similarity between the spatial distribution of the SLPa and the SLPa pattern found for the El Niño composites (Figure 4(a)). Nevertheless, the SLPa are intensified and shifted south relative to the El Niño case shown in Figure 4(a), while a lower-than-normal pressure band is located over Central North America, conditions that enhance the Northern Hemisphere storms that reach low latitudes (Gershunov and Barnett, 1998b). This configuration of the SLPa spatial distribution was called a constructive pattern by Gershunov and Barnett (1998b). In addition, significant negative SLPa (at 95–99% confidence levels) are located near each coast of North America, along with cyclonic circulation that weakens the trades and the jet over the Caribbean Sea (Figure 9(a)). Rainfall anomalies indicate
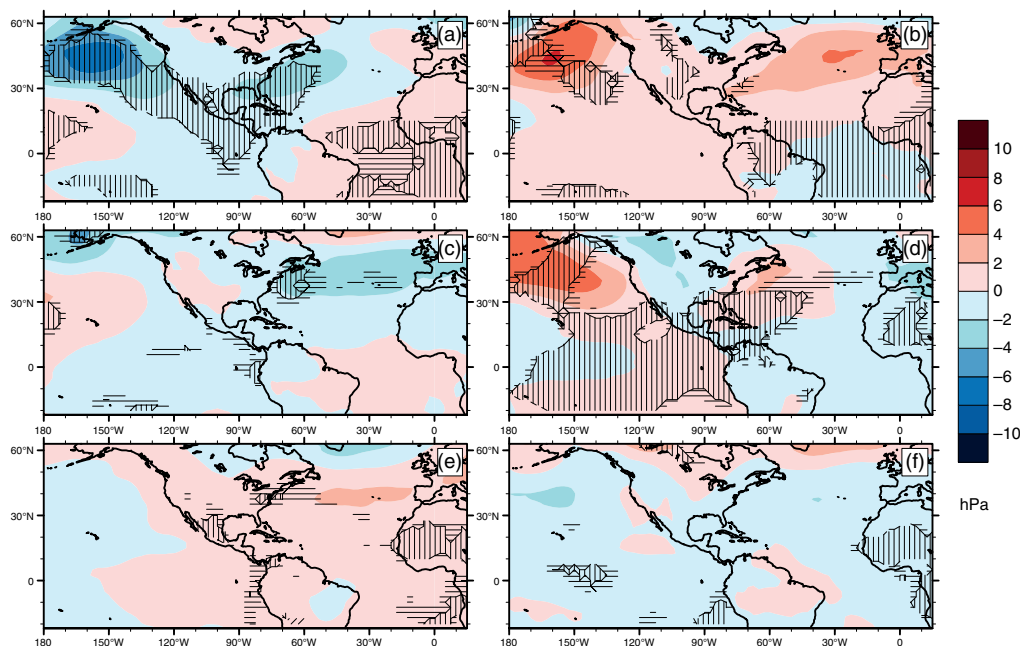
Figure 8. February mean SLP anomalies for the El Niño and PDO phase sub-composites: (a) El Niño and PDO+, (b) La Niña and PDO+, (c) El Niño and PDO−, (d) La Niña and PDO−, (e) neutral and PDO+, and (f) neutral and PDO−. Contours are spaced every 1 hPa. Shaded regions are significant anomalies with confidence levels of 90–95% (horizontal lines), 95–99% (vertical lines), and >99% (slant lines).

drier-than-normal conditions over Central America and the Yucatan Peninsula and wetter-than-normal conditions in southern Mexico (Figure 10(a)). Significant anomalies in rainfall are found in south-western Mexico (positive), Nicaragua, and Panama (negative).

The other constructive case is that of La Niña and negative PDO (PDO−; Figure 8(d)). In this case, the spatial distribution of SLPa is similar to the SLPa pattern found in La Niña composites (Figure 4(b)). La Niña signal in the SLPa is modulated by the PDO−, producing more intense and extended SLPa. This condition can also block storms from the north, preventing them from reaching southern latitudes (Gershunov and Barnett, 1998b). Significant SLPa over the eastern North America are accompanied by anticyclonic circulation, enhancing the trades and the CLLJ (Figure 9(d)). Rainfall anomalies present conditions that are drier than normal over Mexico and wetter than normal over Central America and the Yucatan Peninsula (Figure 10(d)).

In the combination of El Niño with PDO−, or of La Niña with PDO+, the ENSO signal is modulated differently in comparison with the constructive cases mentioned above. Therefore, the condition in which ENSO and PDO are out of phase is regarded as a destructive pattern. Note that in Figure 8(b) the spatial distribution of the SLPa is different from that of the constructive case (Figure 8(d)), the high-pressure anomaly centres being shifted to 160°W (over the north Pacific) and 30°W (north

Atlantic). In the Atlantic, the trades are enhanced and, in addition, the wind over the Caribbean changes in direction (becoming south-easterly, Figure 9(b)) compared with the constructive case. Precipitation anomalies display similar distributions but with wetter conditions in Central America (Figure 10(b)).

In the El Niño and PDO− case (Figure 8(c)), the SLPa pattern is also distorted. In the Pacific, the SLPa are located farther north and their extent and intensity are decreased. In the Atlantic, the SLPa are located farther east and their intensity is also reduced. The circulation linked to the SLPa in the Atlantic does not greatly modify the trades over the Caribbean (Figure 9(c)). Rainfall anomalies (Figure 10(c)) display a distribution similar to that of their constructive counterparts, though south-western Mexico is drier than normal. Note that the rainfall anomalies are not statistically significant in Mexico or Central America.

The influence of the PDO on the perturbations of the Central American climate is measured during neutral ENSO conditions (Figure 8(e) and (f)). The SLPa spatial distribution in the Atlantic is similar during each phase, but with opposite sign. Consequently, the magnitude of the SLPa is less than when combined with ENSO events. On the other hand, negative SLPa are found over the Pacific during each PDO phase, though negative SLPa are intensified during PDO−. Moreover, in each PDO phase, the observed SLPa do not produce
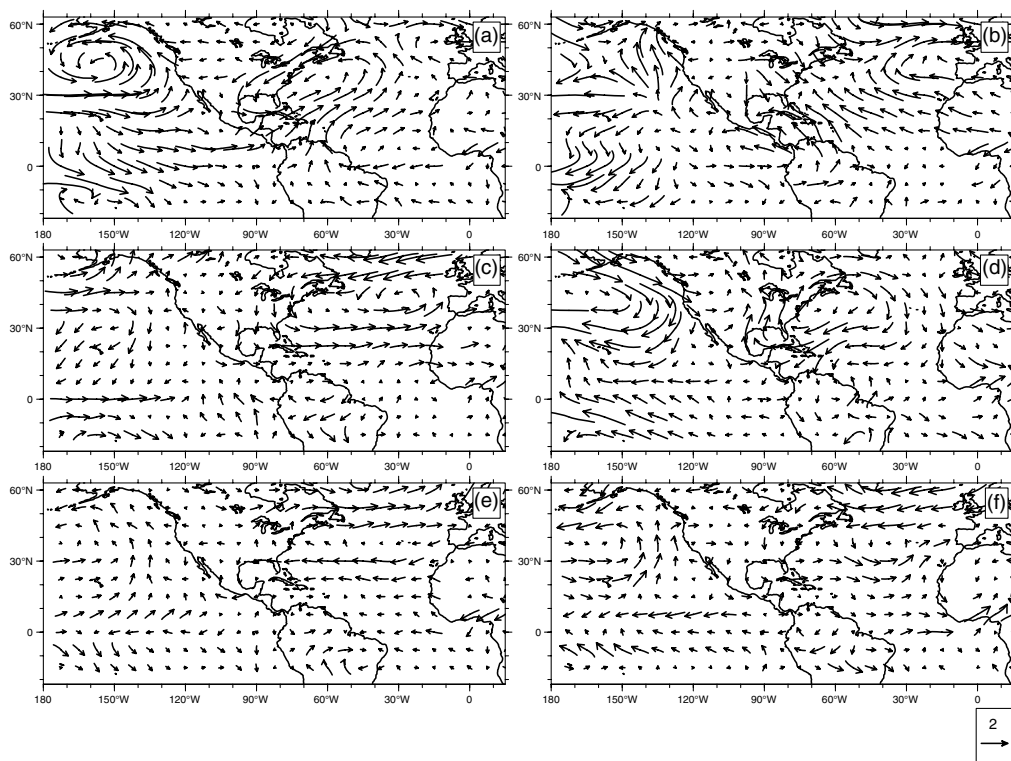
Figure 9. February horizontal wind anomalies at 925 hPa for (a) El Niño and PDO+, (b) La Niña and PDO+, (c) El Niño and PDO−, (d) La Niña and PDO−, (e) neutral and PDO+, and (f) neutral and PDO−. The reference vector is in m s^{-1}.

marked changes in the horizontal wind at 925 hPa over the Caribbean, so the association between the PDO and the perturbation in the CLLJ's intensity and direction is negligible or non-existent. Although the rainfall anomalies (Figure 10(e) and (f)) tend to be positive during PDO+ (PDO−) phases in most of the study domain, these results are not statistically significant.

The divergence field is shown in Figure 11. In the constructive cases (Figure 11(a) and (d)), the divergence anomaly pattern represents an intensification of the pattern found during both the El Niño and La Niña phases, besides having the opposite sign in each case. During El Niño (La Niña) positive (negative) anomalies are observed mainly over Costa Rica and Panama, and over the north-eastern coast of South America, separated by negative (positive) anomalies over Colombia and Venezuela. In the destructive cases, however, each combination behaves differently. During the El Niño and PDO− case (Figure 11(c)), larger changes are observed from 15°N towards the North Pole, over continental North America, and in the equatorial eastern Pacific. Note that the same region displays similar behaviour in the changes in distribution of the precipitation anomalies (Figure 10(a) and (c)). The other destructive case, i.e. La Niña and PDO+ (Figure 11(b)), occurs in a

different manner: negative anomalies are intensified over Costa Rica, Panama, and South America, but significant positive anomalies are centred on 40°N and 90°W where reduced precipitation is observed. In the neutral cases, nevertheless, relevant changes happen only near the equator over continental South America. Regarding the influence of the PDO on rainfall, it is worth mentioning that the modulated divergence helps to explain some observed changes in the spatial distribution of precipitation, though there are other mechanisms related to combinations of the PDO with PNA and/or El Niño. These mechanisms are associated with changes in the distribution of the latent and sensible heat flux anomalies, modulating mainly the SST anomalies in the Gulf of Mexico (Muñoz *et al.*, 2010) that could also be associated with changed precipitation distribution in the mid latitudes or with the changed storm tracks observed in the Northern Hemisphere by Gershunov and Barnett (1998a) and Zárate-Hernández (2013).

5. Summary and conclusions

This paper presents a study of current knowledge about the variability of the CLLJ during winter (February)
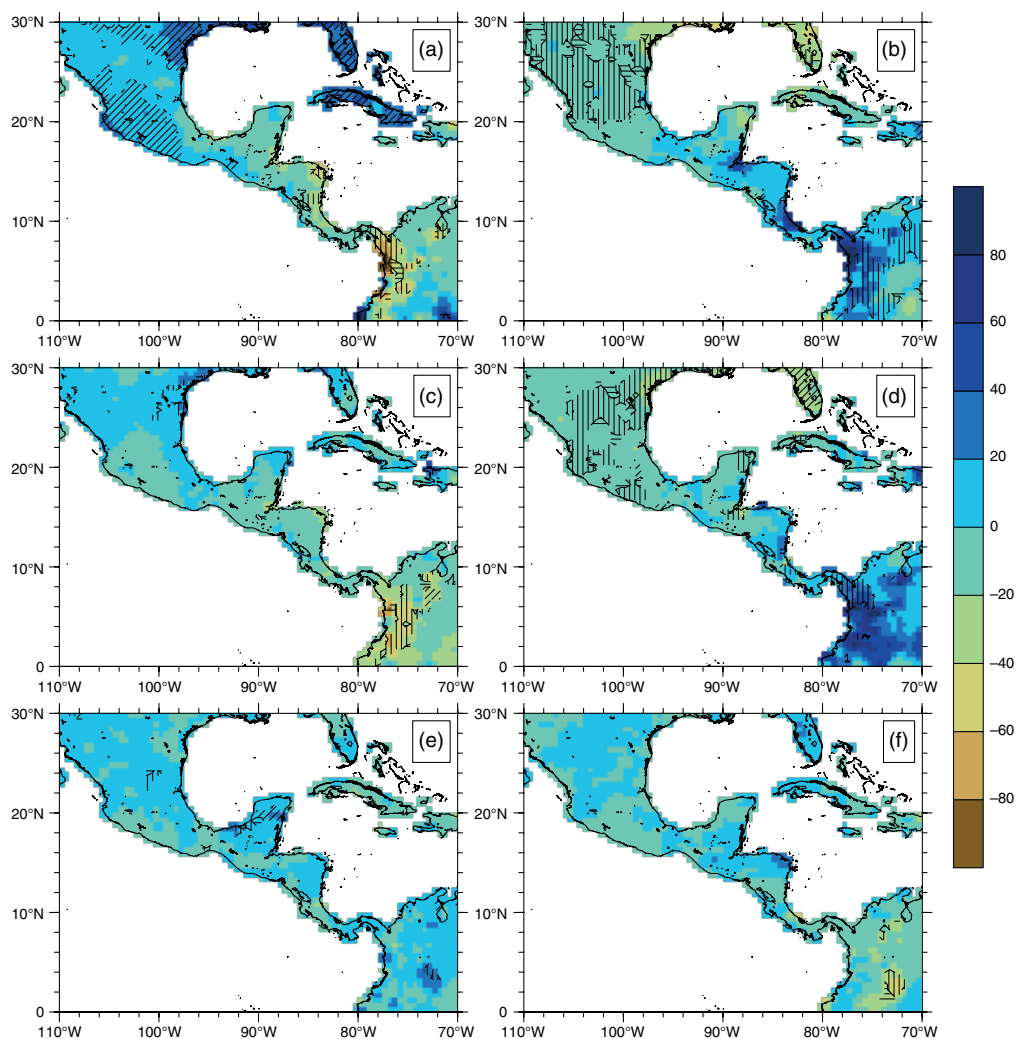
Figure 10. February anomalies of cumulative monthly precipitation in millimetres (mm) for (a) El Niño and PDO+, (b) La Niña and PDO−, (c) El Niño and PDO−, (d) La Niña and PDO−, (e) neutral and PDO+, and (f) neutral and PDO−. Shaded regions are significant anomalies with confidence levels of 90–95% (horizontal lines), 95–99% (vertical lines), and >99% (slant lines).

and about its impact on precipitation anomalies over the Central American region. Using reanalysis data products for horizontal wind at 925 hPa and SLP for the 61-year period from 1950 to 2010, we study the large-scale environment of the CLLJ by calculating monthly mean anomalies. GPCC precipitation data were used to estimate the anomalies of the monthly cumulative rainfall. A CLLJ anomaly index at 925 hPa was defined as the areal average of the February monthly means for the region bounded by 12.5–17.5°N and 70–80°W. We found that the CLLJa is significantly correlated with El Niño, the PDO, and the PNA, and significantly negative correlated with the NAO

and AO. Results also indicate that, in winter, the CLLJ interacts with regional-scale elements such as the MJO and with cold surges originating in the Northern Hemisphere that arrive in the Intra-Americas Sea Region. However, the MJO reportedly exerts more influence on the weather of North America during neutral years (Xue *et al.*, 2002).

The interaction between El Niño and the PDO was studied using composite analysis. During warm (cold) events, the SLPa align with the PNA teleconnection pattern, and cyclonic (anticyclonic) circulation is observed, resulting in westerly (easterly) wind over the Caribbean Sea, weakening (enhancing) the jet intensity. The PDO
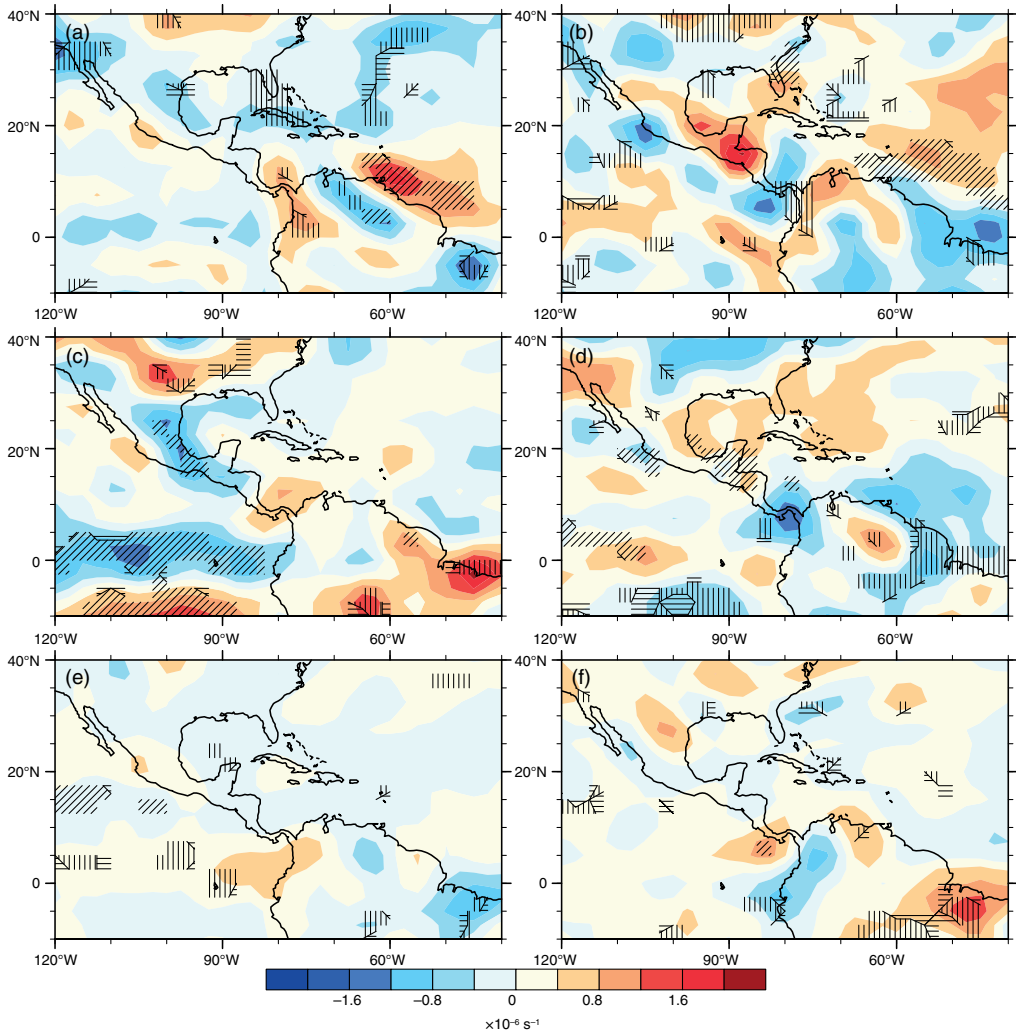
Figure 11. February divergence anomalies at 925 hPa for (a) El Niño and PDO+, (b) La Niña and PDO+, (c) El Niño and PDO−, (d) La Niña and PDO−, (e) neutral and PDO+, and (f) neutral and PDO−. Contours levels are spaced every 0.4×10^{-6} s^{-1}.

enhances or attenuates the ENSO signal in the SLPa (i.e. during El Niño events concomitant with a positive PDO, the PNA teleconnection pattern is enhanced), whereas during El Niño in combination with negative PDO, the PNA pattern is not observed, resulting in no significant modification of the circulation over the Caribbean Sea. Moreover, changes in the circulation due to the PDO phases during La Niña episodes are observed in the direction change of the meridional wind anomalies in the Caribbean Basin. Cold events plus positive (negative) PDO result in an anomalous northward (southward) wind component. Due to the Rossby problem adjustment, the relationship between the SLPa and the CLLJ anomalies

needs further study. Despite large changes in the circulation pattern found due to the influence of the PDO, changes in the monthly cumulative precipitation anomaly were minimal over the Central American Isthmus. The small perturbations in rainfall were related to small fluctuations in the divergence in the tropical regions of the American continent.

The interactions found among the different climate elements studied here emphasise the current need for integrated analysis of the Central American climate. However, such analysis presents many difficulties, as meteorological measurements are unfortunately scarce in this region. Reanalysis, on the other hand, is not sufficient

for several reasons: (1) the temporal and spatial resolution of the data are not necessarily the same or sufficient to capture the main characteristics of the climate elements; (2) the time series in the databases are limited in duration; and (3) removing the noise from the climatology data is difficult. This study, however, contributes significantly to our understanding of the atmospheric dynamics of the Intra-Americas Sea Region, regarding identifying and establishing the relationships between the CLLJ fluctuations in winter and the main climate variability modes.

Acknowledgements

References

Alfaro E. 2002. Some characteristics of the annual precipitation cycle in Central America and their relationships with its surrounding tropical oceans. *Top. Meteorol. Oceanogr.* **9**: 109–119.

Amador JA. 1998. A climatic feature of the tropical Americas: the trade wind easterly jet. *Top. Meteorol. Oceanogr.* **5**: 91–102.

Amador JA. 2008. The Intra-Americas sea low-level jet. *Ann. N. Y. Acad. Sci.* **1146**: 153–188, doi: 10.1196/annals.1446.012.

Amador JA, Chacón JR, Laporte S. 2003. Climate and climate variability in the Arenal basin of Costa Rica. In *Climate, Water and Trans-Boundary Challenges in the Americas*, Díaz H, Morehouse B (eds). Kluwer Academic Publishers: Holland, The Netherlands, 317–349.

Amador JA, Alfaro EJ, Lizano OG, Magaña VO. 2006. Atmospheric forcing of the eastern tropical Pacific: a review. *Prog. Oceanogr.* **69**(2–4): 101–142, doi: 10.1016/j.pocean.2006.03.007.

Amador JA, Alfaro EJ, Rivera ER, Calderón B. 2010. Climatic features and their relationship with tropical cyclones over the Intra-Americas seas. In *Hurricanes and Climate Change*, Elsner JB, Hodges RE, Malmstadt JC, Scheitlin KN (eds). Springer: The Netherlands, 149–173.

Ambaum MHP, Hoskins BJ, Stephenson DB. 2001. Arctic Oscillation or North Atlantic Oscillation? *J. Clim.* **14**: 3495–3507, doi: 10.1175/1520-0442(2001)014<3495:AOONAO>2.0.CO;2.

Cook KH, Vizy EK. 2010. Hydrodynamics of the Caribbean low-level jet and its relationship to precipitation. *J. Clim.* **23**(6): 1477–1494, doi: 10.1175/2009JCLI3210.1.

Dee DP, Uppala SM, Simmons AJ, Berrisford P, Poli P, Kobayashi S, Andrae U, Balmaseda MA, Balsamo G, Bauer P, Bechtold P, Beljaars ACM, van de Berg L, Bidlot J, Bormann N, Delsol C, Dragani R, Fuentes M, Geer AJ, Haimberger L, Healy SB, Hersbach H, Hólm EV, Isaksen L, Kållberg P, Köhler M, Matricardi M, McNally AP, Monge-Sanz BM, Morcrette J-J, Park B-K, Peubey C, de Rosnay P, Tavolato C, Thépaut J-N, Vitart F. 2011. The ERA-Interim reanalysis: configuration and performance of the data assimilation system. *Q. J. R. Meteorol. Soc.* **137**: 553–597, doi: 10.1002/qj.828.

DeWeaver E, Nigam S. 2002. Linearity in ENSO's atmospheric response. *J. Clim.* **15**: 2446–2461.

Durán-Quesada AM. 2012. *Sources of Moisture for Central America and Transport Based on a Lagrangian Approach: Variability, Contributions to Precipitation and Transport Mechanisms*. PhD thesis, Universidade de Vigo, Ourense, Spain.

Gamble DW, Parnell DB, Curtis S. 2008. Spatial variability of the Caribbean midsummer drought and relation to north Atlantic

high circulation. *Int. J. Climatol.* **28**(3): 343–350, doi: 10.1002/joc.1600.

Gershunov A, Barnett T. 1998a. ENSO influence on intraseasonal extreme rainfall and temperature frequencies in the contiguous United States: observations and model results. *J. Clim.* **11**(7): 1575–1586, doi: 10.1175/1520-0442(1998)011<1575:EIOIER>2.0.CO;2.

Gershunov A, Barnett T. 1998b. Interdecadal modulation of ENSO teleconnections. *Bull. Am. Meteorol. Soc.* **79**(12): 2715–2725, doi: 10.1175/1520-0477(1998)079<2715:IMOET>2.0.CO;2.

Gill AE. 1982. *Atmosphere–Ocean Dynamics*. Academic Press: London.

Herrera E, Magaña V, Caetano E. 2015. Air–sea interactions and dynamical processes associated with the midsummer drought. *Int. J. Climatol.* **35**: 1569–1578, doi: 10.1002/joc.4077.

Hidalgo HG, Durán-Quesada AM, Amador JA, Alfaro EJ. 2015. The Caribbean low-level jet, the inter-tropical convergence zone and precipitation patterns in the Intra-Americas Sea: a proposed dynamical mechanism. *Geogr. Ann. Ser. A: Phys. Geogr.* **97**(1): 41–59.

Hoerling M, Kumar A, Zhong M. 1997. El Niño, La Niña, and the nonlinearity of their teleconnections. *J. Clim.* **10**(8): 1769–1786, doi: 10.1175/1520-0442(1997)010<1769:554 ENOLNA>2.0.CO;2.

Holton JR. 2004. *An Introduction to Dynamic Meteorology*. Academic Press: San Diego, CA.

Janowiak J, Gruber A, Kondragunta C, Livezey R, Huffman G. 1998. A comparison of the NCEP-NCAR reanalysis precipitation and the GPCP rain gauge-satellite combined dataset with observational error considerations. *J. Clim.* **11**(11): 2960–2979, doi: 10.1175/1520-0442(1998)011<2960:ACOTNN>2.0.CO;2.

Jury M, Malmgren BA. 2012. Joint modes of climate variability across the inter-Americas. *Int. J. Climatol.* **32**: 1033–1046, doi: 10.1002/joc.2324.

Jury M, Malmgren BA, Winter A. 2007. Subregional precipitation climate of the Caribbean and relationships with ENSO and NAO. *J. Geophys. Res. Atmos.* **112**: D16107, doi: 10.1029/2006 JD007541.

Kalnay E, Kanamitsu M, Kistler R, Collins W, Deaven D, Gandin L, Iredell M, Saha S, White G, Woollen J, Zhu Y, Leetmaa A, Reynolds R, Chelliah M, Ebisuzaki W, Higgins W, Janowiak J, Mo KC, Ropelewski C, Wang J, Jenne R, Joseph D. 1996. The NCEP/NCAR 40-year reanalysis project. *Bull. Am. Meteorol. Soc.* **77**: 437–471, doi: 10.1175/1520-0477(1996)077<0437:TNYRP>2.0.CO;2.

Magaña V, Amador JA, Medina S. 1999. The midsummer drought over Mexico and Central America. *J. Clim.* **12**: 1577–1588, doi: 10.1175/1520-0442(1999)012<1577:TMDOMA>2.0.CO;2.

Martin ER, Schumacher C. 2011a. Modulation of Caribbean precipitation by the Madden-Julian Oscillation. *J. Clim.* **24**(3): 813–824, doi: 10.1175/2010JCLI3773.1.

Martin ER, Schumacher C. 2011b. The Caribbean low-level jet and its relationship with precipitation in IPCC AR4 models. *J. Clim.* **24**(22): 5935–5950, doi: 10.1175/JCLI-D-11-00134.1.

Muñoz E, Enfield D. 2011. The boreal spring variability of the Intra-Americas low-level jet and its relation with precipitation and tornadoes in the eastern United States. *Clim. Dyn.* **36**: 247–259, doi: 10.1007/s00382-009-0688-3.

Muñoz E, Busalacchi AJ, Nigam S, Ruiz-Barradas A. 2008. Winter and summer structure of the Caribbean low-level jet. *J. Clim.* **21**(6): 1260–1276, doi: 10.1175/2007JCLI1855.1.

Muñoz E, Wang C, Enfield D. 2010. The Intra-Americas sea springtime surface temperature anomaly dipole as fingerprint of remote influence. *J. Clim.* **23**: 43–56, doi: 10.1175/2009JCLI3006.1.

Ranjha R, Svensson G, Tjernström M, Semedo A. 2013. Global distribution and seasonal variability of coastal low-level jets derived from ERA-Interim reanalysis. *Tellus A* **65**: 20412, doi: 10.3402/tellusa.v65i0.20412.

Schneider U, Becker A, Finger P, Meyer-Christoffer A, Rudolf B, Ziese M. 2011. GPCC full data reanalysis version 6.0 at 0:5: monthly land-surface precipitation from rain-gauges built on GTS-based and historic data, doi: 10.5676/DWD_GPCC/FD_M_V6_050.

Taylor MA, Alfaro EJ. 2005. Climate of Central America and the Caribbean. In *Encyclopedia of World Climatology*. Encyclopedia of Earth Sciences Series, Oliver J (ed). Springer: The Netherlands, 183–189, doi: 10.1007/1-4020-3266-837, Bodmin, Cornwall (GB).

Wang C. 2007. Variability of the Caribbean low-level jet and its relations to climate. *Clim. Dyn.* **29**: 411–422.

Wang C, Enfield DB. 2003. A further study of the tropical western hemisphere warm pool. *J. Clim.* **16**: 1476–1493, doi: 10.1175/1520-0442-16.10.1476.

Wang C, Fiedler PC. 2006. ENSO variability and the eastern tropical Pacific: a review. *Prog. Oceanogr.* **69**(2–4): 239–266, doi: 10.1016/j.pocean.2006.03.004.

Wang C, Lee S-K. 2007. Atlantic warm pool, Caribbean low-level jet, and their potential impact on Atlantic hurricanes. *Geophys. Res. Lett.* **34**: L02703, doi: 10.1029/2006GL028579.

Xue Y, Higgins W, Kousky V. 2002. Influences of the Madden Julian Oscillation on temperature and precipitation in North America during ENSO-neutral and weak ENSO winter. *A Workshop on Prospects for Improved Forecast and Weather Short-Term Climate Variability on Subseasonal (2 weeks to 2 months) Times Scales*, NASA/Goddard Space Flight Center, Greenbelt, Maryland.

Zárate-Hernández E. 2013. Climatología de masas invernales de aire frío que alcanzan Centroamérica y el Caribe y su relación con algunos índices árticos. *Top. Meteorol. Oceanogr.* **12**(1): 35–55.

Paper II

Interannual variability of the midsummer drought in Central America and the connection with sea surface temperatures

Tito Maldonado[1,2,4], Anna Rutgersson[2], Eric Alfaro[3,4,5], Jorge Amador[3,4], and Björn Claremar[2]

[1]Center for Natural Disaster Sciences, Uppsala University, Villav. 16, 752 36, Uppsala, Sweden
[2]Department of Earth Sciences, Uppsala University, Villav. 16 752 36, Uppsala, Sweden
[3]School of Physics, University of Costa Rica, San Pedro de Montes de Oca, 11501-2060 San Jose, Costa Rica
[4]Center for Geophysical Research, University of Costa Rica, San Pedro de Montes de Oca, 11501-2060 San Jose, Costa Rica
[5]Centre for Research in Marine Sciences and Limnology, University of Costa Rica, San Pedro de Montes de Oca, 11501-2060 San Jose, Costa Rica

Correspondence to: Tito Maldonado (tito.maldonado@geo.uu.se)

Abstract. The midsummer drought (MSD) in Central America is characterised in order to create annual indexes representing the timing of its phases (start, minimum and end), and other features relevant for MSD forecasting such as the intensity and the magnitude. The MSD intensity is defined as the minimum rainfall detected during the MSD, meanwhile the magnitude is the total precipitation divided by the total days between the start and end of the MSD. It is shown that the MSD extends along the Pacific coast, however, a similar MSD structure was detected also in two stations in the Caribbean side of Central America, located in Nicaragua. The MSD intensity and magnitude show a negative relationship with El Niño 3.4 and a positive relationship with the Caribbean low-level jet (CLLJ) index, however for the Caribbean stations the results were not statistically significant, which is indicating that other processes might be modulating the precipitation during the MSD over the Caribbean coast. On the other hand, the temporal variables (start, minimum and end) show low and no significant correlations with the same indexes.

The results from canonical correlation analysis (CCA) show good performance to study the MSD intensity and magnitude, however, for the temporal indexes the performance is not satisfactory due to the low skill to predict the MSD phases. Moreover, we find that CCA allows producing forecasts of the MSD intensity and magnitude using sea surface temperatures (SST) with leading times of up to 3 months. Using CCA as diagnostic tool it is found that during June, an SST dipole pattern upon the neighbouring waters to Central America is the main variability mode controlling the inter-annual variability of the MSD features. However, there is also evidence that the regional waters are playing an important role in the annual modulation of the MSD features. The waters in the PDO vicinity

might be also controlling the rainfall during the MSD, however, exerting an opposite effect at the north and south regions of Central America.

1 Introduction

The geographical features of Central America imprint the characteristics of the regional climate and weather at the isthmus. The region is conformed by a large and high mountain system surrounded by the Pacific and Atlantic oceans, which induces the maritime climate conditions governing in the region (Taylor and Alfaro, 2005). The interaction between the easterly winds (trades), which in turns are the dominant wind regime, and topography divide the region into two different climate areas: the Pacific located leeward of the main wind and the Caribbean presenting windward conditions.

The annual rainfall cycle for the entire region has already been well documented for Central America (Alfaro, 2002), and for the Eastern Tropical Pacific (ETP, Magaña et al. 1999; Amador et al. 2006). In the Pacific region the annual precipitation cycle exhibits a bimodal behaviour (Magaña et al., 1999; Taylor and Alfaro, 2005; Amador et al., 2006). The first precipitation maximum occurs during May-June when the nearby ocean waters have warmed to around 29 °C over the eastern Pacific warm pool, and the easterly winds have decreased, enhancing convection in the region. During July-August a relative precipitation minimum is observed, along with a decrease in the sea surface temperatures (SSTs) over the eastern Pacific warm pool, and an increase of the easterly winds. This reduction in the rainfall is known as the midsummer drought (MSD, Magaña et al. 1999; Amador et al. 2006). The second precipitation maximum occurs during August-September-October (ASO) and is accompanied by a reduction of the trades and a relative increase of the SSTs up to 28.5 °C over the eastern Pacific warm pool. It is also during this quarter of the year that the hurricane season is more active in the Tropical North Atlantic (Amador et al., 2006).

On the other side, upon the Caribbean coast of Central America the annual precipitation cycle contrasts the one in the Pacific mainly during the boreal winter months, when wetter and more humid conditions are found over the eastern coast of Central America (Taylor and Alfaro, 2005; Amador et al., 2006). A similar bimodal cycle, however, has been extensively reported over the Greater Antilles (Chen and Taylor, 2002; Taylor et al., 2002; Spence et al., 2004; Ashby et al., 2005). The reduction in rainfall experienced during the summer months over the western Caribbean is argued to have a similar pattern to that in the Pacific (Martin and Schumacher, 2011). Little is known about the origins of the MSD in both, the Pacific and Caribbean. The processes involved in such rainfall decrease are most probably different to those operating in the western Central America and Mexico, however, both MSDs appear to share the Caribbean low-level jet (CLLJ) as main process increasing the moisture flux in the Caribbean, which suppresses convection and decreases rainfall (Magaña et al., 1999; Wang, 2007; Muñoz et al., 2008; Amador, 2008; Whyte et al., 2008). In this study, we

focus on the variability of the MSD in the Pacific, nevertheless, we also examine two stations in the Caribbean side, to contrast the features present in both MSDs.

The development of the MSD has been explained in terms of the interaction of changes in the divergent (convergent) low-level winds over the warm waters nearby Mexico and Central America (Magaña et al., 1999). Recent studies such as Karnauskas et al. (2013) and Herrera et al. (2014) have proposed different hypothesis about the origin of the MSD. Karnauskas et al. (2013) argue that the MSD originates as a response to one single precipitation-enhancing mechanism occurring twice, contrary to a suppressing mechanism. The latitudinal dependence in the two peaks of precipitation surge as response to the biannual crossing of the solar declination, which leads to the two peaks in convective instability and hence rainfall. This hypothesis, nevertheless, does not explain the almost simultaneous occurence of the MSD in both southern Mexico and Central America (Magaña et al., 1999). On the other hand, Herrera et al. (2014) describe the origins of the MSD studying the air-sea interaction between the CLLJ (Amador, 1998, 2008; Muñoz et al., 2008; Maldonado et al., 2015) and the ocean waters in the neighbourhood of the Pacific coast. Their findings show that the CLLJ peaks in July, provokes a cooling of the SSTs over the Pacific and a westward shift of low-level moisture convergence that combined with subsidence produce the MSD.

The understanding of the variability of the MSD is still a scientific challenge (Herrera et al., 2014), due to its high spatial and temporal variability (Amador et al., 2006; Amador, 2008). Previous studies have analysed the influence of the SST anomalies in the precipitation regime in Central America. Enfield and Alfaro (1999) have shown that the magnitude of the precipitation during the rainy season (from May to October) in Central America is highly modulated by the SST anomalies at both oceans. Alfaro (2007) and Fallas-López and Alfaro (2012b) studied the predictability of the rainfall using canonical correlation analysis (CCA) with SST as predictor. Both studies found that the SST modify the response on precipitation in different ways during each maximum, the first rainfall peak being modulated mainly by the SST over the tropical Atlantic, and the secondary maximum being controlled by a dipole in the SST anomalies over the neighbour oceans to the Central American coast. Moreover, Fallas-López and Alfaro (2012a) found that the MSD intensity is dependent on several global climate indexes such as the Atlantic Multi-Decadal Oscillation (AMO), Niño 3 (N3), and Pacific Decadal Oscillation (PDO). Maldonado and Alfaro (2011) and Maldonado et al. (2013) utilised CCA to explore the distribution of precipitation extreme events during the second precipitation maximum finding that during the second rainfall maximum, the total precipitation and temporal distribution of precipitation events are controlled by a dipole in the SSTs between the Pacific and the Caribbean-North Atlantic waters. Given the above evidence, it would be expected that SST is involved in the MSD variability at inter-annual scales. In fact, Alfaro (2014) found that warm (cool) conditions of Niño 3.4 tend to be associated to drier (wetter) MSD events in some regions of the North Pacific and Central Valley of Costa Rica.

Other climate processes occur simultaneously with the MSD, and could also alter the precipitation during June-August (JJA) e.g the intensification of the North Atlantic Sub-tropical High (NASH, Wang 2007), the Western Hemisphere Warm Pools (WHWM, Wang and Enfield 2001, 2003), the North American Monsoon (Vera et al., 2006) and the CLLJ (Amador, 1998, 2008). Recently, Hidalgo et al. (2015) also found that the latitudinal position of the precipitation centre of mass is correlated with the intensity of the CLLJ, i.e a weaker (stronger) jet is associated to the northward (southward) shift of the latitudinal precipitation centre of mass, resulting in rainfall above normal during JJA that might be also associated with variations of the MSD events.

A better understanding of the variability of the MSD would then contribute to the knowledge about the weather and climate dynamics in the region, also to the information given to the economic and social sectors. These sectors, such as water resources, agriculture, and hydro-electrical power production are benefited in terms of obtaining better data for planning, mitigation and prevention to severe dry conditions, e.g. the droughts reported in the North Pacific region of Costa Rica during July 2014 (Chinchilla-Ramírez, 2014). Therefore, the targets of this study are first to contribute to the understanding of the climate in the region, and second to provide a systematic method for MSD forecasting.

This study consists of an analysis of the connection between the features of the MSD observed in the Pacific and Caribbean coast of Central America and the anomalies in the SST of the regional waters by means of a combination of principal component analysis (PCA) and canonical correlation analysis (CCA). The precipitation observations, however, are first examined in order to determine the data quality and to characterised the MSD per station. The MSD is described in terms of start, timing, end, duration, depth (intensity) and total precipitation (magnitude). This representation is also used to produce annual indexes of those variables. Previous reports have already characterised the existence of the MSD in Costa Rica (Ramírez, 1983; Hernández, 2013; Alfaro, 2014; Solano, 2015), nonetheless, in this study the portray is expanded to include the entire the region.

This manuscript is organised as follows: in Section 2 is described all the information relevant to the databases used in this study. Section 3 is a explanation of the methodology applied in this analysis. In Section 4 the result and Section 5 the discussion and concluding remarks are presented.

2 Data

A total of 25 gauge stations with daily observations of precipitation provided by the meteorological services in Central America are used. Their location is shown in Fig. 1a, and the information about the coordinates of each station is given in Table 1. Note that the majority (23) of the stations are situated along the Pacific coast with only two stations located along the Caribbean coast. The two Caribbean stations possess relevant features to describe the precipitation behaviour in the Caribbean slope, such as their location at the CLLJ exit and their contrasting annual precipitation cycle to
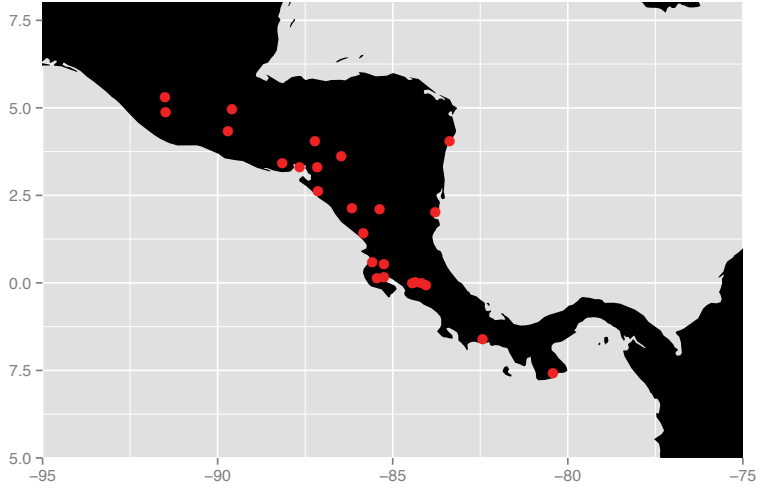
(a)
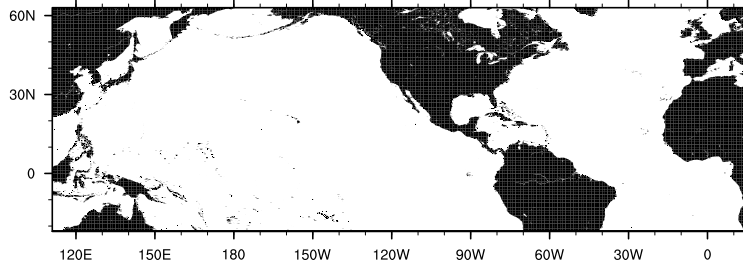
(b)

Figure 1. a) Spatial distribution of the gauge stations in Central America. b) SST domain used as predictor for CCA. The area captures the most important climate modulators for Central America, see Maldonado et al. (2013).

that in the Pacific. Thus, in order to achieve a better representation of the complete region, we consider the Caribbean stations for the analysis. The gaps in the time-series are filled using the methodology described in Alfaro and Soley (2009), which uses autoregressive models of order 1. This method can filter persistent signals comparable to the length of the filter, and the estimated values are consistent with the statistical properties of the time series without external superposition of the data. The precipitation time series length is from 1961 to 2012.

Table 1. Geographical position of the gauge stations in degrees north for latitude and degrees west for longiutde.

Station	LAT	LON
La Argentina	10.03	84.35
Fabio Baudrit	10.00	84.43
Juan Santa Maria	10.00	84.17
Liberia	10.58	85.58
Nicoya	10.15	85.45
Santa Cruz	10.17	85.25
Bagaces	10.53	85.25
CIGEFI	9.94	84.04
Bluefields	12.02	83.78
Ocotal	13.62	86.47
Chinandega	12.63	87.13
Juigalpa	12.10	85.37
Managua	12.14	86.16
Puerto Cabezas	14.05	83.38
Rivas	11.44	85.83
David	8.40	82.43
Los Santos	7.42	80.42
San Miguel	13.43	88.15
Asuncion Mita	14.33	89.71
Huehuetenango	15.32	91.50
LaborOvalle	14.87	91.48
La Fragua	14.96	89.58
Amapala	13.29	87.65
Choluteca	13.32	87.15
Tegucigalpa	14.06	87.22

The extended reconstructed sea surface temperatures (ERSSTv3b, Xue et al. 2003; Smith et al. 2007) are used in this study. The SST anomalies are constructed using a combination of observed data along with models and historical sampling grids. This global database has a horizontal resolution of 2.5 by 2.5 degrees. The domain bounded by -22° to 63° N and 111° to 15° E (Fig. 1b) is considered in order to capture the signal of the most important climate variability modes for the Central American isthmus such as El Niño Southern Oscillation (ENSO), the Pacific Decadal Oscillation (PDO), the Atlantic Multi decadal Oscillaction (AMO), the North Atlantic Oscillation (NAO), and the Tropical North Atlantic (TNA), which in turns, have shown to be relevant in terms of variability of rainfall during the season JJA. The SST anomalies are used as predictors in the CCA models.

The Niño 3.4 index (Trenberth, 1997) provided by the International Research Institute for Climate and Society (IRI, http://iridl.ldeo.columbia.edu/, last view 2015/07/14) is used to estimate the relationship between this index and relevant features of the MSD by means of empirical contingency tables for conditional data.

Horizontal wind data at 925 hPa is provided by the NCEP/NCAR reanalysis (Kalnay et al., 1996; Kistler et al., 2001) which has a horizontal resolution of 2.5 by 2.5 degrees. The wind data is used to calculate the CLLJ index as in Amador (2008) and Maldonado et al. (2015).

3   Methods

Based on the methodology developed in Alfaro (2014), and also applied by Solano (2015), the daily precipitation times series are filtered using a running triangular weight average with a window of 31 days, to avoid or minimise interruptions of the MSD due to weakening of the trades and/or approaching of the ITCZ, as suggested by Ramírez (1983) and Alfaro (2014). An algorithm to systematically identify the features of the MSD is applied to the filtered daily precipitation time series. This algorithm seeks for the timing of each phase of the MSD (start, minimum, and end), besides the intensity and magnitude of the MSD. Notice that this algorithm provides an annual value of each quantity, which are used as indexes to characterise the MSD later in this study. The start of the MSD is considered as the moment when the decrease in precipitation initiates, usually after May-Jun. The end of the MSD is when the precipitation stops increasing, normally taking place around September-October. The minimum occurs in between the start and end of the MSD. The MSD intensity is defined as the minimum rainfall detected during the MSD (or the depth of the valley in Fig. 2), meanwhile the magnitude is the total precipitation divided by the total number of days between the start and end of the MSD. The description of the whole MSD detecting process is explained as follows: first, the algorithm scans for the precipitation minimum in the filtered time series within a reasonable range of days for the existence of the MSD, determined by the climatologies of each station, i.e. typically from 1 June to 30 August. If the precipitation minimum falls outside this period, it is not considered a MSD event. Second, the nearest inflection points to the minimum are sought to determine the start and the end of the MSD. The shortest distance allowed between the inflection points and the minimum is 5 days. Consequently, the shortest MSD would have a duration of 10 days. Moreover, the inflection points have the restriction that the difference of precipitation between them and the minimum should be at least 20% per day. It is worth mentioning, that not all the years present the inflection points and the minimum. For the scope of this study, hence those years missing any of the MSD phases are removed. The causes for those fails in the detection of the MSD phases are several, however, they can be attributed to anomalous years with a extended dry season at the beginning of the year, combined with an earlier and severe MSD, or anomalous drier condition during the secondary precipitation maximum, years with no MSD at all, and in most cases due to missing
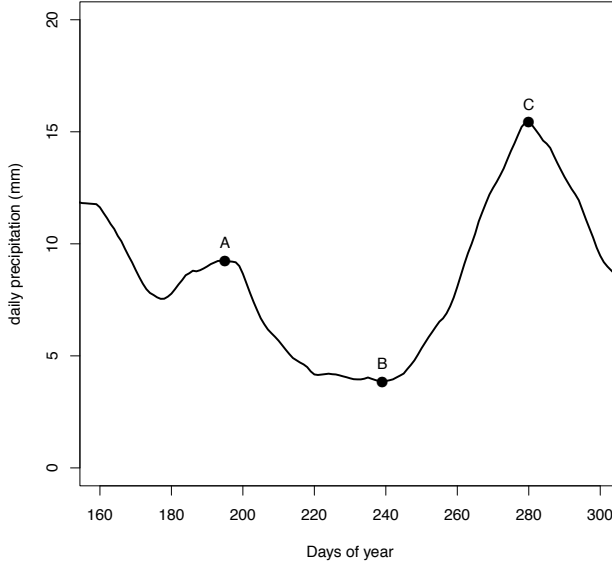
Figure 2. Filtered daily time series for the observed precipitation in station La Argentina during 1990. The dots represent the beginning (A), minimum (B) and end (C) of the MSD. In this year the MSD started by day 195 (14 July), reached the minimum at day 239 (27 August) and ended by day 280 (7 Oct).

data in the observations. Figure 2 shows the schematics of this algorithm. A statistical summary of the features of the MSD is shown in Fig. 3 and 4.

The contingency tables method seeks for a significant predictive relationship between two variables, being one independent and the other dependent (Alfaro et al., 2003; Fallas-López and Alfaro, 2012a). The time series are divided into three categories: below normal, normal and above normal (BN, N, AN, respectively) using the percentiles 33rd and 67th. Fallas-López and Alfaro (2012a) have shown that using these categories provides a good measure of the possible states of El Niño and the MSD indexes, besides, the information obtained is easy to use for the public. Thus, the contingency tables are estimated for conditional events to study the dependence of the MSD features (intensity and magnitude) with ENSO events (independent variable). As mentioned above, the years in which the algorithm does not detect any of the phases or no MSD at all, are dismissed. The statistical significance is estimated by means of bootstrapping with no replace (Gershunov and Barnett, 1998). With bootstrapping, a synthetic time series normally distributed is generated from random noise, then, we estimated contingency tables for the artificial time series. This process is repeated several times to obtain a number of random frequencies normally distributed, which in this case is 1000 repetitions, thus, we obtain 1000 contingency tables per station. If the value of the observed absolute frequency is greater than the 90th of the synthetic frequencies, then the observation is sig-

8

nificant at 0.1 significance level. The same can be said for the 0.05 and 0.01 of significance level. Moreover, an estimated of the Pearson correlation between the MSD intensity (magnitude) and the Niño 3.4 index are shown in Fig. 5.

As a tool to investigate the variability of the MSD, we use Canonical correlation analysis (CCA, Wilks 2011) which is a statistical technique that searches for pairs of patterns in two multivariate data sets (fields), and constructs sets of transformed data variables by projecting the original data onto those patterns. These new variables maximise the interrelationships between the two fields. The new variables can be used, analogously to the regression coefficient in the multiple regression. The new variables or vector weights are also known as canonical vectors, and their projection with their respective fields as canonical variates. CCA can be useful in different applications, such as: i) to obtain diagnostic aspects of the coupled variability of two fields, in the case when the time series of observations of the two fields are simultaneous, or ii) to perform statistical forecasts, in the case when the time series of observations of one field precede the other (e.g. Alfaro 2007; Maldonado and Alfaro 2011; Fallas-López and Alfaro 2012b; Maldonado et al. 2013).

In this study CCA is used as a diagnostic tool, however, models for statistical forecasting can be built for future use. Consequently, CCA is employed in order to analyse the relationship between the SSTs monthly anomalies (SSTA, also denoted field X) with each of the indexes (start, minimum, end, intensity and magnitude of MSD) estimated to represent each of the features of the MSD (each index would be the field Y, for the corresponding model), that is, we seek for a statistical relationship between the large and regional scale features of the SSTA and the characteristics of the MSD in each of the stations (local scale). The above CCA methodology is based on Maldonado et al. (2013) and it is implemented as follows: the fields (SSTA, MSD indexes) are first reduced by means of principal component analysis (PCA) to assure stability in the CCA parameters. A maximum of 17 EOFs and CCA modes in the filtering stage are allowed. This threshold was suggested by Gershunov and Cayan (2003) and Alfaro (2007) to avoid overparameterisation. The optimal combination of EOFs and CCA modes are calculated by means of the goodness index (R^2, Fig. 6). Notice that any set EOFs will produce unique CCA modes for that especific set, then, once the best combination of EOFs is determined, that set EOF is capturing the maximum variability in each field (X and Y), separately, for each specific CCA model (intensity and magnitude). The maximum possible number of CCA modes, however, is determined first by the minimum number of EOFs between both fields. Then with the goodness skill, the maximum number of CCA modes is found for the best fit to avoid any overparameterisation in the model $\hat{Y} = b^T \cdot X$, where the elements of b are the ordinary least-squares regression coefficients computed with CCA, and $\hat{Y}$ is the predicted value of Y. The R^2 is computed using cross-validation models with 1-month window from 1961-2012 for each station in all the models. This metric also allows identifying the best month to predict any of the MSD features. It is worth mentioning that at the end the models would not necessarily have 17 EOF and CCA modes. Stations having indexes with more than 30% of missing data (i.e. fails detecting

MSD events) are discarded. In total, 21 stations are left for the CCA models. Precipitation data are transformed to a normal distribution using percentiles, to achieve better performance in the EOF. The 21 stations having less than 30% of missing data are filled using the long-term means of each index. Note that filling the data in this step is not the same procedure described above.

4 Results

4.1 General features of the MSD

Figs. 3 and 4 show a statistical summary of the timing of the MSD phases. Each phase exhibits subtle differences throughout the stations. Those discrepancies suggest to study this phenomenon separately per station. For example, from Fig. 3, one can see that in the southern part of Central America (Panama, Costa Rica, Nicaragua) the MSD tends to start, develop and end earlier than in the northern part (El Salvador, Guatemala, Honduras), in agreement with previous studies such as Alfaro (2002) and Herrera et al. (2014). In the southern stations, typically, the start of the MSD is detected by 20 June, the minimum is reached by 19 July and the end by 20 August, meanwhile at the north the start is observed by 22 June, the minimum by 24 July and the end around 24 August. Note that the difference can be up to 20 days in each phase from south to north if the stations are analysed separately. The results in Fig. 4 also show the high temporal and spatial variability existent throughout the region agreement with Alfaro (2002) and Amador (2008), but that feature is also observed at local scales as noted by Ramírez (1983); Hernández (2013); Alfaro (2014), and Solano (2015).

The algorithm captures similar MSD structure in stations located over the eastern Nicaragua (Bluefields and Puerto Cabezas) at the Caribbean region. In addition, the stations located at the Caribbean coast present later development of the MSD, starting in average by 29 June, the minimum in 21 July, and the end at 14 August, therefore, being later and shorter in the Caribbean than in the Pacific side of Central America, showing a marked difference between the eastern and western Central America. This MSD structure over the Caribbean has been previously studied by Martin and Schumacher (2011), which concluded that the MSD in the Caribbean is controlled by different external forcings than the one operating in the Pacific sector.

This observed latitudinal difference in the timing in each MSD phase is examined using a t-test (not shown). The results, nevertheless, show no statistical difference among the stations at 90% of significance level, except for the start index in Bluefields station, indicating that in the Caribbean slope the MSD is out-of-phase at least at the start. Thus, it can be argued that the MSD over the Pacific occur simultaneously as found by Magaña et al. (1999).

The intensity and magnitude of the MSD also show high spatial variability (Fig. 5), with a strong contrast between the Pacific and the Caribbean coasts. The Pacific side presents drier MSDs than in the Caribbean basin. In the western Central America, the mean intensity is 4.06 mm (σ = 1.85 mm)
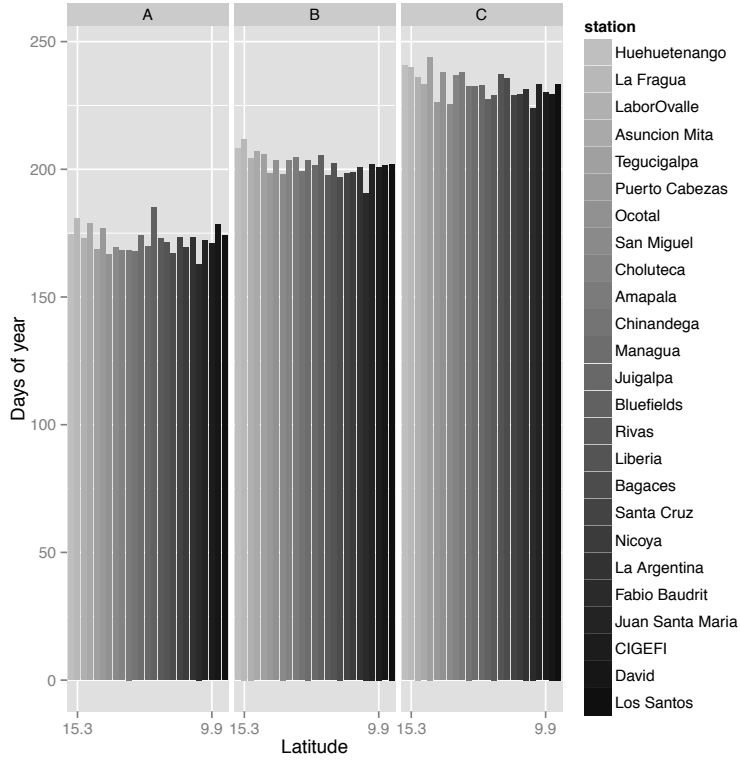
Figure 3. Mean values of the indexes describing the timing of the MSD phases: A) start, B) minimum, and C) end. The x-axis has latitude coordinates being north to the left.

and mean magnitude of 6.50 mmday^{-1} (σ = 2.00 mmday^{-1}), with the highest score detected in David, Panama with an intensity of 7.70 mm (σ = 2.01 mm), and a magnitude of 10.45 mm (σ = 2.20 mmday^{-1}). On the Caribbean side, Bluefields and Puerto Cabezas show the highest records in intensity and magnitude. The mean intensity recorded in Bluefields is 16.64 mm (σ = 5.50 mm), and Puerto Cabezas 8.81 mm (σ = 3.68 mm), whereas the mean magnitude scored is 19.93 mmday^{-1} (σ = 5.39 mmday^{-1}) and 11.31 mmday^{-1} (σ = 3.30 mmday^{-1}). As above, using t-test is determined that the differences in the MSD intensity and magnitude indexes amongst the stations are statistically significant at 90% of significance level.

Inter-annual variability of the MSD intensity and magnitude is examined in Fig. 5. Correlations with Niño 3.4 index are shown in Fig. 6a,c. Notice that all the stations show a significant negative correlation, except one (San Miguel, El Salvador), nevertheless in both cases the correlation is relatively low (0.24 for intensity and 0.18 for magnitude), hence, this result can be discarded. Tables 2 and 3 show a summary of the contingency tables calculated. In both cases, the extreme values of the
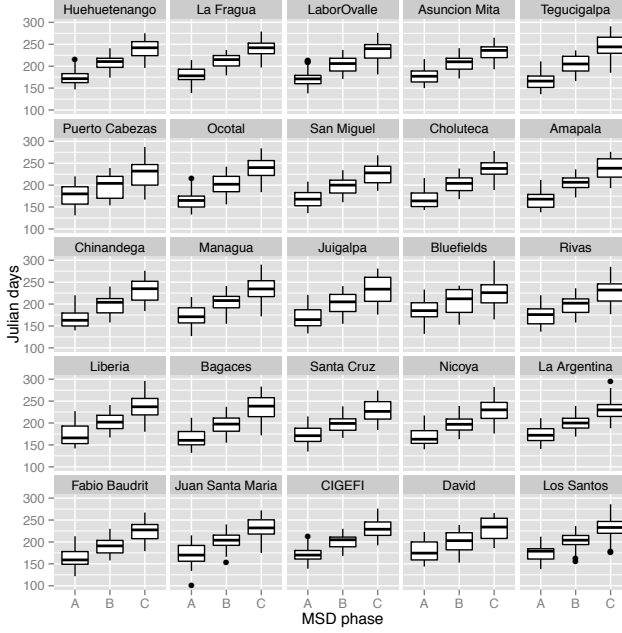
Figure 4. Box-plot of the indexes describing the MSD timing. In the x-axis are each of the events defining the MSD, start (A), minimum (B), and end (C). In the y-axis are the time-coordinates in Julian days. The upper and lower limits of each box correspond to the first and third quartiles (the 25th and 75th percentiles). The upper (lower) whisker extends from the hinge to the highest (lowest) value that is within 1.5 times inter-quartile range of the hinge. Data beyond the end of the whiskers are outliers and plotted as dots. The median is the bold line in each box. Note that the panels are distributed from north to south, left to right and top to bottom.

MSD intensity and magnitude present a connection with ENSO events, however, those conditions are not observed in all the stations, despite some of them have a significant correlation with Niño 3.4 (e.g. Liberia and Juigalpa). Notice that the results for the Caribbean stations are not statistically significant. Alfaro (2014) and Solano (2015) have found similar results for stations in Costa Rica; and Fallas-López and Alfaro (2012a) reported the same relationship with other stations in Central America. This association between the SST anomalies in the Nino 3.4 region and the MSD intensity and magnitude over the west cost of Central America can be connected with low-level wind anomalies over the Caribbean Sea. Previous studies have found a relationship between the fluctuation of the CLLJ and precipitation during the summer months (Wang, 2007; Amador, 2008). Figure 6b,d show the correlation of the intensity and magnitude of the MSD with the CLLJ index. Similarly, most of the stations show positive significant correlations, except the stations in the Caribbean. It is known that in the summer months (JJA) during warm (cold) ENSO episodes the CLLJ is stronger (weaker) than normal (Amador, 2008) with a correlation of -0.53 (p-value < 0.01). Hidalgo et al. (2015) also
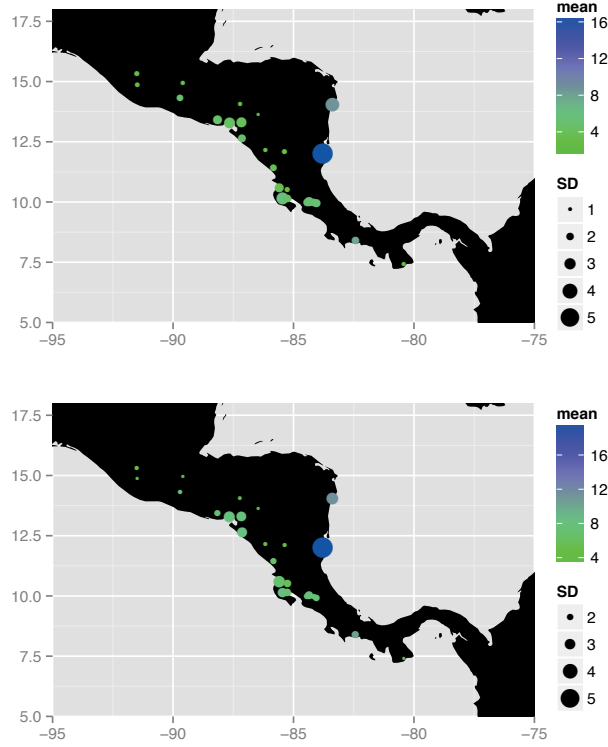
Figure 5. Mean and standard deviation for the MSD intensity (mm, top) and magnitude (mmday^{-1}, bottom) for the period 1961-2012. Note the color scale is not the same in both figures, since the intensity and magnitude are not necessarily of the same order of magnitude. The dots size represents the standard deviation.

noted that during stronger (weaker) CLLJ the ITCZ is located south (north) from the normal position, leading to a reduction (increase) in the total precipitation during boreal summer (JJA), thus, affecting the MSD. Therefore, the bottom line of this result is that the ENSO events modulate the intensity and magnitude of the MSD, and the evidence reveals that the observed changes in these metrics are connected with the modulation of the CLLJ, functioning as the mechanism that transfers El Niño signal into the precipitation field, and consequently shaping the MSD. It is worth to highlight again that from these results, those processes explain only the inter-annual variability of the MSD in the Pacific coast. The same estimations were done for the other variables (start, minimum, end), however, the results do not shown significant correlations with El Niño and CLLJ index (not shown).
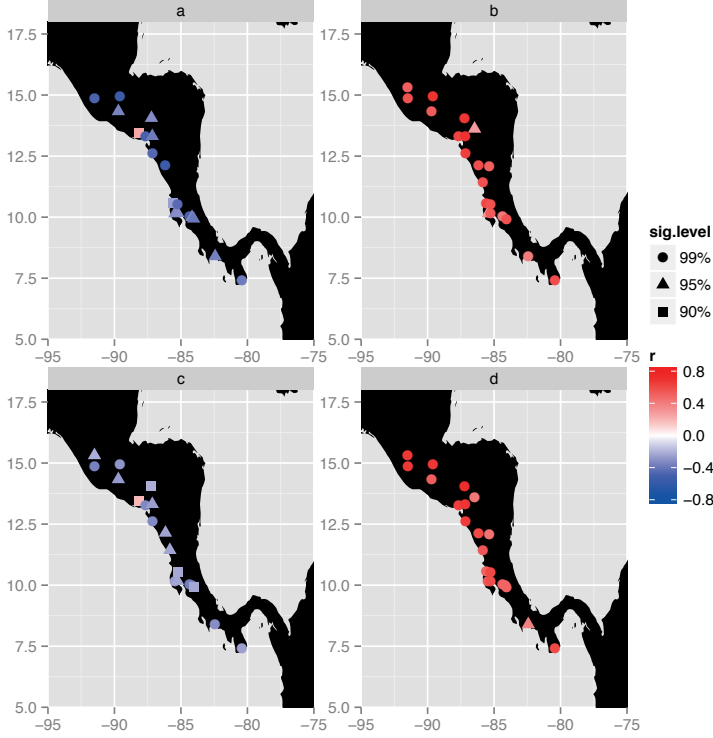
Figure 6. Top Pearson correlation between MSD intensity and a) CLLJ index and b) Niño 3.4 indexes. Bottom the same metric but for the MSD magnitude with c) CLLJ and d) Niño 3.4 indexes. Niño 3.4 index is taken for June. The CLLJ index is estimated from the daily time series, using the definition by Amador (2008) for July.

4.2 Canonical correlation analysis

Models based on CCA are tailored for each of the indexes describing the features of the MSD, defined in Section 3. Using the SST anomalies as predictor (X field), CCA identifies SST patterns that are related to the perturbations of the MSD features (Y field, predictant). The goodness index (R^2) is shown in Fig. 7. The intensity and magnitude show the best skill score compared to the other indexes. These results show that the models to study the timing of the MSD phases have a poor performance using the CCA technique. Consequently, those models are not considered in the further analysis. Both CCA models for MSD intensity and magnitude show one of the highest values of R^2 in April, which means in operational terms, information concerning the MSD intensity and magnitude can be retrieve up to 3 months in advance of an event. This would be valuable for preparation and planning of the societal, economical and agricultural activities during the MSD

Table 2. Summary of contingency tables for each station. The tables were estimated using Niño 3.4 index and the mean intensity per year. The categories were defined using the 33rd (below normal, BN) and 67th (above normal, AN). Years in which the algorithm failed detecting any of the phases of the MSD, were removed. The star (*) represents cases in which the observed condition in column 2 and 3 dominates, and has statistical significance > 90%

Station	SST AN and Intensity BN	SST BN and Intensity AN	r (Kendall)	p-value
La Argentina	*	*	-0.38	0.00
Fabio Baudrit			-0.05	0.62
Juan Santa Maria	*	*	-0.34	0.00
Liberia			-0.21	0.05
Nicoya		*	-0.24	0.02
Santa Cruz	*	*	-0.26	0.01
Bagaces		*	-0.30	0.01
CIGEFI		*	-0.30	0.02
Bluefields			-0.04	0.77
Ocotal	*		-0.27	0.01
Chinandega	*		-0.33	0.00
Juigalpa			-0.21	0.04
Managua	*	*	-0.39	0.00
Puerto Cabezas			-0.02	0.87
Rivas			-0.13	0.26
David	*	*	-0.32	0.00
Los Santos		*	-0.22	0.03
San Miguel			0.25	0.01
Asuncion Mita			-0.22	0.04
Huehuetenango	*		-0.14	0.16
Labor Ovalle	*		-0.35	0.00
La Fragua	*	*	-0.42	0.00
Amapala		*	-0.40	0.00
Choluteca	*		-0.28	0.01
Tegucigalpa	*	*	-0.26	0.02

period. Notice that both models also shown the highest results in July, concurrently with the existence of the MSD, and the CLLJ.

In this study, we analyse the SSTA patterns identified by the model in June, since for that month, CCA models show a relative high R^2, and there is also a 1-month leading time for forecasting the MSD. Besides, the SST do not change significantly from June to July, when the CCA models have the best performance, thus, the SST in July is expected to be close to the SST in June. The best com-
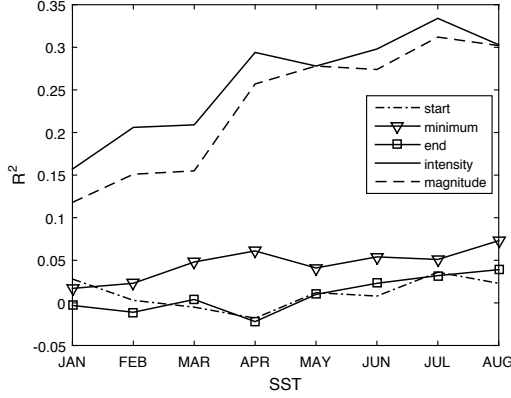
Figure 7. Goodness index (R^2) estimated as the average of the Pearson correlation between synthetic time series generated by cross-validation models and the observed MSD features per station.

bination of EOF and CCA modes for the MSD intensity are $X = 14$, $Y = 4$ EOFs and 2 CCA modes, and for the MSD magnitude $X = 11$, $Y = 6$ EOFs and 3 CCA modes, meaning that for each model (for intensity and magnitude respectively) the best fit is achieved when using 2 and 3 modes (canonical variates) respectively, capturing the maximum influence of the SST on the precipitation field, and specifically in the modulation of the MSD. Figure 8 shows the Pearson correlation between the predicted time series generated using cross-validation models and the observations of both intensity and magnitude in each station. In each case, the station exhibits relative high significant correlation, about 0.35 in average.

The X loadings (correlation between the canonical vectors of the SST and the SSTA) of the first mode controlling the MSD intensity shows a dipolar pattern in the correlation with the SSTAs surrounding Central America (Fig. 9a,b). The highest positive correlations are found over the Pacific in the El Niño region, whereas the highest negative correlation are found over the Tropical North Atlantic and near to the Brasil coast. The influence of this variability mode on the precipitation in Central America has been previously studied by Enfield and Alfaro (1999); Maldonado and Alfaro (2011) and Maldonado et al. (2013), but for the secondary peak of precipitation during August-October (ASO), thus, this results shows that the rainfall during the MSD is governed by the same variability mode present during the highest precipitation season in Central America. On the other hand, for the MSD magnitude, the first mode exerts more influence of the SSTA over the El Niño region, and the regional waters close the west Mexican coast. Notice that in both cases also high positive correlations are found near the western coast of Mexico revealing that both models are affected by the influence of regional waters, varying with the same phase that the superficial temperatures in the El Niño region. The Y loadings in both models are negatively correlated with most of the stations (Fig. 9c,d). That means for a state in which the water over the Pacific is warmer (colder) than normal,

Table 3. Same as Table 2 but for MSD magnitude.

Station	SST AN and Magnitude BN	SST BN and Magnitude AN	r (Kendall)	p-value
La Argentina	*		-0.38	0.00
Fabio Baudrit			-0.04	0.71
Juan Santa Maria	*	*	-0.36	0.00
Liberia	*		-0.17	0.10
Nicoya	*		-0.26	0.01
Santa Cruz	*	*	-0.23	0.03
Bagaces		*	-0.23	0.06
CIGEFI		*	-0.23	0.07
Bluefields			-0.06	0.66
Ocotal			-0.06	0.55
Chinandega	*	*	-0.32	0.00
Juigalpa			-0.08	0.43
Managua		*	-0.25	0.01
Puerto Cabezas			0.02	0.87
Rivas			-0.24	0.03
David	*	*	-0.32	0.00
Los Santos	*		-0.26	0.01
San Miguel			0.19	0.06
Asuncion Mita	*		-0.28	0.01
Huehuetenango	*	*	-0.21	0.01
Labor Ovalle	*		-0.35	0.00
La Fragua	*		-0.29	0.01
Amapala		*	-0.33	0.01
Choluteca	*		-0.26	0.01
Tegucigalpa			-0.21	0.05

plus the SST over the Atlantic colder (warmer) than normal, the intensity and magnitude of the MSD drier (wetter). This results also connects the MSD period with the second rainfall peak, that is, SSTs conditions for drier MSDs, would persist leading to less rainfall during the second peak, following the results in Maldonado et al. (2013). The temporal scores (canonical variates) of this mode in both models show that this mode has mainly inter-annual variations (Fig. 9e,f).

The X loadings of the second mode are shown in Fig. 10a and b. The MSD intensity is dominated by negative correlations with SST anomalies in the Tropical North Atlantic, the Caribbean and Gulf of Mexico and the eastern Pacific, being more important than the first region. The X loadings for the MSD magnitude on the other hand, reveal a tripolar configuration in the North Pacific. This tripolar setting is located in the region where the PDO develops. The PDO has shown more influence in the
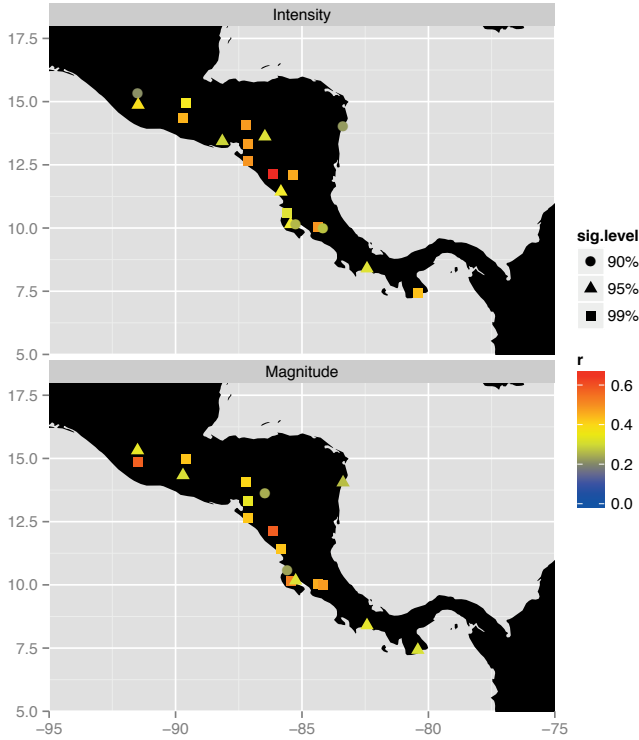
Figure 8. Pearson correlation of the CCA models with the time series of intensity (top) and magnitude (bottom) of MSD.

southern USA and northern Mexico than in Central America (Muñoz et al., 2010; Maldonado et al., 2015), and that could be the reason that its influence is observed in the second mode. The Y loadings in both cases (Fig. 10c,d) show a non-uniform distribution of the correlation. For the MSD intensity (Fig. 9c), the stations are positively correlated with this mode, meanwhile, the MSD magnitude (Fig. 10d) shows a clear division between northern and southern Central America, being the former region (Guatemala, El Salvador, Honduras and west Nicaragua) negatively correlated and the latter region (Costa Rica, Panama and east Nicaragua) positively correlated. The temporal scores for the intensity model exhibit mainly inter-annual variability with a negative trend after 1990 (Fig. 9e), while the temporal scores of the magnitude (Fig. 10f) present a decadal variation, that again possibly relates to the influence of the PDO.

The MSD magnitude is the only feature with a third mode, the X loadings (Fig. 11a) reveal that this mode is dominated by regional SSTs in the Pacific and Tropical North Atlantic. The north and south Pacific show a dipole being positive and negative correlations respectively. The Y loadings
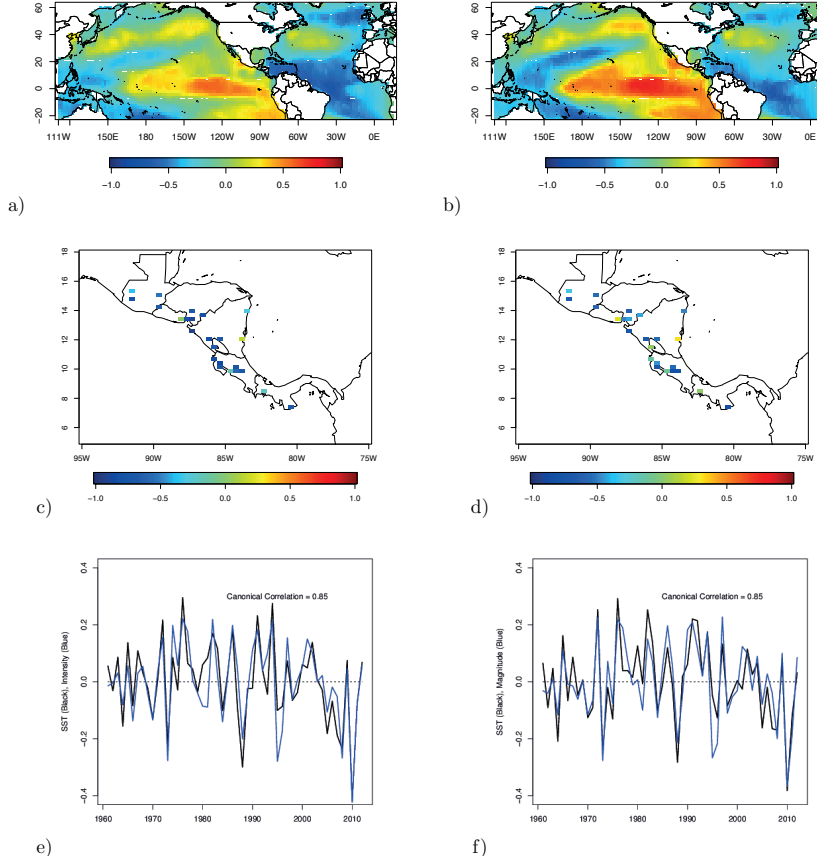
Figure 9. CCA mode 1 for both MSD intensity and magnitude. In the left column are the X (upper) and Y(middle) loadings, and the time scores (bottom) for the intensity. In the right column the same but for the magnitude.

(Fig. 11b) show a north/south division being positively correlated to the north and negatively to the south, while the temporal scores (Fig. 11c) reveal an interannual variation of this mode.

5 Discussion and conclusions

The MSD is characterised using daily time series of rainfall for 25 stations located mainly in the Pacific coast of Central America during the 1961 – 2012 period. An algorithm to detect the MSD phases is developed in order to compare the timing of the MSD start, date of minimum, and end in each station. This algorithm clearly captures the development of the MSD over the Pacific, but also a similar MSD-like structure in two stations located in the Caribbean coast. The results confirm
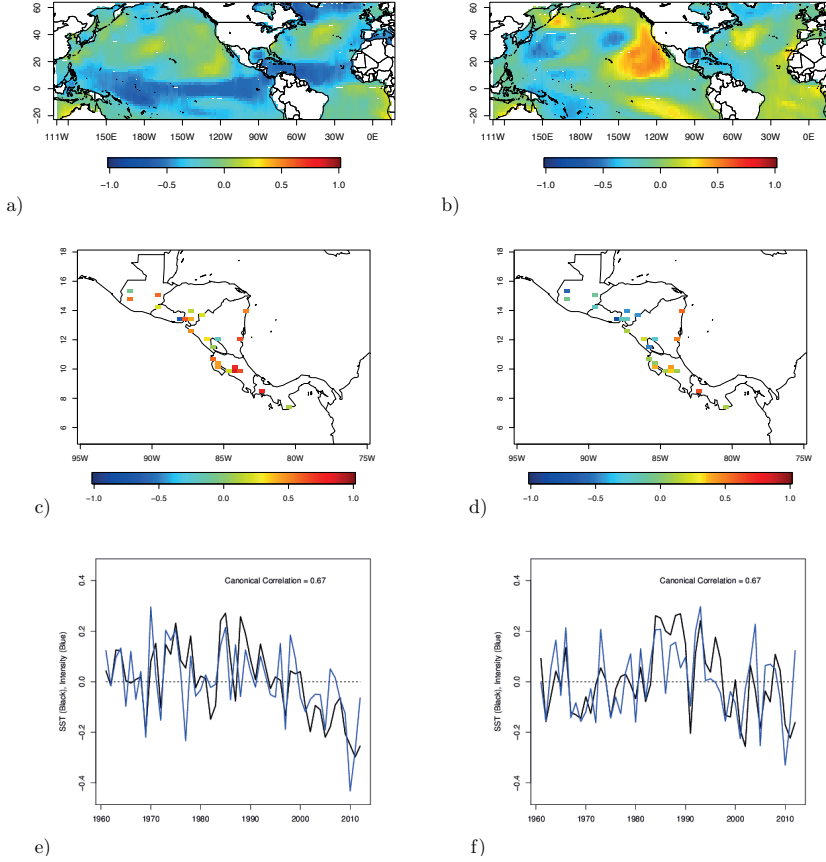
Figure 10. Same as Fig. 9 but for Mode 2.

previous observations showing the high spatial and temporal variability of the MSD, thus, suggesting the need of a more detailed analysis. We , thus, analyse the features of the MSD individually per station, using a combination of empirical analysis (contingency tables) and a more sophisticated statistical method as the canonical correlation analysis to diagnose the variability of the MSD in terms of changes in the SSTA of the surrounding waters.

The MSD intensity and magnitude are correlated with the Niño 3.4 and the CLLJ index in stations located over the western side of Central America. These results reveal a significant negative correlation in almost all the stations with ENSO phases, i.e. warm (cold) anomalies in the Niño 3.4 region, corresponding to an enhanced (decreased) CLLJ intensity, are associated with drier (wetter) MSD. The results of the correlation with the CLLJ show also a positive association of such process, indicating that with a stronger (weaker) jet the MSD intensifies (decreases). This indicates that the
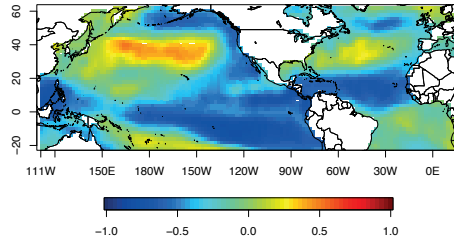
(a)
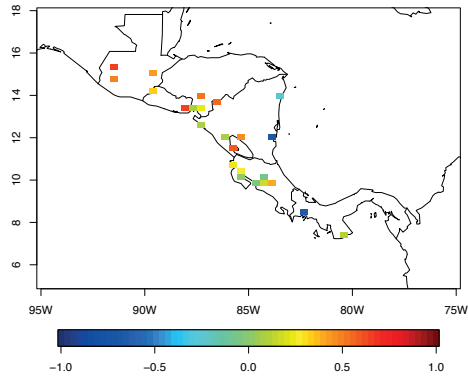
(b)
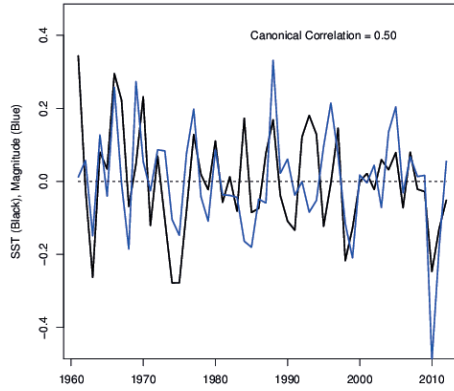
(c)

Figure 11. CCA mode 3 for MSD magnitude. X (a) and Y(b) loadings, and (c) the time scores.

21

CLLJ is involved in the mechanism connecting the SST anomalies in the Pacific with precipitation fluctuations, however, other processes such the migration of the ITCZ, the North American Monsoon and perturbations in the SLP fields over the Amazon could also be engaged with anomalous MSD (Hidalgo et al., 2015). The two stations placed in the Caribbean side do not reveal results statistically significant, hence, suggesting that other elements are involved explaining the annual rainfall variability during their MSD period.

The outputs of CCA show that the MSD intensity is mainly modulated by a dipolar configuration in the SST anomalies formed between the Pacific and the Tropical North Atlantic and Caribbean sea, meanwhile, the first mode controlling the MSD magnitude shows more influence from El Niño and the regional waters close to the western coast of Mexico and Central America. This variability mode in both models has an inter-annual scale, with negative effects in precipitation, i.e. when this mode is positive for both intensity and magnitude, a reduction in rainfall is observed in almost all the stations. Similar SST dipole has been reported to influence the anomalies in rainfall during the months of the highest precipitation events (August-November), and it has been associated with intensification/reduction of the trades, leading to a decrease/increase of precipitation in Central America during the second rainfall period, however, these results show this mode is present prior to the quarter ASO and is also modulating the precipitation during boreal summer.

The second mode in both models presents more complex structures, and it is difficult to distinguish a general pattern affecting the intensity as well as magnitude of the MSD. For the intensity model, the SST show a negative correlation pattern over the equatorial Pacific and North Atlantic waters, nevertheless, the latter region dominates; the time series for this mode show a negative trend after 1990. Meanwhile, for the magnitude, a tripolar configuration over the vicinity of the PDO development region is found. Also negative correlations are found over the Gulf of Mexico. The influence of the PDO should be taken with caution and needs more analysis since the PDO has shown more influence in the southern USA and northern Mexico than in Central America. The time series exhibited inter-decadal variability. As previously mentioned, the correlations between both variables (intensity and magnitude) and this mode, however, do not depict a clear pattern in the stations; for the MSD intensity the correlations reveal a positive association with the SSTA, meanwhile, for the MSD magnitude shows a division between the north and south Central America, being the north (Guatemala, Honduras, El Salvador and west Nicaragua) affected negatively and the south and Caribbean (Costa Rica, Panama and east Nicaragua) positively. It is clear that the second mode is not controlling the precipitation in both models in the same way . The North Atlantic waters become more important for the MSD intensity, hence, could be associated with the same controlling mechanism present during the first precipitation maximum (Alfaro, 2007; Fallas-López and Alfaro, 2012b). While for the MSD magnitude the tripolar configuration might suggest the influence of the PDO, also noted in the contrasting effects of this mode between north and south Central America.

The MSD magnitude is the only variable with higher CCA modes. The third mode reveals the influence of regional waters close to the Central America Pacific and a dipole formed between the north (positive) and south (negative) Pacific, affecting with opposite sign the eastern (negative) and western (positive) part of Central America. This mode presents an inter-annual variability scale. The CCA allows identifying patterns of the SST affecting variables describing the MSD such as the intensity and magnitude, however, it shows a poor performance related to the temporal variables. Another benefit achieved using CCA was the identification of particular months suitable for prediction of the intensity and magnitude of the MSD, being capable of forecasting up to 3 months in advance, which is a reasonable time in terms of practical matters related to prevention and planing for the season. Finally, it is worth pointing out that this analysis also provide a systematic method to study the MSD features, that can be used for statistical forecasts of such phenomenon.

References

Alfaro, E.: Some Characteristics of the Annual Precipitation Cycle in Central America and their Relationships with its Surrounding Tropical Oceans, Tópicos Meteorológicos y Oceanográficos, 9, 1–13, http://imn.ac.cr/publicaciones/revista/2002/Diciembre/1-Alfaro-Dic02.pdf, 2002.

Alfaro, E.: Uso del análisis de correlación canónica para la predicción de la precipitación pluvial en Centroamérica, Ingeniería y Competitividad, 9, 33–48, http://bibliotecadigital.univalle.edu.co/xmlui/handle/10893/1622, 2007.

Alfaro, E.: Caracterización del "veranillo" en dos cuencas de la vertiente del Pacífico de Costa Rica, América Central (Characterization of the Mid Summer Drought in two Pacific slope river basins of Costa Rica, Central America). Spanish., International Journal of Tropical Biology, 62, 1–15, https://www.academia.edu/9493294/Caracterizaci%C3%B3n_del_veranillo_en_dos_cuencas_de_la_vertiente_del_Pac%C3%ADfico_de_Costa_Rica_Am%C3%A9rica_Central_Characterization_of_the_Mid_Summer_Drought_in_two_Pacific_slope_river_basins_of_Costa_Rica_Central_America_._Spanish, 2014.

Alfaro, E. and Soley, J.: Descripción de dos métodos de rellenado de datos ausentes en series de tiempo meteorológicas, Revista de Matemáticas: Teoría y Aplicaciones., 16, 59–74, http://revistas.ucr.ac.cr/index.php/matematica/article/view/1419, 2009.

Alfaro, E., Soley, J., and Enfield, D.: Uso de una Tabla de Contingencia para Aplicaciones Climáticas (Use of a Contingency Table for Climatic Applications), p. 51, ESPOL and FUNDESPOL, Guayaquil, Ecuador, 2003.

Amador, J. A.: A Climatic Feature of the Tropical Americas: The Trade Wind Easterly Jet, Top. Meteor. Oceanogr., 5, 91–102, http://imn.ac.cr/publicaciones/revista/1998/diciembre/1-Amador,Jorge-dic98.pdf.pdf, 1998.

Amador, J. A.: The Intra-Americas Sea Low-level Jet Overview and Future Research, Annals of the New York Academy of Sciences, 1146, 153–188, doi:10.1196/annals.1446.012, http://onlinelibrary.wiley.com/doi/10.1196/annals.1446.012/abstract, 2008.

Amador, J. A., Alfaro, E. J., Lizano, O. G., and Magaña, V. O.: Atmospheric forcing of the eastern tropical Pacific: A review, Progress In Oceanography, 69, 101–142, doi:10.1016/j.pocean.2006.03.007, http://www.sciencedirect.com/science/article/pii/S0079661106000292, 2006.

Ashby, S. A., Taylor, M. A., and Chen, A. A.: Statistical models for predicting rainfall in the Caribbean, Theor. Appl. Climatol., 82, 65–80, doi:10.1007/s00704-004-0118-8, http://link.springer.com/article/10.1007/s00704-004-0118-8, 2005.

Chen, A. A. and Taylor, M. A.: Investigating the link between early season Caribbean rainfall and the El Niño+1 year, Int. J. Climatol., 22, 87–106, doi:10.1002/joc.711, 2002.

Chinchilla-Ramírez, G.: Resumen Meteorológico Julio 2014. Boletín Meteorológico Mensual, http://www.imn.ac.cr/boletin_meteo/historial/2014/BMET072014.pdf, 2014.

Enfield, D. B. and Alfaro, E. J.: The Dependence of Caribbean Rainfall on the Interaction of the Tropical Atlantic and Pacific Oceans, Journal of Climate, 12, 2093–2103, doi:10.1175/1520-0442(1999)012<2093:TDOCRO>2.0.CO;2, http://journals.ametsoc.org/doi/abs/10.1175/1520-0442(1999)012%3C2093%3ATDOCRO%3E2.0.CO%3B2, 1999.

Fallas-López, B. and Alfaro, E. J.: Uso de herramientas estadísticas para la predicción estacional del campo de precipitación en América Central como apoyo a los Foros Climáticos Regionales. 2: Análisis de Correlación Canónica., Revista de Climatología, 12, http://webs.ono.com/reclim8/reclim12g.pdf, 2012a.

Fallas-López, B. and Alfaro, E. J.: Uso de herramientas estadísticas para la predicción estacional del campo de precipitación en América Central como apoyo a los Foros Climáticos Regionales. 1: Análisis de tablas de contingencia., Revista de Climatología, 2012, 12: 61-79, http://webs.ono.com/reclim7/reclim12e.pdf, 2012b.

Gershunov, A. and Barnett, T.: ENSO influence on intraseasonal extreme rainfall and temperature frequencies in the contiguous United States: Observations and model results, J. Climate, 11, 1575–1586, doi:10.1175/1520-0442(1998)011<1575:EIOIER>2.0.CO;2, 1998.

Gershunov, A. and Cayan, D. R.: Heavy Daily Precipitation Frequency over the Contiguous United States: Sources of Climatic Variability and Seasonal Predictability, Journal of Climate, 16, 2752–2765, doi:10.1175/1520-0442(2003)016<2752:HDPFOT>2.0.CO;2, http://journals.ametsoc.org/doi/abs/10.1175/1520-0442%282003%29016%3C2752%3AHDPFOT%3E2.0.CO%3B2, 2003.

Hernández, K.: Estudio de la evaporación en Costa Rica y su aplicación para determinar el inicio y la conclusión de la época seca y lluviosa., Tesis de Grado, Licenciatura, Escuela de Física, Universidad de Costa Rica, San José, Costa Rica, 2013.

Herrera, E., Magaña, V., and Caetano, E.: Air–sea interactions and dynamical processes associated with the midsummer drought, Int. J. Climatol., pp. n/a–n/a, doi:10.1002/joc.4077, http://onlinelibrary.wiley.com/doi/10.1002/joc.4077/abstract, 2014.

Hidalgo, H. G., Durán-Quesada, A. M., Amador, J. A., and Alfaro, E. J.: The Caribbean Low-Level Jet, the Inter-Tropical Convergence Zone and Precipitation Patterns in the Intra-Americas Sea: A Proposed Dynamical Mechanism, Geografiska Annaler: Series A, Physical Geography, 97, 41–59, doi:10.1111/geoa.12085, http://onlinelibrary.wiley.com/doi/10.1111/geoa.12085/abstract, 2015.

Jury, M. R. and Malmgren, B. A.: Joint modes of climate variability across the inter-Americas, Int. J. Climatol., 32, 1033–1046, doi:10.1002/joc.2324, http://onlinelibrary.wiley.com/doi/10.1002/joc.2324/abstract, 2012.

Kalnay, E., Kanamitsu, M., Kistler, R., Collins, W., Deaven, D., Gandin, L., Iredell, M., Saha, S., White, G., Woollen, J., Zhu, Y., Leetmaa, A., Reynolds, R., Chelliah, M., Ebisuzaki, W., Higgins, W., Janowiak, J., Mo, K. C., Ropelewski, C., Wang, J., Jenne, R., and Joseph, D.: The NCEP/NCAR 40-Year Reanalysis Project, Bull. Amer. Meteor. Soc., 77, 437–471, doi:10.1175/1520-0477(1996)077<0437:TNYRP>2.0.CO;2, http://dx.doi.org/10.1175/1520-0477(1996)077<0437:TNYRP>2.0.CO;2, 1996.

Karnauskas, K. B., Seager, R., Giannini, A., and Busalacchi, A. J.: A simple mechanism for the climatological midsummer drought along the Pacific coast of Central America, Atmósfera, 26, 261–281, doi:10.1016/S0187-6236(13)71075-0, http://www.sciencedirect.com/science/article/pii/S0187623613710750, 2013.

Kistler, R., Collins, W., Saha, S., White, G., Woollen, J., Kalnay, E., Chelliah, M., Ebisuzaki, W., Kanamitsu, M., Kousky, V., van den Dool, H., Jenne, R., and Fiorino, M.: The NCEP–NCAR 50–Year Reanalysis: Monthly Means CD–ROM and Documentation, Bull. Amer. Meteor. Soc., 82, 247–267, doi:10.1175/1520-0477(2001)082<0247:TNNYRM>2.3.CO;2, http://dx.doi.org/10.1175/1520-0477(2001)082<0247:TNNYRM>2.3.CO;2, 2001.

Magaña, V., Amador, J. A., and Medina, S.: The Midsummer Drought over Mexico and Central America, Journal of Climate, 12, 1577–1588, doi:10.1175/1520-0442(1999)012<1577:TMDOMA>2.0.CO;2, http://journals.ametsoc.org/doi/abs/10.1175/1520-0442%281999%29012%3C1577%3ATMDOMA%3E2.0.CO%3B2, 1999.

Maldonado, T. and Alfaro, E.: Predicción estacional para ASO de eventos extremos y días con precipitación sobre las vertientes Pacífico y Caribe de América Central, utilizando análisis de correlación canónica, InterSedes, 12, 78–108, http://www.intersedes.ucr.ac.cr/ojs/index.php/intersedes/article/view/301, 2011.

Maldonado, T., Alfaro, E., Fallas-López, B., and Alvarado, L.: Seasonal prediction of extreme precipitation events and frequency of rainy days over Costa Rica, Central America, using Canonical Correlation Analysis, Adv. Geosci., 33, 41–52, doi:10.5194/adgeo-33-41-2013, http://www.adv-geosci.net/33/41/2013/, 2013.

Maldonado, T., Rutgersson, A., Amador, J., Alfaro, E., and Claremar, B.: Variability of the Caribbean low-level jet during boreal winter: large-scale forcings, 2015.

Martin, E. R. and Schumacher, C.: The Caribbean Low-Level Jet and Its Relationship with Precipitation in IPCC AR4 Models, Journal of Climate, 24, 5935–5950, doi:10.1175/JCLI-D-11-00134.1, http://journals.ametsoc.org/doi/abs/10.1175/JCLI-D-11-00134.1, 2011.

Muñoz, E., Busalacchi, A. J., Nigam, S., and Ruiz-Barradas, A.: Winter and Summer Structure of the Caribbean Low-Level Jet, Journal of Climate, 21, 1260–1276, doi:10.1175/2007JCLI1855.1, http://journals.ametsoc.org/doi/abs/10.1175/2007JCLI1855.1, 2008.

Muñoz, E., Wang, C., and Enfield, D.: The Intra-Americas Sea springtime surface temperature anomaly dipole as fingerprint of remote influence, J. Climate, 23, 43–56, doi:http://dx.doi.org/10.1175/2009JCLI3006.1, 2010.

Ramírez, P.: Estudio Meteorológico de los Veranillos en Costa Rica., Nota de investigación. 5, Instituto Meteorológico Nacional, Ministerio de Agricultura y Ganadería., San José, Costa Rica, 1983.

Smith, T., Reynolds, R., Peterson, T. C., and Lawrimore, J.: Improvements to NOAA's Historical Merged Land–Ocean Surface Temperature Analysis (1880–2006), J. Climate, 21, 2283 – 2296, 2007.

Solano, E.: Análisis del comportamiento de los períodos caniculares en Costa Rica en algunas cuencas del Pacífico Norte y del Valle Central entre los años 1981 y 2010., Tesis de Grado, Licenciatura, Escuela de Física, Universidad de Costa Rica, San José, Costa Rica, 2015.

Spence, J. M., Taylor, M. A., and Chen, A. A.: The effect of concurrent sea-surface temperature anomalies in the tropical Pacific and Atlantic on Caribbean rainfall, Int. J. Climatol., 24, 1531–1541, doi:10.1002/joc.1068, http://onlinelibrary.wiley.com/doi/10.1002/joc.1068/abstract, 2004.

Taylor, M. A. and Alfaro, E. J.: Climate of Central America and the Caribbean, in: Encyclopedia of World Climatology, edited by Oliver, J. E., pp. 183–186, Springer, Netherlands, 2005.

Taylor, M. A., Enfield, D. B., and Chen, A. A.: Influence of the tropical Atlantic versus the tropical Pacific on Caribbean rainfall, Journal of Geophysical Research: Oceans, 107, 10–1–10–14, doi:10.1029/2001JC001097, http://onlinelibrary.wiley.com/doi/10.1029/2001JC001097/abstract, 2002.

Trenberth, K. E.: The Definition of El Niño, Bulletin of the American Meteorological Society, 78, 2771–2777, doi:10.1175/1520-0477(1997)078<2771:TDOENO>2.0.CO;2, http://journals.ametsoc.org/doi/abs/10.1175/1520-0477(1997)078%3C2771%3ATDOENO%3E2.0.CO%3B2, 1997.

Vera, C., Higgins, W., Amador, J., Ambrizzi, T., Garreaud, R., Gochis, D., Gutzler, D., Lettenmaier, D., Marengo, J., and Mechoso, C. R.: Toward a unified view of the American monsoon systems, Journal of Climate, 19, 4977–5000, http://journals.ametsoc.org/doi/pdf/10.1175/JCLI3896.1, 2006.

Wang, C.: Variability of the Caribbean Low-Level Jet and its relations to climate, Clim Dyn, 29, 411–422, doi:10.1007/s00382-007-0243-z, http://link.springer.com/article/10.1007/s00382-007-0243-z, 2007.

Wang, C. and Enfield, D. B.: The Tropical Western Hemisphere Warm Pool, Geophysical Research Letters, 28, 1635–1638, doi:10.1029/2000GL011763, http://onlinelibrary.wiley.com/doi/10.1029/2000GL011763/abstract, 2001.

Wang, C. and Enfield, D. B.: A Further Study of the Tropical Western Hemisphere Warm Pool, J. Climate, 16, 1476–1493, doi:10.1175/1520-0442(2003)016<1476:AFSOTT>2.0.CO;2, http://journals.ametsoc.org/doi/abs/10.1175/1520-0442%282003%29016%3C1476%3AAFSOTT%3E2.0.CO%3B2, 2003.

Whyte, F. S., Taylor, M. A., Stephenson, T. S., and Campbell, J. D.: Features of the Caribbean low level jet, International Journal of Climatology, 28, 119–128, doi:10.1002/joc.1510, http://onlinelibrary.wiley.com/doi/10.1002/joc.1510/abstract, 2008.

Wilks, D. S.: Statistical Methods in the Atmospheric Sciences, Volume 100, Third Edition, Academic Press, Amsterdam ; Boston, 3 edition edn., 2011.

Xue, Y., Smith, T., and Reynolds, R.: Interdecadal changes of 30-yr SST normals during 1871-2000, JOURNAL OF CLIMATE, 16, 1601–1612, doi:10.1175/1520-0442-16.10.1601, 2003.